An Investigation into the Role of Collagen VI in the Myocardium

Bianca Leonie Anzellotti

A thesis submitted in partial fulfilment of the requirements for a Master of Biomedical Sciences. The University of Auckland. 2023

Abstract

The role of collagen VI in the myocardium is still largely unknown. Mostly being linked to muscular dystrophies such as Bethlem muscular dystrophy and Ullrich congenital muscular dystrophy, a lack of collagen VI deposition leads to severe matrix deficiencies in skeletal muscle and causes overall degradation of muscle fibres. Research within the myocardium in human heart failure has shown an increase in deposition of collagen VI along remodelled t-tubules which are structurally essential for calcium-induced calcium release. Furthermore, recent research from the Crossman lab demonstrates a reduced ejection fraction in the hearts of collagen VI alpha 1 (Col6α1) knockout rats. Moreover, isolated cardiac myocytes from the knockouts demonstrate increased calcium transients and a propensity for arrhythmia. Loss of ejection fraction and disturbed calcium handling are prominent features of heart failure. This led to the proposition that collagen VI may be a target for heart failure therapies, however the lack of knowledge of how this molecule functions in the myocardium motivated this thesis.

It was hypothesized the absence of collagen would lead to reduced force production of the myocardium as indicated by reduced ejection fraction in knock outs and that this was caused by either a loss of mechanical linkage to the extracellular matrix and/or disturbed calcium handling. Moreover, these hypothesized changes likely result from a disconnection between the extracellular matrix and the dystrophin-glycoprotein complex that is essential for normal muscle function.

Free running trabeculae were dissected from the hearts of male collagen VI knockout rats and wild type rats. These trabeculae were then superfused in an oxygenated buffer and attached to a force transducer to measure stress. Trabeculae were loaded with Fura-2 AM indicator to measure calcium dynamics. Stress and calcium dynamics were measured at four stimulation frequencies (0.2Hz, 2Hz, 2.6Hz and 5.6Hz), in five extracellular calcium concentrations (1mM, 1.5mM, 2mM, 2.5mM and 3mM) and response to beta-adrenergic stimulation by addition of isoproterenol. The aim of these experiments was to determine if there were any differences in force production and/or intracellular calcium content of knockout trabeculae in comparison to wild type trabeculae. Furthermore, super-resolution microscopy was used to determine if the protein biglycan can form a link between collagen VI and the dystrophin-glycoprotein complex in cardiac myocytes.

Knockout trabeculae displayed a statistically significant biphasic change in active stress in response to stimulation frequency. A similar but non-significant pattern was observed in wild type trabeculae likely due to a low sample number. Knockout trabeculae showed statistically significant increases of active stress in response to increasing extracellular calcium and a similar but non-significant change was observed in wild type trabeculae. Trabeculae from both groups demonstrated increases in active stress in

response to isoproterenol, although not significant likely due to large variance. Unexpectedly, there was no increase in calcium transient in parallel with increases in active stress. Although it is possible that non-calcium dependant mechanisms could be involved, this does not correlate with published data. Subsequently it was determined that the sensitivity of the calcium detection in the microscope used was poor compared to published studies and likely impacted the ability to detect changes.

Active stress was increased up to a third in the knockouts but was not statistically significant. However, variance in both active stress and intracellular calcium in knockout trabeculae resulted in the study being statistically underpowered. An increased variance in active stress within the myocardium could lead to dyssynchronous contraction and explain the reduced ejection fraction in the knockout heart. Supporting this dyssynchronous hypothesis, two of the six knockout trabeculae demonstrated spontaneous arrhythmic activity compared to none of the wild type trabeculae. Interestingly, there was a statistically significant decrease in passive stress suggesting that collagen VI contributes to the stiffness of the myocardium. This suggests a possible mechanism of desynchrony contraction driven by calcium overload. The absence of collagen VI would likely increase myocyte stretch and increased calcium storage via stretch activated channels.

Preliminary super-resolution imaging demonstrated biglycan was located at the myocyte surface and t-tubules and was also within molecular bind distance of collagen VI in the wild type rat heart supporting the hypothesis that collagen VI forms a mechanical connection between the myocyte and the extracellular matrix. The findings of the thesis provide some support for the hypothesis that there is disorganisation in the knockout cardiomyocytes resulting in varied active stress and calcium dynamics. Moreover, similar changes in muscle function, stress, calcium and arrhythmias have been found in animal studies on Duchenne muscular dystrophy that have mutations in dystrophin. However, due to low statistical power and technical issues with the experiments, further research on collagen VI in the myocardium is needed in order to validate this hypothesis.

Acknowledgements

To David, thank you for mentoring me, listening to my countless questions, and always having answers. You would always make me feel less stressed after our meetings and I couldn't have written this thesis without you. Thank you to Dr Marie Louise Ward for access to your lab and to Amelia Power for your technical assistance.

To my mum and dad, thank you for supporting me even from a distance, from a young age you have embedded an overwhelming drive in me to do my best and I cannot thank you enough. Thank you, mum, for the many afternoon tea video calls and thank you dad for believing in me and always being a call away when I had problems which I didn't know how to solve myself - you were and are always my first call.

To Ciaran, thank you for listening to me, cooking for me, taking me for coffee, motivating, inspiring me, and loving me. I've never met anyone as kind-hearted as you, thank you for allowing me to grow. To Daniel and Donna, thank you for your unrelenting support and ability to always listen and look after me when I needed dinner or just time away from my work.

Finally, to Lulu and Daxter my main support team - thank you for going on walks with me, loving me and most importantly, thank you for being my best friends.

Table of Contents

List of Figures

List of Tables

List of Abbreviations

RrR	ryanodine receptor
RV	right ventricle
DGC	dystrophin glycoprotein complex
DAG	dystrophin-associated glycoprotein
Ca^{2+}	calcium ion
Na^{+}	sodium ion
ADP	adenosine diphosphate
T-tubules	transverse tubules
SERCA	sarcoplasmic reticulum Ca^{2+}-ATPase
NCX	sodium-calcium exchanger
FFR	force frequency relationship
HF	heart failure
HFpEF	heart failure with preserved ejection fraction
HFrEF	heart failure with reduced ejection fraction
LVEF	left ventricular ejection fraction
PKA	protein kinase A
Tnl	protein troponin complex
WGA	wheat germ agglutinin
JPH2	junctophilin 2
BIN-1	myc box-dependent-interacting protein 1
IDCM	idiopathic dilated cardiomyopathy
COL	collagen
UCMD	ullrich congenital muscular dystrophy
DMD	duchenne muscular dystrophy
MI	myocardial infarction
ANG II	angiotensin II
DAPI	4′,6-diamidino-2-phenylindole
a-SMA	alpha smooth muscle actin
SLRP	small leucine rich proteoglycan
LRR	leucine rich repeat
MATN-1	matrilin-1
TGF-β	transforming growth factor-beta
TNF-α	tumor necrosis factor alpha

WT	wild type
KO	knockout
MDX	Duchenne muscular dystrophy mouse model
O_2	oxygen
KHB	krebs–henseleit buffer
BDM	2,3-butanedione monoxime
PFA	paraformaldehyde
DMSO	dimethyl sulfoxide
PBS	phosphate-buffered saline
LSD	least significant difference
ANOVA	analysis of variance
LVDP	left ventricular developed pressure
NO	nitric oxide
ROS	reactive oxygen species
DMD	Duchenne muscular dystrophy
BMD	Becker muscular dystrophy
TRPC	transient receptor potential canonical
PKG	protein kinase G
SOCE	store-operated Ca^{2+} entry

CHAPTER 1 - INTRODUCTION

1.1 Heart anatomy and physiology

1.11 Cardiac tissue, trabeculae and cardiomyocytes

The heart exists as four chambers, two atria and two ventricles as shown in Figure 1. Deoxygenated blood from circulation in the body enters the right atrium via the superior and inferior vena cava, then is pumped from the right ventricle to the lungs through the left and right pulmonary arteries to become reoxygenated. After becoming reoxygenated, the blood re-enters the left atrium of the heart via the left and right pulmonary veins and is pumped around the body from the left ventricle through the aorta. Heart muscle consists of cardiomyocytes, which as the name implies are muscle cells unique to the heart. Inside the ventricles of the heart are two types of free running muscles called trabeculae and papillary muscles (Shown in Figure 1.1B). The main differences between the two is that trabeculae are free running but sit along the walls of the ventricles and are very thin whereas papillary muscles do not run along the walls of the ventricles and are more cylindrical and thicker in comparison. Generally, when undertaking physiological experiments with heart muscles, papillary muscles are considered too thick for oxygenation via dispersion from an oxygenated solution (Fatemifar et al., 2018).

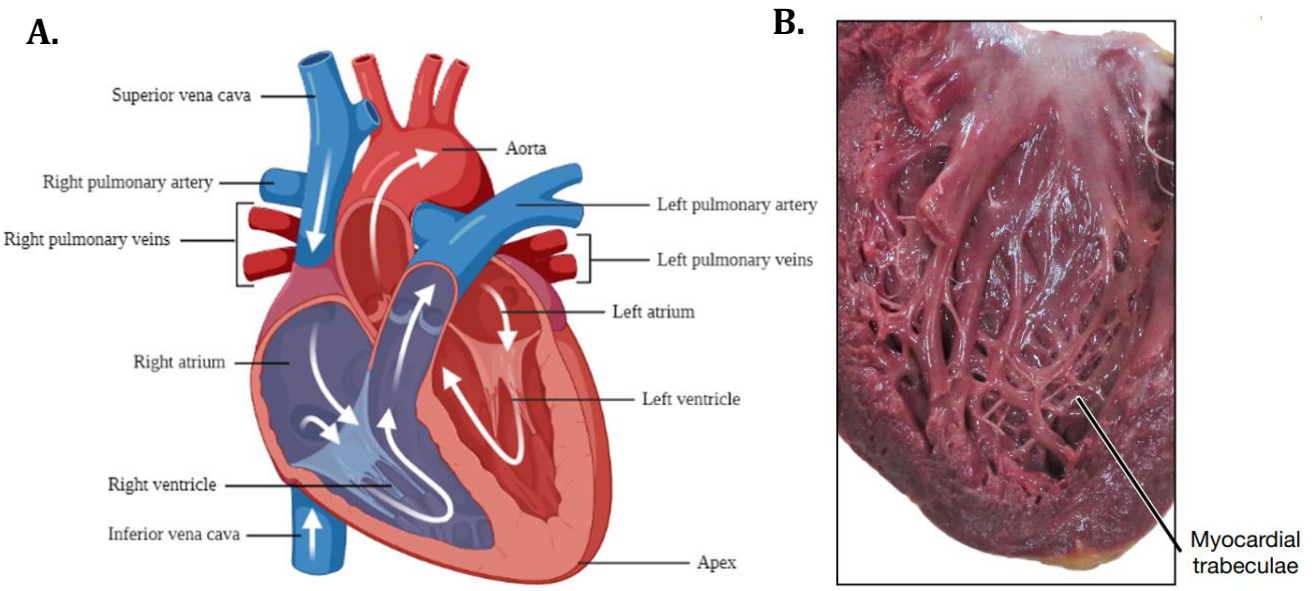

Figure 1.1: Anatomy of heart

A. A labelled diagram of the heart (created at BioRender.com). Blue vessels and chambers show the flow of deoxygenated blood, which comes into the heart and goes to the lungs, whilst red chambers and vessels. **B.** An image taken from (Meyer et al., 2020)of the inside of the left ventricle of a human heart showing labelled myocardial trabeculae.

In the cardiac muscle there are intercalated discs between adjacent muscle cells which function as anchorage points for contractile proteins and for cytoplasmic connections so that cardiomyocytes can rapidly spread action potentials to all adjacent cells to allow for fast muscle contraction (Goodenough & Paul, 2009). These discs generally run perpendicular to the direction of muscle fibres and contain gap junctions for depolarisation between cardiomyocytes (Sun et al., 2020). Cardiomyocytes are rod shaped, shorter, have gap junctions between them and are denser in comparison to skeletal muscle cells. Shown in Figure 1.2 is a confocal image of cardiac tissue from a rat labelled for ryanodine receptors (RyR), which are located on the endoplasmic reticulum membrane and are responsible for calcium release into cells and collagen IV, which is a core component for the basement membrane of cells. The outline of the cardiomyocytes and how they are joined together to form cardiac muscle tissue can be seen clearly with these two labels as shown below.

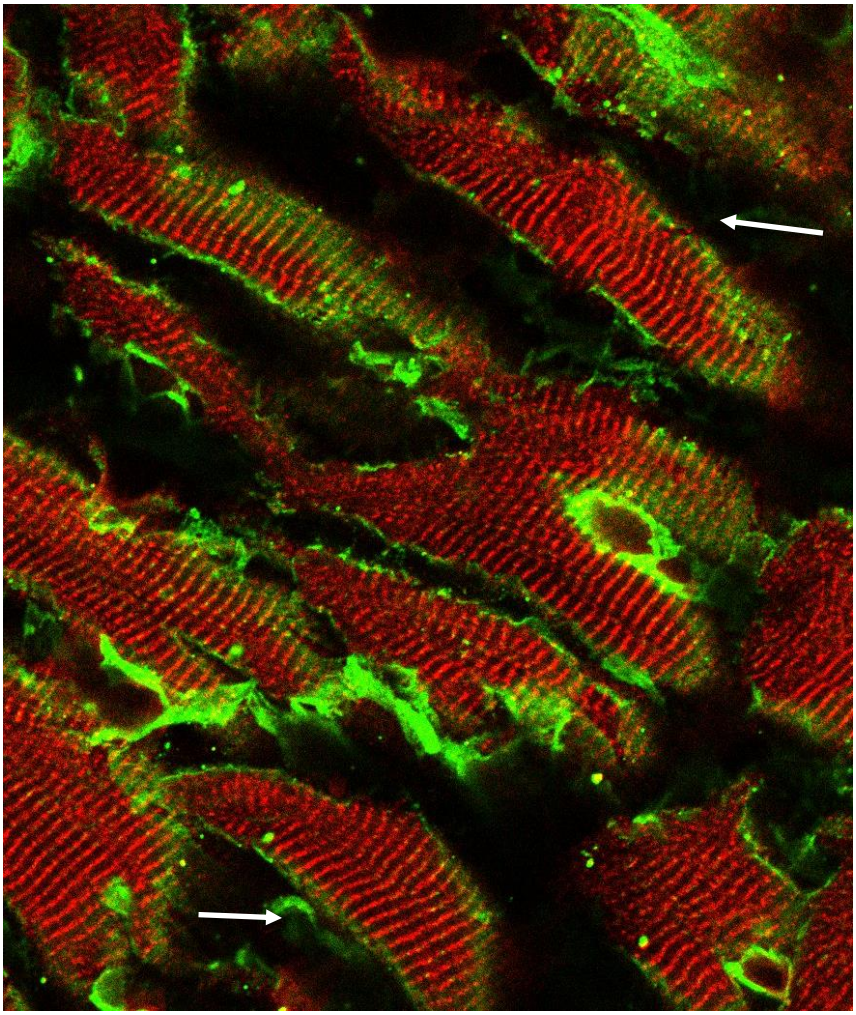

Figure 1.2: Confocal image of a rat RV sample

A confocal image of a sample from the right ventricle (RV) of a rat with RyR (red) and collagen IV (green) labelling, showing the shape and configuration of cardiomyocytes within cardiac tissue. Single cardiomyocytes can be seen (white arrows) with RyR being located within t-tubules whilst the collagen IV label is located around the outside of cardiomyocytes.

Image taken by B.A with assistance from Dr David Crossman

1.12 The costamere complex

A costamere is a connection between the sarcolemma and myofibrils around the Z and M lines as shown in Figure 1.3A (Feher, 2017) which helps with lateral force transmission between neighbouring myofibrils along to the myofibrils under the plasma membrane and then to tendons in skeletal muscle (García-Pelagio et al., 2006). The costamere complex also exists in cardiomyocytes as shown in Figure 1.3B with an image of rat cardiac tissue. Shown is the costamere complex connecting the sarcolemmal membrane and the z-line of the sarcomere. This force transmission is additive to the more well-known muscle force being the through fibres to the intercalated disc.

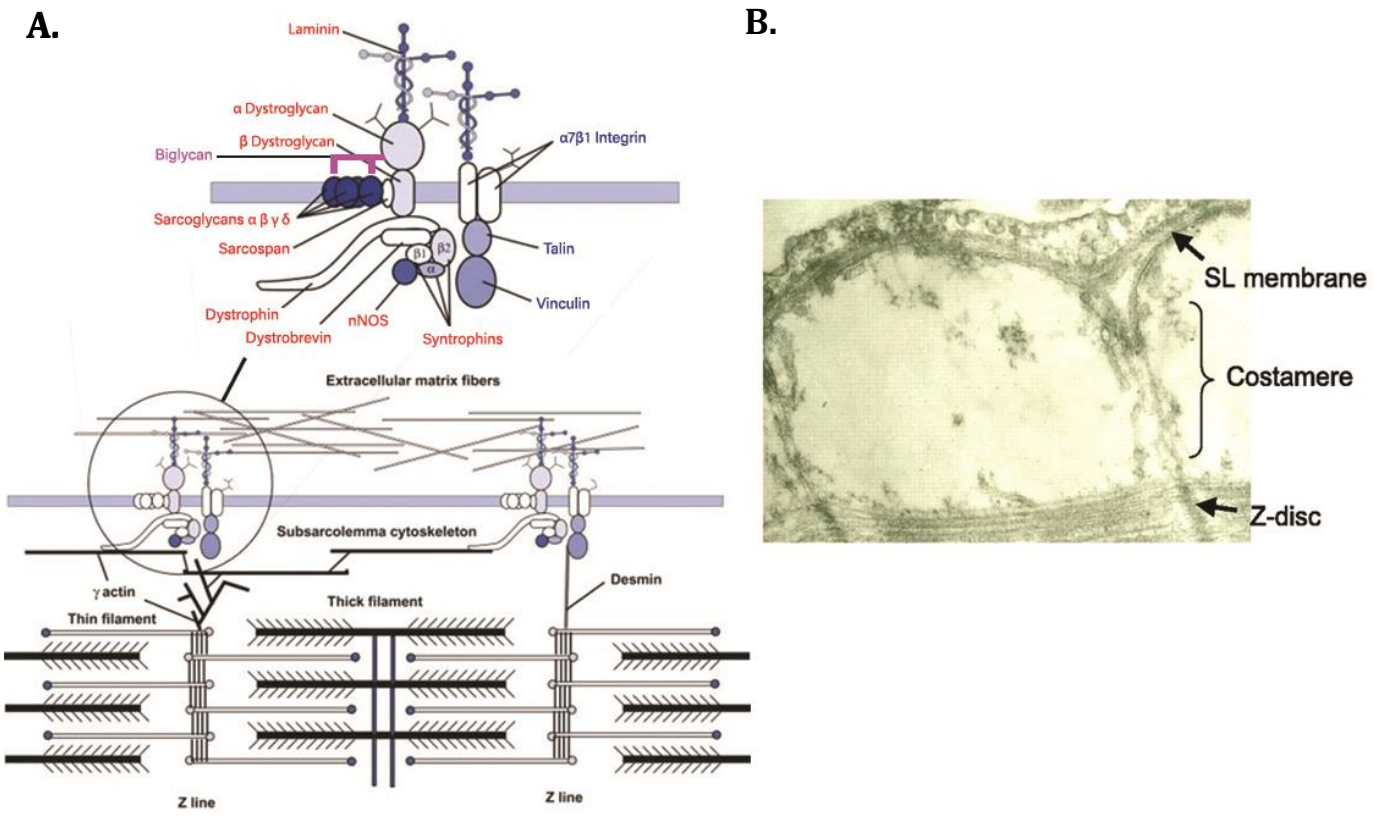

Figure 1.3: A diagram of the costamere complex in skeletal muscle

A. A diagram of how the costamere complex, the DCG and the sarcomere's associated proteins interact with each other. Circled is the costamere complex containing the DGC (red), vinculin-talin-integrin complex (blue) and lamins in the phospholipid bilayer of cells, connecting the extracellular matrix to the intracellular components of myocytes. Biglycan (purple) connects to and holds sarcoglycans α and γ to α-dystroglycan in the DGC. **B.** An electron micrograph of longitudinal rat cardiac muscle tissue in low osmolarity to allow for cellular swelling to occur in order to clearly see the costamere complex within the tissue.

Figures adapted from:

A. (Feher, 2017)

B. (Samarel, 2005)

The costamere consists of two protein complexes known as the dystrophin-glycoprotein complex (labelled in Figure 1.3A in red) and the vinculin-talin-integrin complex (labelled in Figure 1.3A in blue) with studies labelling components from each complex showing that both complexes show a costameric/Z-line distribution along the plasma membrane and that all proteins tested were found to colocalise together (Anastasi et al., 2009).

1.13 The dystrophin glycoprotein complex (DGC)

Dystrophin is a cytoskeletal protein found on the inner surface of the sarcolemma of muscles with an actin-binding domain on the amino terminal and a transmembrane complex of glycoproteins called dystrophin-associated glycoproteins (DAGs), some of which interact directly with elements of the extracellular matrix on the C terminal. Together these proteins are known as the dystrophin glycoprotein complex (DCG). Attached to the DCG are multiple syntrophins which are adaptor proteins known to recruit various signalling proteins and sodium channels, linking the extracellular matrix and intracellular signalling complexes through the DCG (Bhat et al., 2019). Mutations in skeletal muscle DCGs has also been linked to muscle dystrophies and when phosphorylated, dystrophin has been shown to reduce its binding affinity for actin and the syntrophins (Rando, 2001).

With one of the functions of collagen VI in the myocardium hypothesised to be holding the biglycan on the plasma membrane to the sarcoglycans in the DGC (Crossman et al., 2017), there is potential that in the collagen VI knockout rat model there would be disruptions in the dyads within the heart. If the costamere is affected and becomes disorganised in the form of no longer having the correct costameric distribution along the plasma membrane, calcium flux and contractions would be negatively affected. These negative affects potentially would be observed via looking at the knockout model's response to various frequencies in comparison to controls.

1.2 Excitation-contraction coupling

Excitation-contraction coupling is a process in which the excitation (or action potential) on the surface of a cell membrane is paired to a contraction of nearby muscle fibres. When excitation occurs, there is a resulting influx of calcium (Ca^{2+}) ions across the cell membrane that triggers are much larger release of Ca^{2+} from the sarcoplasmic reticulum a process termed calcium induced Ca^{2+} release. Upon excitation, the increased cytoplasmic Ca^{2+} ions bind to troponin molecules on the thin filaments of the sarcomere allowing for myosin molecules to become available for binding to the thick filaments. When bound

together, the thick and thin filaments of the sarcomere slide together by releasing adenosine diphosphate (ADP) forming a contraction of the muscle. Figure 1.4A shows an illustration of a cardiac sarcomere which is the individual contractile unit responsible for mechanical movement of the heart. Below this image is a corresponding electron micrograph (Figure 1.4B) of a sarcomere in cardiac tissue.

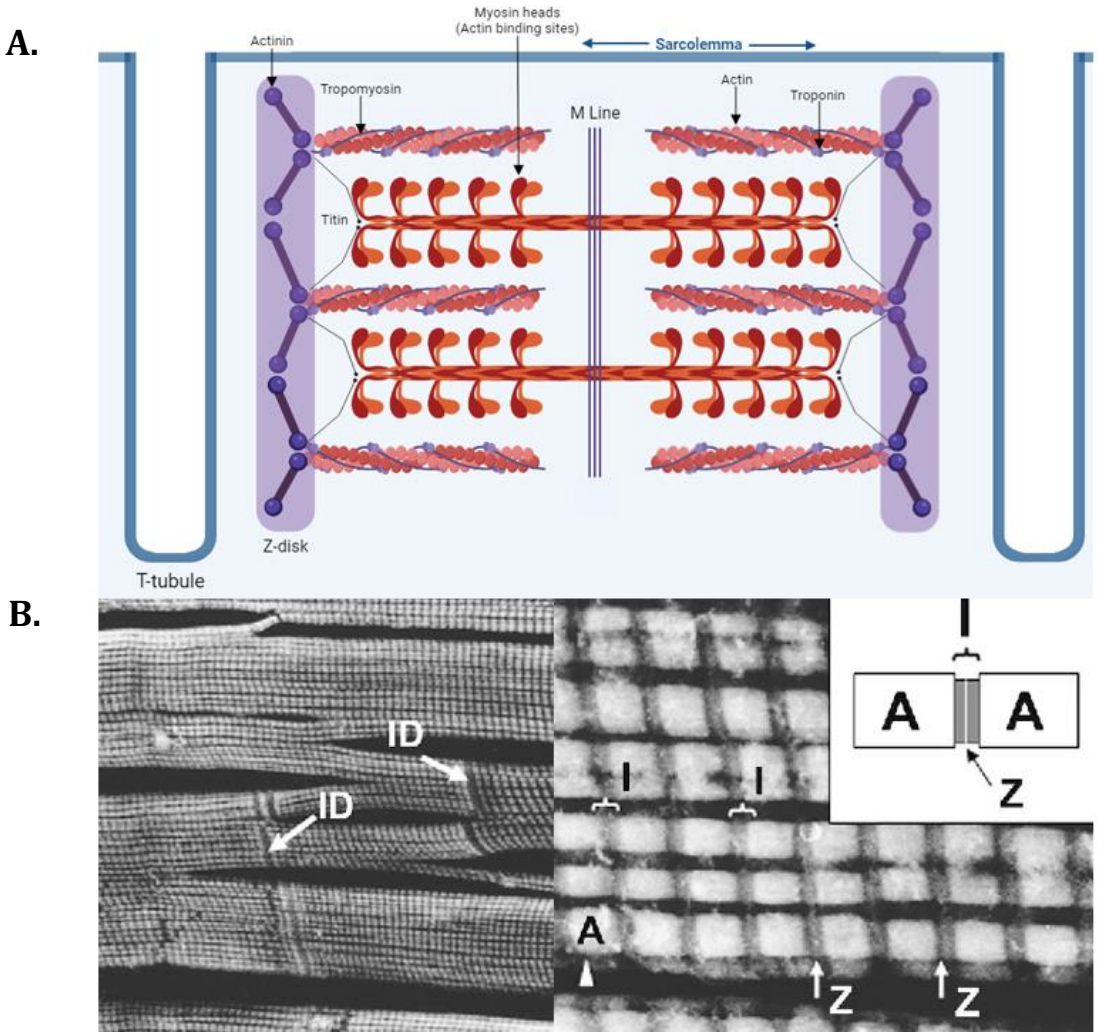

Figure 1.4: Diagram and image of the sarcomere

A. Diagram of a cardiac sarcomere, identifying both thick and thin filaments along with their associated molecules. **B.** An electron micrograph from (Kanzaki et al., 2010)of cardiac tissue showing Z lines of sarcomeres and intercalated disks marked with ID.

(Figure 1.4A created by B.A via biorender.com)

1.21 T-tubules and calcium dynamics

T-tubules are known as invaginations of the sarcolemma in muscle tissue. They have a prominent role in calcium induced calcium release in the heart with additional roles including mediating storage of calcium in the sarcoplasmic reticulum, structure and integrity of cells and

communication between cells. T-tubules are imperative for proper membrane depolarisation and contraction as they rapidly convey excitation (also known as the upstroke in action potential) to the centre of cells in approximately 2ms (Sacconi et al., 2012). A diagram in Figure 1.5 depicts the main components on the t-tubule membrane. Upon receiving a signal via the t-tubule system, molecules such as calcium ions (Ca^{2+}) can enter the cytosol of the cell via L-type Ca^{2+} channels. When entering the cytosol, the calcium travels across the cardiac dyad into the ryanodine receptors (RyR) on the sarcoplasmic reticulum, which allows release of calcium from stores (D. Bers, 2001). After the release of a large amount of calcium from the sarcoplasmic reticulum, the calcium can bind to the thin filaments in the sarcomere to allow for the binding of myosin and the resulting contraction of the muscle.

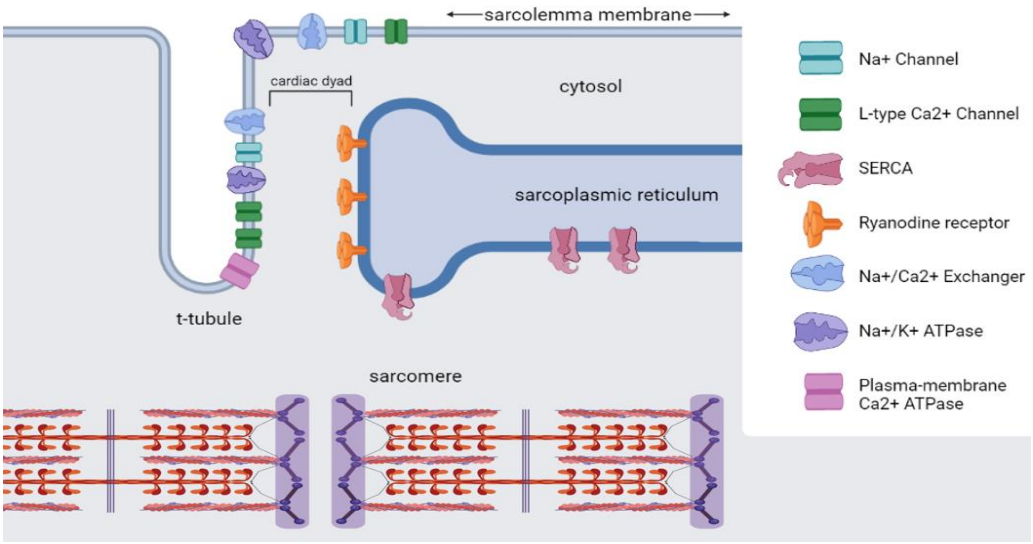

Figure 1.5: A diagram of the main structure and components of the t-tubule

The t-tubule membrane is composed of many proteins responsible for exchanging calcium, sodium and potassium. Exchange of these molecules allows for excitation across the sarcolemma and t-tubule membranes via the increase in cytosolic calcium.

Created by B.A (biorender.com)

1.22 Cardiac dyads and calcium dynamics

Tightly controlled movement of calcium is vital for synchronous contraction and dyads are a key cellular structure enabling this process. Dyads form a tightly regulated signalling complex, between the sarcolemma and the sarcoplasmic reticulum, the intracellular calcium store. The structure of a cardiac dyad, its placement along the Z-lines (shown in Figure 1.6A) of sarcomeres and its arrangement of the ion channels and proteins within it are essential for the initiation of a contraction (Lu et al., 2022).

Dyads are considered essential for forming Ca^{2+} microdomains within cardiomyocytes due to their structural configuration, forming a junctional cleft approximately 12nm to 18nm-wide across (Lu & Pu, 2020) that concentrates incoming Ca^{2+} current to levels required to trigger Ca^{2+} release from the sarcoplasmic reticulum. On the sarcolemma side of the dyad is the voltage sensitive L-type Ca^{2+} channel that opens on depolarisation allowing the signal via a calcium current into the dyad where it then initiates a much large calcium release from the sarcoplasmic reticulum via the calcium-sensitive ryanodine receptor (RyR), generating the cytosolic calcium transient that activates the cross-bridge cycling that powers contraction during systole. Relaxation or diastole occurs when calcium is pumped back into the sarcoplasmic reticulum via sarcoplasmic reticulum Ca^{2+}-ATPase (SERCA) (Itzhaki et al., 2011), and across the sarcolemma via sodium-calcium exchangers (NCX) and plasma membrane Ca^{2+}-ATPase to restore resting cytosolic calcium levels (Takeuchi & Matsuoka, 2022).

Modelling studies show nanoscale changes in the dyad structure will diminish the concentration of trigger Ca^{2+} below what is required to initiate the calcium transient (Lu & Pu, 2020). Disruption of the dyadic arrangement is a common finding in cardiomyocytes from mammals with heart failure (Jones et al., 2018) and was found to create improper propagation of signals resulting in impaired excitation-contraction coupling in a rat model (Wu et al., 2012). Shown in Figure 1.6 is the comparison of the dyad organisation between control sheep cardiomyocytes and diseased cardiomyocytes. Compared to the control dyads, the loss of t-tubules in the disease sample shows not only a loss of the total dyads, but also a change in dyad structure resulting in increased distance between the sarcoplasmic reticulum and the plasma membrane. The efficacy of calcium influxes into L-type Ca^{2+} channels within the dyad is moderated by multiple systems, with one paper noting a reduced calcium synchronicity and induced t-tubule disorganisation at eight weeks when testing mechanical stretch-sensitive molecules in cardiac muscle from rats by pressure overloading and unloading via thoracic aortic constriction/relaxation (Ibrahim et al., 2012).

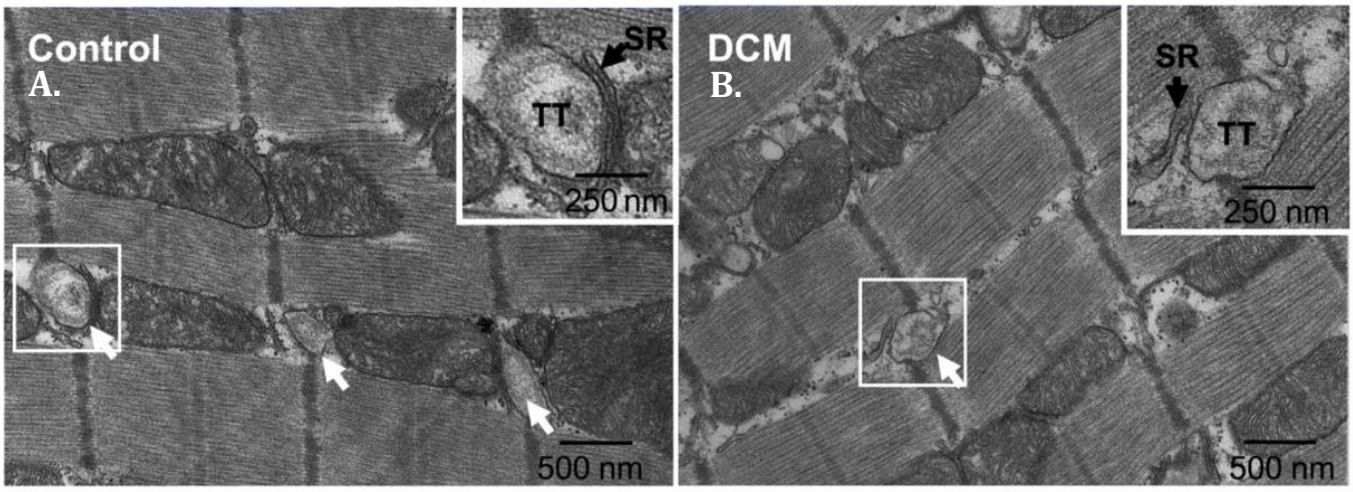

Figure 1.6: A closer view of cardiac dyads within cardiomyocytes

These images are confocal micrographs taken from murine cardiomyocytes with transversely oriented dyads from both a control animal **(A)** and a diseased animal **(B)**. The dark vertical lines are the Z-line of sarcomeres in cells and the t-tubules are labelled TT. The sarcoplasmic reticulum is labelled at SR with the white boxes in each image a single dyad and a closer image in the top right corner.

Image adapted from: (Zhang et al., 2013)

Due to Ca^{2+} being an integral molecule for signals and contractions, it is linked to the modulation of many processes containing proteins which are required for the handling of calcium and in turn, is responsible for many abnormalities displayed in cardiac muscle. An example of an abnormality is the promotion of arrhythmias via incorrect calcium movements such as with calcium sparks (Sutanto et al., 2020). A calcium spark is one of many calcium releases from the sarcoplasmic reticulum which join upon stimulation to form the calcium transient (Cheng & Lederer, 2008). Uncoordinated electrical activity such as early or delayed depolarisations can occur outside of the automaticity of the sinoatrial node (Sutanto et al., 2020). Early depolarisations can occur due to an excessive repolarisation phase and additional delayed depolarisations can occur due to a spontaneous release of sarcoplasmic calcium into the cytosol (Heijman et al., 2014). Within the same study, it was shown that Ca^{2+} current can be at normal levels, but Ca^{2+} release can be reduced. A different occurrence of dysfunction has also been shown within the dyad where RyR calcium leak, which over time caused the development of atrial fibrillation substrates in a mouse model (Li et al., 2014).

Calcium current is known to be disrupted in cardiomyocytes in heart failure. The loss of t-tubules in heart failure has been linked to the failure of the calcium current which in turn fails to initiate calcium release from the sarcoplasmic reticulum and overall slower, more dyssynchronous releases of calcium further resulting in weaker contractions if any (Heinzel et al., 2008) (Lipsett

et al., 2019). Along a healthy myocardial cell there are evenly spaced dyads and in these dyads, there are corresponding RyRs and L-type Ca^{2+} channels which line up with each other in order to become activated when Ca^{2+} ions come into cells so that the sarcoplasmic reticulum can release more calcium and contractions can occur. The main explanation for failed calcium release and dyssynchronous releases of calcium is in heart failure t-tubule remodelling occurs, after remodelling the distance between each dyad on the plasma membrane as well as the dyadic space within the dyad itself becomes no longer optimal for calcium influx into cells which results in L-type Ca^{2+} channels not being lined up on the plasma membrane, leaving some sarcoplasmic RyRs unable to be activated for further calcium release and resulting contraction (Louch et al., 2010). There are also other phenomena which alter calcium currents including receptor defects and insufficiencies. One such defect is with the RyRs on the sarcoplasmic membrane. When the same restructuring of cardiomyocytes occurs in heart failure, the reduced ability to activate sarcoplasmic calcium release in a rat model was looked at further. Found was that when t-tubules were remodelled, they moved away from the Z-line which would leave the RyRs on the sarcoplasmic reticulum. These RyRs were named "orphaned RyRs" and were found to be responsible for the calcium sparks noted above which altered contractions and created arrhythmias (L.-S. Song et al., 2006). Furthermore, with observed Ca^{2+} mishandling and irregularities in heart failure, a logical step in understanding the role of collagen VI would be to create an experiment where the force produced by contractions of the myocardia and the calcium transients displayed in collagen IV knockout rats can be collected simultaneously, which this paper endeavoured to achieve.

1.3 Force and mechanical insufficiencies in heart failure

The force produced from the myocardium contraction depends on multiple factors, including, the frequency of the stimulus provided, calcium sensitivity of myofilaments, the concentration of calcium inside the sarcoplasm, sarcoplasmic reticulum and the dyad as well as the movement or flux of the calcium ions during diastole and systole (Chung et al., 2016).

1.31 The force frequency relationship (FFR) and its variables

The relationship between the force of a muscle contraction and the activation frequency of the stimulus provided in a muscle is known as the force frequency relationship (FFR). The myocardial FFR (which is commonly known as the staircase phenomenon) also details the relationship between contractile force of the myocardium and frequency in the absence of all

external stimuli (Abu-Khousa et al., 2020). When heart rate increases, ventricular filling time is reduced and therefore so too would the end-diastolic volume achieved. Therefore, to maintain the required high stroke volume at higher heart rates, the systolic contraction force and velocity needs to become larger and faster respectively. Most mammals have a positive ventricular myocardium FFR, meaning, increased contractile force at higher stimulation frequency driven by increased amplitudes of calcium transients. Myocardial FFR varies across mammalian species, with larger mammals showing larger gains in contractile strength in response to increased heart rate (Figure 1.7A). Rodents have a negative FFR at slower stimulation frequencies, meaning the contractile force is greater due to a longer time between stimuli (Endoh, 2004). Yet, as stimulation frequency increases to physiological range, the FFR becomes positive and correlated with calcium transient amplitude. In heart failure, the FFR can become negative or inverted, leading to inability of the heart to respond to increase energetic demands.

In mice which is a common model for heart failure in research, there is a positive FFR however, calcium transient amplitudes within ventricular myocardial cells were not correlated to the change in contractile force leading researchers to conclude that the myocardium itself was sensitive to frequencies (Gao et al., 1998). In comparison, rat studies on ventricular myocardial FFR have shown a strong correlation with calcium transients and contractile force (Backx et al., 1995), meaning that even with positive FFRs, the reason for changes in contractile force is not always the amplitude of calcium transients and when studying any force changes it is important to understand where calcium fits in to the FFR of the species being used. In Figure 1.7B, rat trabeculae had a positive FFR at 1mM extracellular calcium concentration however, when increasing the concentration to 8mM, the calcium transient amplitude and the FFR turns negative (Layland & Kentish, 1999). As stimulus increased, the contractile force was reduced, further confirming the strong correlation between calcium transient amplitude and contractile force shown in rat trabeculae.

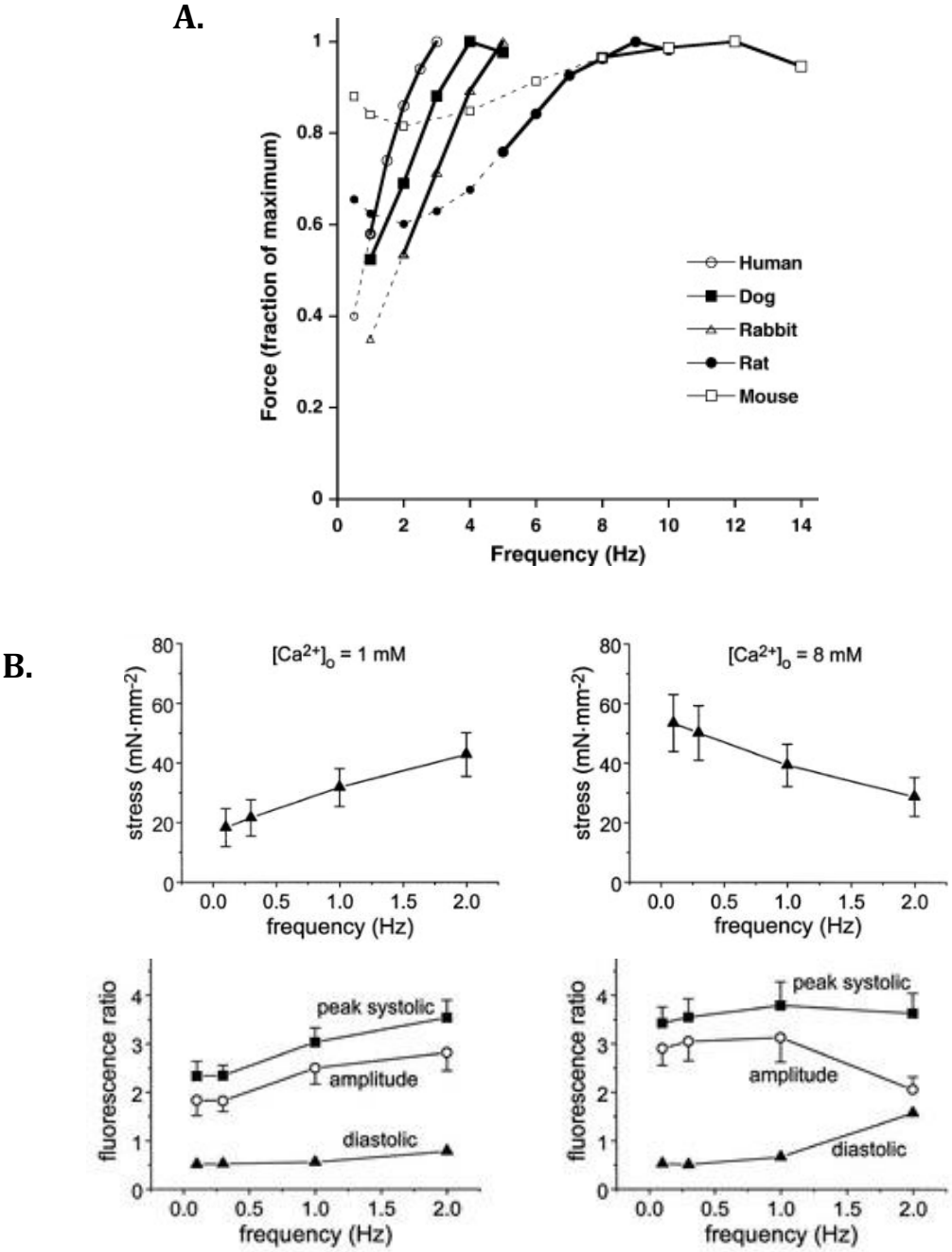

Figure 1.7: Comparisons of various species' myocardial FFRs

A. Averages obtained from contractions of ventricular trabeculae at 37 °C. Solid lines represent in vivo physiological frequency ranges. The rat FFR has a sigmoidal shape starting from around 0.1Hz to 5Hz, whilst humans' FFR curve is almost linear. **B.** Rat ventricular trabeculae stress with changing frequencies at 1mM and 8mM extracellular calcium concentration (top row) and intracellular calcium with frequencies shown as the 340nm/380nm fluorescence ratio. Shown is when extracellular calcium concentration is increased, the intracellular calcium ratio at 1Hz drops in comparison to at 1mM and there is a corresponding change in FFR. Figures adapted from: **A.** (Abu-Khousa et al., 2020) **B.** (Layland & Kentish, 1999)

1.4 Heart failure epidemiology

Heart failure is described as a clinical syndrome in which the heart is not able to supply the body with the correct volume of blood. Unfortunately, there are many reasons for heart failure to occur including coronary artery disease and chronic hypertension (Velagaleti & Vasan, 2007) amongst hundreds of other connections to health and environmental variables being made. The prevalence of this syndrome is vast with etiological research over multiple countries deeming it an epidemic. A paper from 1997 analysed patient data in the United States with heart failure having a prevalence of more than 5.8 million cases (Braunwald, 1997), with data analysis from 2012 exceeding these numbers (Kemp & Conte, 2012). These papers explain that although over time symptom management and the state of technology has improved the quality of life of patients who have diagnosed heart failure, there is still more to learn and much to clarify. A report from 2020 in the AME Medical Journal detailed the world-wide prevalence of heart failure as when searching for the syndrome on the Global Health Data Exchange registry, authors totalled 64.34 million cases (8.52 per 1000 people) which accounted for 9.91 million years lost to disability and $346.17 billion US dollars of expenditure (Benjamin et al., 2017).

There are also multiple variables within the human population which differ in heart failure prevalence and disease progression such as age and gender. One of the earliest heart failure population studies known as the Framingham heart study from 1993 determined that men had a statistically significant increase in the incidence rates of congestive heart failure when compared with women (Ho et al., 1993). Another notable study showing this trend was the Hillingdon heart failure study from 1999 in which the population of men showed higher incidence in every age group when compared to women (Figure 1.8A).

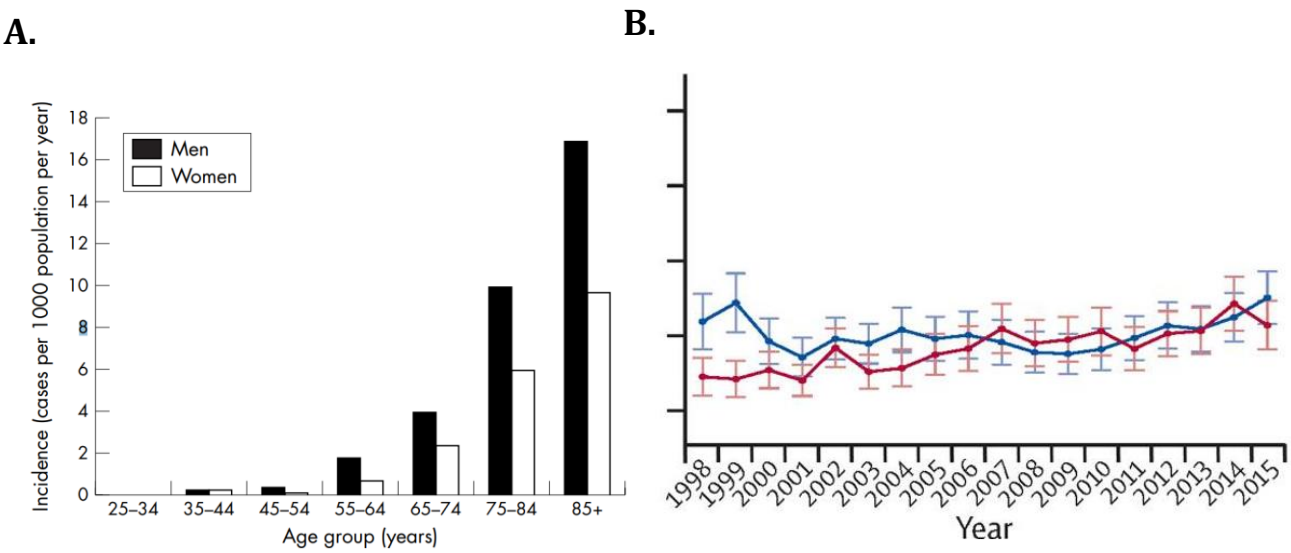

Figure 1.8: Gender-based heart failure incidences

A. This figure shows the incidence of heart failure by age group and gender in the Hillingdon heart failure study with men having increased incidences of heart failure in each group except the 35-44 age group. **B.** Shows the large incidence difference shown between the genders (red for females, blue for males) in heart failure incidence before the year 2000 (such as the reported differences in **A.**), with increasing incidences overall for women across the years, mirroring men's incidences around the 2013 year.

Figure 1.8A adapted from (Cowie et al., 1999)

Figure 1.8B adapted from (Lawson et al., 2019)

Potentially, age and the increasing lifespans of humans may be the reason for a new increase in incidence of heart failure in women compared to men, just as the trend shows in Figure 1.8B. In more recent population studies on heart failure, incidences in men are still greater than women, however it has been shown that the relationship between specific factors such as obesity is much greater in women when looking at heart failure with preserved ejection fraction (HFpEF) in comparison to men (Savji et al., 2018). Another cohort study in the UK (Figure 1.8B) looked at heart failure incidence between 1998 and 2017 which showed women having similar rates as men with all incidences rising from 2000 to 2015 (Lawson et al., 2019).

With negative effects on both the worldwide population and the economy, the field of heart failure research is vast as many are attempting to understand the changes that occur in the heart to warrant the physiological and mechanical changes being observed in patients.

1.41 Incidence, impacts on morbidity and mortality in New Zealand

The impacts of heart failure on the community specifically are large with significantly high predicted percentiles of primary patients in New Zealand alone (Fitzgerald et al., 2008). From 2006 to 2018, it was found that in the New Zealand population there was increasing hospitalisations for heart failure in the younger population (20-49 years) compared to a decrease in the elderly (60-80 years) population (D. Z. L. Chan et al., 2022). Authors from this paper deem heart failure to be an important healthcare problem in New Zealand which is the main reason for research into its mechanisms.

1.42 Māori and Pacifica populations

The mortality rate for heart disease in the Māori population has been significantly higher with reports as early as 1991 showing it to be 1.6 times higher than their European counterparts (Sabatelli et al., 2012) and this is a common occurrence within the New Zealand population throughout history. Interventions for the Māori population were significantly lower than non-Māori counterparts in a study occurring over four years (Luther et al., 2012). A retrospective analysis of Māori and non-Māori 45-year-olds in New Zealand who died due to heart failure between 1988 and 1998 determined that socioeconomic deprivation was associated with hospitalisation and death (Riddell, 2005). It is common knowledge in New Zealand that the Māori and Pacifica populations are in the lower socioeconomic group (W. C. Chan et al., 2008). However, there is research to suggest that the prevalence difference in heart disease is greater than what can be accounted for from socioeconomic differences. Being in this group exposes these communities to environmental exposures such as lifestyle, access to medical care and diet which have been linked to increases in heart failure as well. Research has also shown that in New Zealand, Māori patients admitted with heart failure were significantly younger than New Zealand-European patients having a mean age of 62 years compared to 78 years respectively ($p<0.01$) (Wall et al., 2013).

1.5 Heart failure clinical presentation

Heart failure is separated into two groups: heart failure with reduced ejection fraction (HFrEF) and heart failure with preserved ejection fraction (HFpEF). For both types of heart failure, the blood pumped out of the heart is reduced compared to a healthy heart and what differentiates them is the mechanism of failure (Atherton et al., 2018). There is no worldwide treatment plan for each of these types of heart

failure. Instead, each country has its own medical guidelines on how to diagnose and treat heart failure based on symptoms and the severity of the disease. For heart failure with preserved ejection fraction, there is still a lack of specific treatment for patients with most being prescribed calcium channel blockers for the treatment of hypertension amongst the other medications listed above (Wang et al., 2022).

1.51 Heart failure with reduced ejection fraction (HFrEF)

Heart failure with reduced ejection fraction (HFrEF) occurs when there is a left ventricular ejection fraction (LVEF) which is 40% or less and is accompanied by both progressive left ventricular dilatation and adverse cardiac remodelling (Murphy et al., 2020). HFrEF is the most common type of heart failure, occurring in 50% of cases in the United States in 2017 (Benjamin et al., 2017) and 59% of patients from New Zealand in 2018 (Lam et al., 2018). HFrEF is caused by an initial injury or a disease which directly affects the heart and further leads to a reduction in ventricular contractions (Bloom et al., 2017).

In healthy hearts, the Frank Starling principle states that when there is an increase in cardiac performance when there is an increase in end-diastolic ventricular volume (Frank, 1895). Therefore, the response in cardiac performance is attributed to venous filling pressure. With a linear increase in work and respiration rates there was a corresponding linear increase of the end-diastolic volume (Starling & Visscher, 1927).

In the instance of a reduction in left ventricular contractions, the compensation occurs in the form of increased stroke volume (Konhilas et al., 2002) because of this principle. In HFrEF, after initially decreasing in stroke volume due to injury and a reduction in left ventricular contraction strength, there is a resulting incomplete emptying of the ventricular chamber. To solve the problem, the ventricles force of contractions increases and this leads to the increase in stroke volume described by the Frank Starling principle (Berliner et al., 2020). Eventually, there becomes a decrease in the volume of blood the heart can pump compared to the volume of blood required which leads to a further impaired ventricular contractions, increases in left atrial pressure and overall congestion of the heart (Lilly, 2012).

1.52 Heart failure with preserved ejection fraction (HFpEF)

Heart failure with preserved ejection fraction (HFpEF) is described as impaired relaxation leading to a resistance in the filling of the left ventricle and a corresponding congestion in the heart

(Lekavich et al., 2015). Whilst there is no confirmed one cause of HFpEF, there are many theories of how it occurs with one research group detailing an uncoupling of left ventricular systolic elastance and arterial elastance which would result in vascular dysfunction and an arterial stiffening (Borlaug & Kass, 2011). This would then reduce the ability of the left ventricle to relax when filling and therefore pressure would increase within the ventricle. This is only one theory and currently there are many factors associated with HFpEF which extend multiple areas of pathophysiology with some being increased venous and arterial resistance, hormonal activation coupling and systemic inflammation. Notably, a recent promising biomarker of HFpEF is the collagen VI- derived pro-peptide called endotrophin (Chirinos et al., 2022) which is known to mediate inflammation, fibrosis and dysregulation in patients (Reese-Petersen et al., 2021). Due to the extracellular matrix remodelling which occurs in heart disease, there is an upregulation of extracellular matrix proteins including collagen VI which is further responsible for the increase in expression of endotrophin. This research concludes that the circulating endotrophin levels were independently associated with future poor outcomes HFpEF and with further is promising in the future for diagnosis of patients.

Initially HFpEF was not recognised as a diagnosis. The reason for this is that there is no way to diagnose the disease at bedside as the main problem with HFpEF is that left ventricular end-diastolic pressure is not easily measured in patients, and almost every possible symptom of the disease can manifest as another illness such as dyspnoea for example being generalised as a symptom of pulmonary disease rather than cardiac performance (Pfeffer et al., 2019).

HFpEF prevalence rates have increased over time (Steinberg et al., 2012) and when compared to HFrEF, increasing at a larger rate (R. T. Campbell et al., 2012). Patients hospitalised with HFrEF have statistically better outcomes overall compared to HFpEF (R. T. Campbell et al., 2012) however, mortality rates from unrelated heart events which occur in patients with HFpEF are higher when compared with HFrEF (Lee et al., 2011). Pathophysiology explaining HFpEF is incompletely understood with a large number of contributing factors including and not limited to; systemic vascular functioning, left atrial functioning and left ventricular systolic reserve (Borlaug, 2014). In HFpEF, left atrial and ventricular pressure elevation occurs as a result of both a delay and a decreased ability to relax chamber muscles (Borlaug et al., 2011). There has also been a passive stiffness of the left ventricle which is also an important variable in maintaining the pressure-volume relationship (Zile et al., 2004). Correct pressure to volume ratio is vital to correct functioning of the heart and blood flow around the body, hence without it is when adverse effects begin to occur due to deoxygenation of tissues.

1.53 Fibrosis in heart failure

Fibrosis is when there is an excessive accumulation of the extracellular matrix in and around cells. Fibrosis occurs due to injury of tissue which can be due to a myriad of reasons such as hypoxia, radiation, autoimmune reactions and physical injury. Of the accumulation of the extracellular matrix, collagen is found to be a component commonly in excess. In the heart fibrosis is mainly caused by an injury either from a heart attack or stroke, with monocytes and other immune cells infiltrating tissue after an injury to promote collagen deposition and angiogenesis long term (Kania et al., 2009). Specifically type I and type III collagens are the most well researched components in fibrosis with studies linking the increased deposition of these collagens with the development of heart failure in patients (Polyakova et al., 2011; Querejeta et al., 2004).

1.54 Calcium cycling insufficiencies in heart failure

Calcium is one of the most important ions in the excitation-contraction coupling system and so its availability, movement and abundance is vital to optimal functioning of sarcomeres and therefore muscle contractions.

There are further regulating molecules which alter the filament's calcium sensitivity such as protein kinase A (PKA) which decreases sensitivity via the phosphorylation of the sarcolemmal protein troponin complex (Tnl) (Jideama et al., 2006). Calcium being an integral part of each step of contraction means there are hundreds of interactions still unknown between calcium and other regulators both extracellularly and intracellularly. Shown in Figure 1.9 are the concentrations of calcium required for a myofilament response and then further contraction and corresponding force percentages (D. M. Bers, 2000). The competition is so large that in order to raise the concentration of calcium from a normal diastolic level of 100 nmol/L to the peak amount of 1umol/L it takes more than 100umol/L of calcium (Trafford et al., 1999).

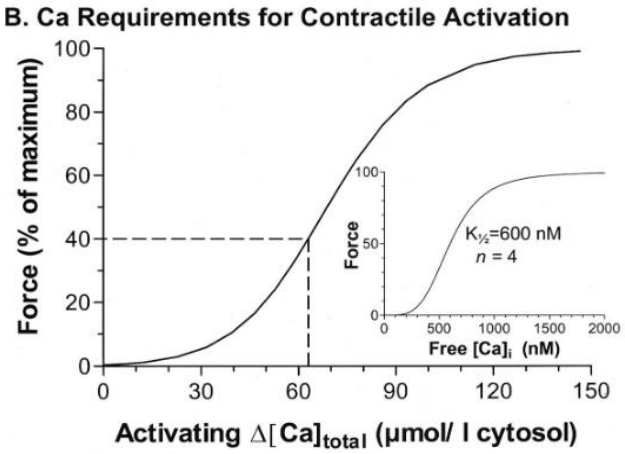

Figure 1.9: Concentrations of Calcium (Ca2+) ions for contractile activation of cardiac myofilaments

A sigmoidal curve for both activating calcium and free calcium against force shows that between 30µmol/L to 90µmol/L I cytosol there is a significant increase in forced produced by myofilaments, as with free calcium between 250nM and 1000nM.

Figure from: (D. M. Bers, 2000)

Research has consistently found in failing hearts there is a diminished capacity to restore sarcoplasmic calcium levels during diastole which may be the reason for both systolic and diastolic dysfunction observed in humans (Morgan et al., 1990). A paper from 2003 which modelled heart failure in rabbits, isolated cardiomyocytes from the left ventricle and sought to differentiate calcium transients compared to control myocytes to determine the change in calcium handling (Baartscheer et al., 2003). Observed in the heart failure cardiomyocytes there was an increase in cytosolic calcium during diastole, while both the sarcoplasmic reticulum and membrane gradients were decreased based on stimulation rate. These findings were corroborated by research indicating a down-regulation of sarco/endoplasmic reticulum Ca^{2+}-ATPase (SERCA) which is responsible for transporting calcium from the cytosol to the sarcoplasmic reticulum (Mercadier et al., 1990). This furthers the hypothesis that in at least some forms of heart failure there are calcium disturbances which underlie these impaired contractions.

1.55 T-tubule remodelling in heart failure

T-tubule remodelling has been a common finding in studies of heart failure with reduced ejection fraction. Originally, alterations in the t-tubule organisation were documented with electron microscopy in 1973, where an observation of enlarged t-tubule diameters was observed in a rat model of HF post-overload hypertrophy (Page & McCallister, 1973). Subsequently, in human cardiomyocytes from hypertrophic cardiomyopathies t-tubules were documented to have dilated or to be completely missing is some cells (Maron et al., 1975). Similar findings were then

documented in patients with ischemic cardiomyopathy (Kaprielian et al., 2000; Schaper et al., 1991). Over a decade after this, in a hypertensive rat model it was discovered that t-tubules were completely changed with re-organisation in the form of loss of transverse elements, but a gain in longitudinal elements - causing a drastically different t-tubule network in comparison to healthy controls (L.-S. Song et al., 2006). Shown in Figure 1.10 are confocal images taken from a rat MI model and the progression of the t-tubule remodelling over time with t-tubule striations being clear and parallel in the control cardiomyocyte and increasing disorganisation of the system over time after MI (Schobesberger et al., 2017).

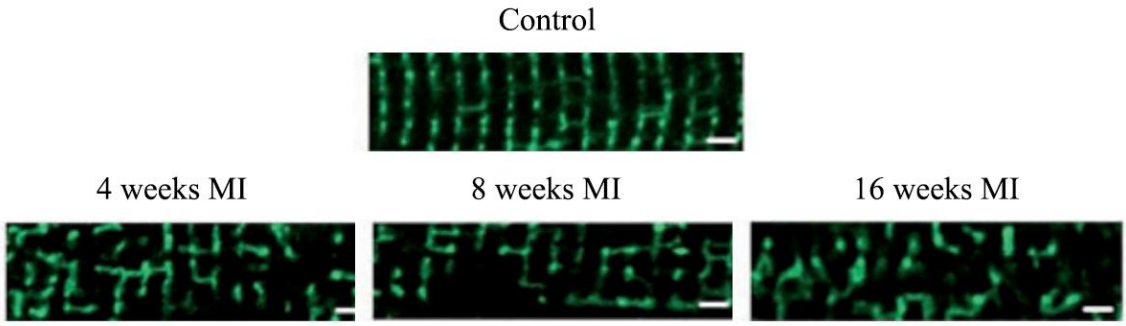

Figure 1.10: Confocal images of progressive t-tubule remodelling in cardiomyocytes post-MI.

As heart failure progresses, the remodelling of t-tubules post-MI can be observed when comparing the disorganisation to the control. Myocytes 4 weeks post-MI exhibited an impaired t-tubule system showing the beginning of loss of t-tubules via the lack of striations in the cardiomyocytes shown and as time increased so too does the disorganisation of the t-tubule system.

Images adapted from: (Schobesberger et al., 2017)

These and many other studies concluded that this re-organisation of the t-tubule network was significant problem in multiple cardiac diseases and became the target for research to understand why it occurred and which pathways were involved. From isolated myocyte models, research then linked this common t-tubule remodelling with a dyssynchronous calcium release which further led to impaired contractions of the myocytes (Ibrahim et al., 2010). A study from 2017 hypothesised that the remodelling of t-tubules was due to changes in the extracellular matrix of cardiac myocytes and investigated the disarrangement of t-tubules labelling with wheat germ agglutinin (WGA) (Crossman et al., 2017). The reasoning for this was that WGA is known to bind to extracellular glycosylated proteins, specifically some proteins from the dystrophin glycoprotein complex (DGC) (K. P. Campbell & Kahl, 1989). The DGC has commonly been a target for heart failure research as this protein complex is essential for muscle function and forms a connection between the extracellular matrix and the cytoskeleton (Lapidos et al., 2004). Further, the DGC is integral in the transmission of force during a muscle contraction and is thought to contribute to heart failure as prior research linked changes in the dystrophin labelling to end-stage

heart failure in patients (Vatta et al., 2002). WGA-positive proteins were found to be elevated in human heart failure, including a 140kDa band that was elevated 5.7-fold in diseased hearts which was identified as collagen VI by mass-spectrometry and western blotting (Figure 1.10).

A main protein hypothesised to have a role connected to the remodelling of t-tubules in heart failure is junctophilin 2 (JPH2). JPH2 is an isoform specific to cardiac tissue with another isoform JPH1 in skeletal tissue. The main function of JPH2 is to assist in maintaining the spacing of cardiac dyads across the membrane and is known to be converted into fragments via calpain during heart injury and stress (Landstrom et al., 2007). When labelled alongside RyR in the right ventricle of monocrotaline-induced heart failure rats, JPH2 labelling was reduced along the plasma membrane, leading researchers to conclude the observation suggested a larger role in the remodelling of t-tubules (Howe et al., 2021). When knocked down in adult male mice, there was a loss of contractility, heart failure and reduced colocalization of RyRs in cardiomyocytes, again linking the protein to heart failure and remodelling (Van Oort et al., 2011). Another scaffolding protein present in the plasma membrane known as myc box-dependent-interacting protein 1 (BIN-1) has also been hypothesised as having a vital role in the remodelling of t-tubules. This is because when investigated it was found that BIN-1 was used for transporting the L-type calcium channel complexes into t-tubules through the t-tubule network which was why when knocked out, all mouse embryos displayed severe cardiomyopathy and resulting death prenatally (J et al., 2003). Further, upon knocking down BIN-1 in adult mice there showed a reduction in membrane folds and an increase in the promotion of susceptibility to ventricular arrythmia (Hong et al., 2014). These aren't the only targets thought to be responsible for the remodelling of t-tubules and across many labs researchers are looking for the full reason as to why t-tubule remodelling occurs, what the main causes are and if they can be reversed in order to help patients recover from heart disease.

1.56 T-tubule remodelling and fibrosis: a link to disorder calcium signalling

A study from the Crossman lab in 2017 hypothesised that the remodelling of t-tubules was due to changes in the extracellular matrix of cardiac myocytes due to increased wheat germ agglutinin (WGA) labelling of t-tubules in the failing human heart (Crossman et al., 2017). The reasoning for this hypothesis was that WGA is known to bind to extracellular glycosylated proteins, including proteins from the dystrophin glycoprotein complex (DGC) (K. P. Campbell & Kahl, 1989). The DGC has commonly been a target for heart failure research as this complex is essential for normal muscle function as it forms a connection between the extracellular matrix and the

cytoskeleton that is required for force transmission during contraction (Rando, 2001). For example, loss of dystrophin labelling is found in end-stage human heart failure and notably reverse after therapeutic mechanical unloading (Vatta et al., 2002). Using proteomics Crossman et al (2017) identified that a major component of the increased WGA-positive proteins in heart failure was collagen VI.

Now researchers in this paper knew that there was a significant increase in collagen VI in heart failure patients and so collagen VI was investigated further. In the same paper, researchers labelled samples with collagen VI and imaged via confocal and super resolution microscopy. Significant increases in the width and distribution size of collagen VI were observed compared to healthy cardiomyocyte samples along with an accumulation of collagen VI within hypertrophied t-tubules (Crossman et al., 2017) (Figure 1.11). When this paper was written, there was already links between fibrosis in the heart in heart failure patients and since it was known the production of collagen was largely from fibroblasts, researchers labelled the number of collagen VI positive fibroblasts in samples. They found that there was a significant increase in the number of collagen VI positive fibroblasts in IDCM patient samples compared to donor samples which can be observed when comparing Figure 1.11D and 1.11G. Finally, ending the paper was the hypothesis that with an increase in collagen VI in the t-tubules there would be a corresponding remodelling and distortion of cellular structure that would disrupt calcium signalling.

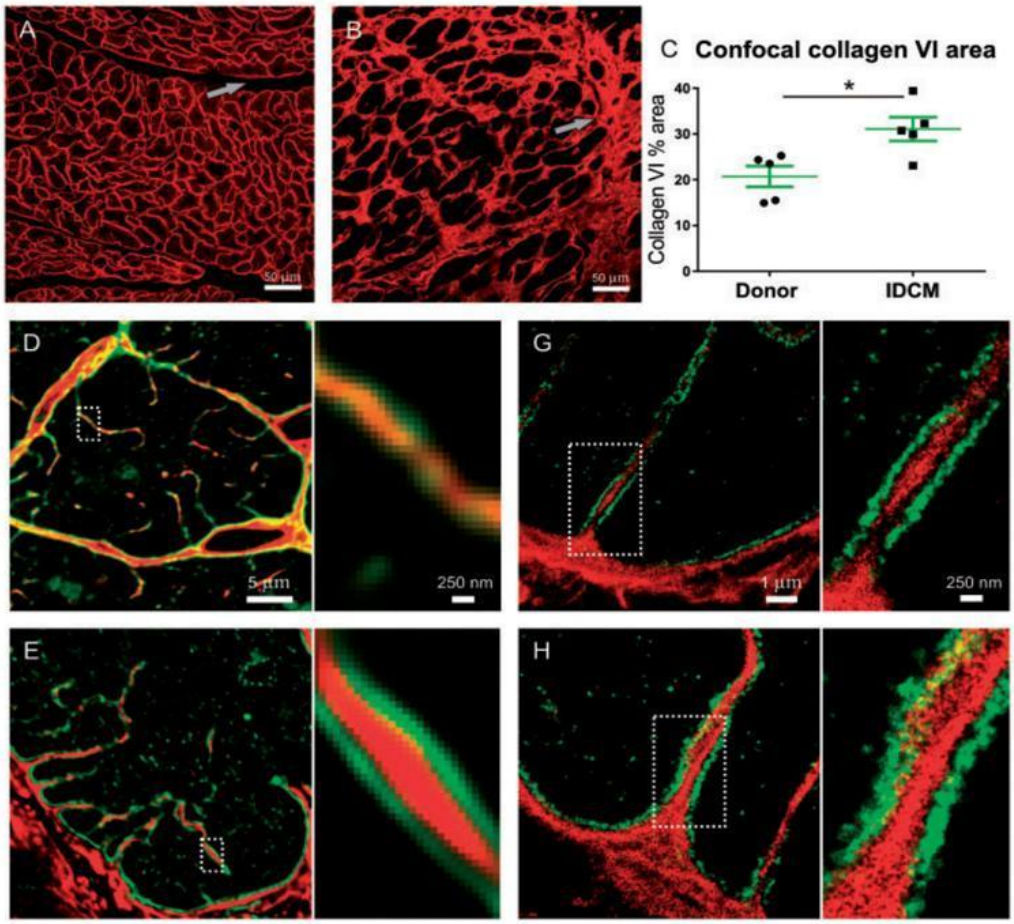

Figure 1.11: Confocal and super-resolution microscopy of collagen VI (red) and dystrophin (green) in healthy donor and IDCM samples

A. Shows collagen VI labelling in the left ventricle from a healthy sample compared to **B** from an IDCM patient. Interstitial spaces shown in **A** with a grey arrow identify regions with no collagen VI labelling in between the sarcolemma, however in comparison there are minimal to no such regions in IDCM patient samples **B** with large amounts of interstitial collagen VI labelling present. **C.** A significantly higher percentage area of collagen VI was confirmed between samples. **D** and **G** show confocal and super-resolution images respectively of t-tubules from a healthy donor sample. **E** and **H** show confocal and super-resolution images respectively of an IDCM patient sample. Between the donor and IDCM images there is a clear increase in collagen VI labelling. Figure adapted from: (Crossman et al., 2017)

With an increase in collagen VI and positive fibroblasts in remodelled t-tubules, there is now cause for a further investigation of collagen VI. Its role in the heart both intracellularly and extracellularly may be an integral step in attempting to better understand heart failure, how and why remodelling occurs and whether it can be stopped or reversed.

1.6 Collagen VI

Collagen VI is one in approximately 25 known proteins in the collagen family which are vital to the structure and integrity of cells. Different collagen VI isomers can be created using different combinations of three out of the six alpha chains (Karsdal, 2019). Collagen VI alpha chains I and II are common to all isomers with the different isomers formed from one of the following four alpha chains III, IV, V and VI. (Figure 1.12A) Collagen VI is assembled in the endoplasmic reticulum from monomers, that dimerise, the dimers then combine to form tetramers before being secreted out the plasma membrane via the Golgi apparatus (Allamand et al., 2011).

Collagen VI isomers are structurally different for their individual functions which include forming shapes of tissues, contributing to the mechanical properties of cells and forming junctions between cells for communication just to name a few (Ricard-Blum, 2011).

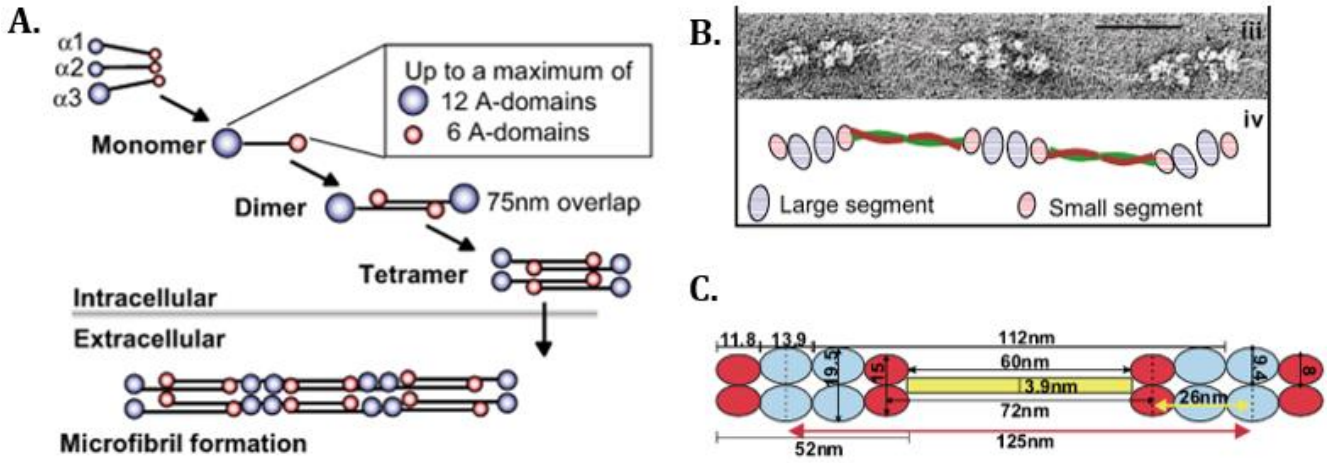

Figure 1.12: Collagen VI microfibril formation and measurements

A. The formation of the collagen VI microfibril out of an alpha 1,2 and 3 monomer. **B.** A virtual XY slice of collagen VI microfibrils from a tomographic reconstruction of a fetal bovine aorta sample with corresponding **C.** A diagram detailing estimates of component size within the microfibril formation.

Figure adapted from: (Baldock et al., 2003)

In humans, mRNA expression of the interchangeable alpha chains COL6A3 and COL6A6 gene are the most abundant found over a large range of fetal and adult tissues including the kidney, thymus, skeletal, lung, cardiac and articular cartilage whereas COL6A5 gene is expressed only in the lung, testis, and colon (note COL6A4 gene is non-functional in humans) (Fitzgerald et al., 2008).

1.61 Collagen VI in skeletal muscle pathology

Research efforts for collagen VI consist mainly in skeletal muscle as muscle dystrophies. They are associated with mutations in three of its genes; COL6A1, COL6A2 and COL6A3. Mutations in these genes cause Bethlem muscular dystrophy and Ullrich congenital muscular dystrophy (UCMD), inherited dominantly and recessively respectively (Baker et al., 2005), with UCMD being the more severe phenotype of the two dystrophies. The clinical presentation of Bethlem muscle dystrophy starts with hypotonia and delayed milestones in motor functioning during childhood. Once adults, patients commonly display evidence of muscle weakness with muscles of the face, elbows, ankles and wrists being commonly affected (Panadés-de Oliveira et al., 2019). Comparatively, UCMD patients experience more severe symptoms including hypotony and weakness resulting commonly in the loss of ability to walk and inability to breathe overnight without non-invasive assistance (Natera-de Benito et al., 2017). For both dystrophies the clinical presentations for the patients are associated with the extent of the collagen VI deficiency.

Cultured fibroblasts isolated from human skeletal muscle samples from patients with different mutations in collagen VI causing UCMD were shown to produce less collagen VI deposition in the extracellular matrix from fibroblasts overall when grown (Figure 1.19). The lack of collagen VI was found to cause the severe matrix deficiencies which resulted in patients experiencing proximal joint contractures, scoliosis, congenital hip dislocations, marked distal joint hyperextensibility and overall congenital muscle weakness (Baker et al., 2005). The mutations leading to Bethlem myopathy have been found to cause a disruption in the anchoring of the myocyte basement membrane to the matrix – further leading to the observed degeneration of muscle fibres (Kuo et al., 1997) in patients.

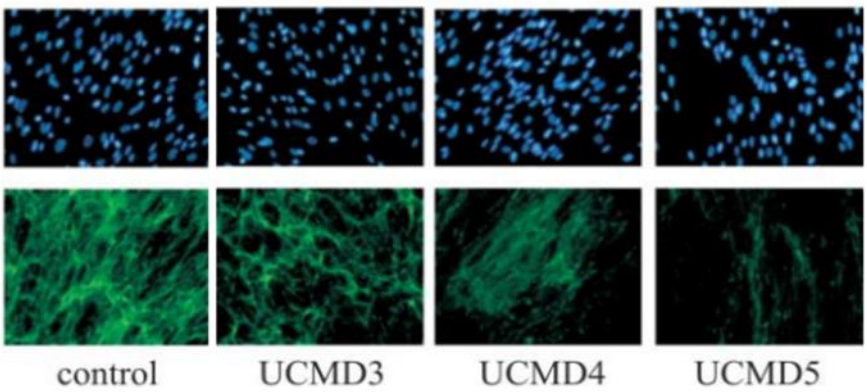

Figure 1.19: Cells grown for 2 days in the presence of sodium ascorbate to promote deposition of collagenous extracellular matrix.

Blue labelling (top row) shows the nuclei of fibroblasts in the sample and the green labelling (bottom row) shows collagen VI. UCMD4 and UCMD5 were collagen VI deficient samples due to UCMD mutations. When compared to UCMD3 and the control samples, UCMD4 and UCMD5 showed significantly less collagen VI.
Figure adapted from: (Baker et al., 2005)

In mutated collagen VI muscle dystrophies in mice models, myocytes have been shown to have dysfunctions in their mitochondrial and sarcoplasmic reticulum functioning – both of which result in disruptions and alterations in autophagy mechanisms of cells leading to spontaneous apoptosis and the associated degeneration of muscle tissue over time (Bernardi & Bonaldo, 2008). This link between collagen VI, mitochondrial and autophagy defects in skeletal muscle has been further demonstrated using collagen VI knockout mice which showed the same changed pathogenesis of mitochondria and autophagy (Irwin et al., 2003). Authors from this paper further hypothesised that the reason for the alterations of processes and organelles in the knockout mice may have been due to an increase in sarcolemmal influxes of calcium which would lead to an intracellular overload, particularly of the mitochondria triggering calcium mediated apoptosis. Although authors in that paper did not observe this, recent unpublished data from the Crossman lab support this hypothesis with large increases in calcium transient observed in isolated cardiac myocytes from collagen VI knockout rats.

There are other links to muscle dystrophies and collagen VI with a paper linking an upregulation of the alpha 6 chain of collagen VI to muscle tissue in patients with Duchenne muscular dystrophy (DMD) (Sabatelli et al., 2012).

1.62 Collagen VI in cardiac pathology

Collagen VI is not the most abundant collagen in cardiac tissue; however, studies have shown that in cardiac tissue in patients with diabetes and patients with hypertension the amount of collagen VI is significantly increased. The same increase in abundance in collagen VI has been echoed in human cardiac tissue in heart failure (Crossman et al., 2017). Collagen VI is also abundant in many other tissues.

Notably collagens I, III and V are well known for being important components of the myocardium supporting myocytes and maintaining the structure required for the cardiac cycle. Of these collagens, their distribution in the heart was found to be 85%, 11% and 3% respectively (Weber

et al., 1988) with other types of collagen at the time found to be a combination of type I and III (Contard et al., 1991). There has been minimal research conducted on collagen VI in the heart to date. A recent study on heart t-tubules found that there was a significant increase in collagen VI upon transverse tubule (t-tubule) remodelling post heart failure in humans (Crossman et al., 2017) and this is the original motivation for the further investigation of collagen VI's role and links inside heart tissue conducted in this thesis.

From early research, it has been shown that the expression of collagen VI is up regulated during wound healing, suggesting a role for this collagen in tissue integrity and remodelling (Oono et al., 1993). More specifically, collagen VI has been shown to play a role in mediating the three-dimensional organisation of fibronectin in the extracellular matrix of cultured fibroblasts (Sabatelli et al., 2001), which is essential for the endogenous cardiac progenitor cell expansion and repair required for the stabilisation of cardiac function after a myocardial infarction (MI) (Konstandin et al., 2013). Fibronectin polymerisation is necessary for collagen matrix deposition (notably type III and IV) and this deposition of collagen has been shown to directly contribute to an increased amount of cardiac myofibroblasts after myocardial injury (Torr et al., 2015). Further, upon inhibiting fibronectin there was an observed attenuation of fibrosis in myocytes after cardiac injury which researchers believe was the reason for the observed improvement in cardiac functioning of mice (Valiente-Alandi et al., 2018). Myocardial fibrosis is linked to many forms of heart disease and occurs due to a transformation in cardiac fibroblasts to a myofibroblast phenotype (Travers et al., 2016). This phenotype is the likely cause of the remodelling of transverse tubules in cardiomyocytes, altering cell signalling functions and causing permanent changes in the functioning of the heart leading to heart failure. We also now know that the heart of an older individual is characterised by fibrous modelling and collagen crosslinking (Horn & Trafford, 2016).

Fibronectin is essential for endogenous cardiac progenitor cell expansion and repair, both of which are required for the stabilisation of cardiac function after MI (Konstandin et al., 2013). Fibronectin polymerisation is also known to be necessary for collagen matrix deposition and this directly contributes to an increased amount of cardiac myofibroblasts after injury (Torr et al., 2015). In a study on human fibroblasts, a far western assay showed that collagen VI and fibronectin were found to directly interact (Sabatelli et al., 2001). Expanding on this further, in the same study researchers cultured fibroblasts from knockout collagen VI mice and found that the fibronectin fibrils were observed to have a different pattern as shown in Figure 1.20.

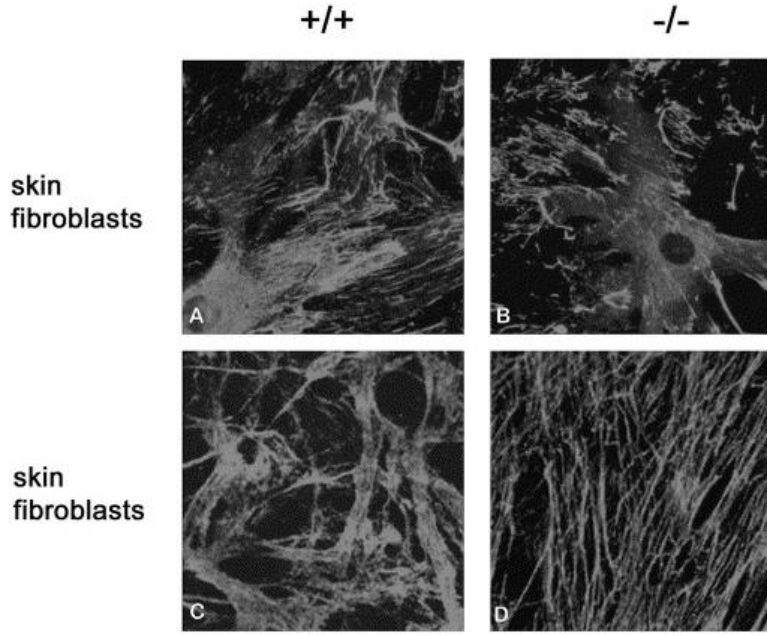

Figure 1.20: Immunofluorescence analysis via confocal microscopy of fibronectin in control mice skin fibroblasts compared to collagen VI knockout skin fibroblasts.

A. and **B.** show a significant difference in the organisation of fibronectin fibrils with fibrils from the collagen knockout VI mice looking parallel and thinner in nature. This finding is also shown in **C.** and **D.** which are confluent skin fibroblasts.

Figure from: (74)

Upon inhibiting fibronectin post-cardiac injury in a study, fibrosis was attenuated in myocytes and the overall cardiac function was seen to improve in mice (Valiente-Alandi et al., 2018). This furthers the importance for collagen VI overall in myocyte remodelling and functioning. Hearts of older individuals are also commonly characterised by fibrous modelling and collagen crosslinking (Horn & Trafford, 2016). In Figure 1.21A, cardiac fibroblasts from rat tissue were plated along with three types of collagen (I, III and VI) found in the heart (Naugle et al., 2006). There is clear evidence of collagen VI inducing myofibroblast differentiation, linking the idea of collagen VI, fibrosis and the remodelling observed after cardiac injury or heart failure. Researchers in the field have already hypothesised collagen VI's role in myocardial fibroblast differentiation to be an induction of the differentiation process. This theory was tested and confirmed from the paper from 2006 which showed in Figure 1.21B that when rat cardiac fibroblasts were induced with ANG II, collagen VI abundance significantly increased and so too did the differentiation of cells (Naugle et al., 2006).

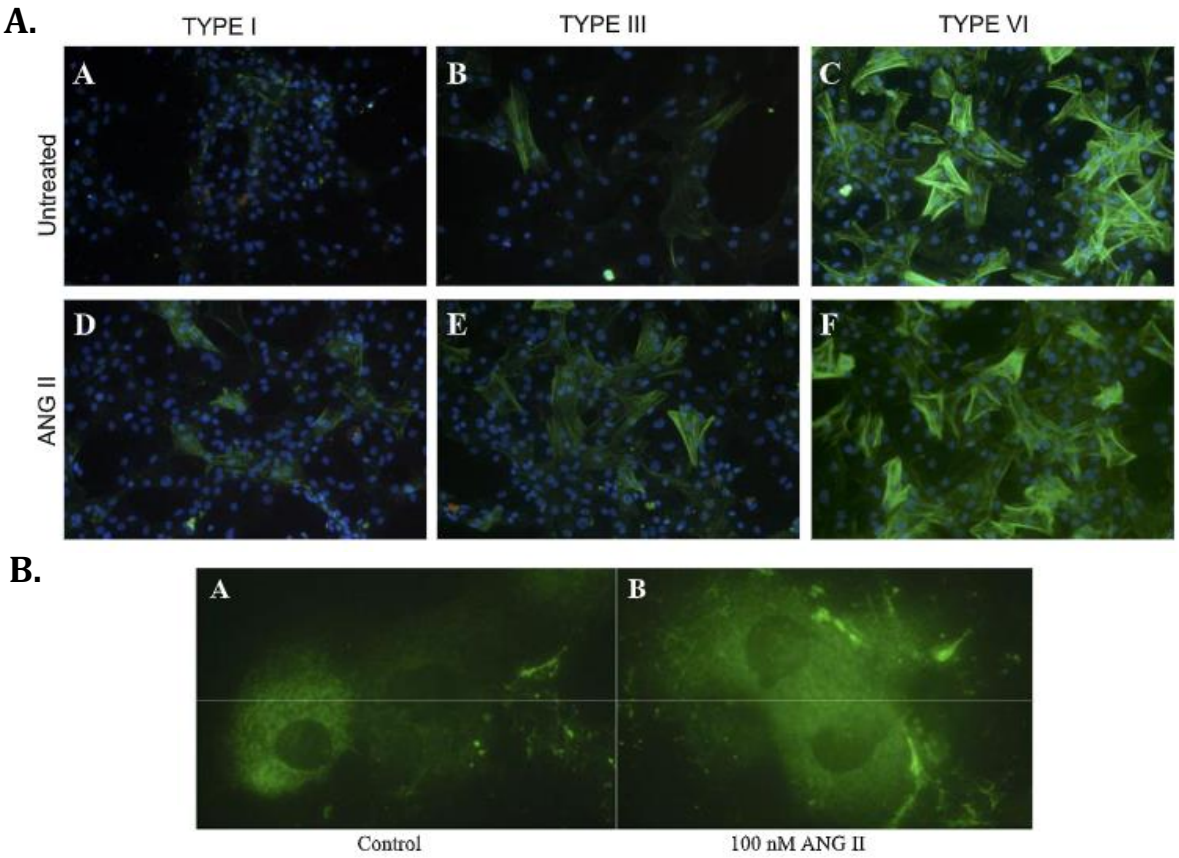

Figure 1.21: Myofibroblast differentiation amongst collagen types I, II and VI and fibroblast differentiation with collagen VI alone

The top figure **A**. shows cultured myofibroblasts with added collagens to each plate both treated with ANG II and left for 24hr and untreated. Blue staining (DAPI) shows the nuclei of cells, and the green stain (Alexa Fluor 488). shows alpha smooth muscle actin (a-SMA) expression which is a marker for differentiation. **B.** Shows two plated cardiac fibroblasts which were both plated for 24hr and then stained for collagen VI. The ANG II treated fibroblast **B** shows an increase in collagen VI.

Figure adapted from: (Naugle et al., 2006)

So now there is knowledge that collagen VI plays an important role in the induction of cell differentiation in myocardial fibroblasts, plus upon heart failure or injury there is an increase in both fibrosis and collagen VI. There are large amounts of research in cardiac failure and fibrosis however, there is limited research into collagen VI, its role in remodelling of cardiac tissue upon injury and how it functions within cardiac tissue.

The finding of myocardial fibrosis in heart disease is the opposite phenotype found in UCMD patients with reduced collagen VI deposition in the extracellular matrix as discussed prior (Baker et al., 2005), however fibrosis overall was still increased. This leads researchers to the assumption that both too much and not enough collagen VI in the extracellular matrix leads to negative effects on myocytes. This balance seems to be negatively affected during myocardial injury, increasing the level of collagen VI, causing damaging effects. A study conducted in a knockout mouse model

observed that mice with the deletion of collagen VI experienced beneficial effects on post myocardial infarction (MI) cardiac functioning and remodelling of heart tissue compared to those with collagen VI still present (Luther et al., 2012). These beneficial results of no collagen VI included significantly reduced infarction size, a significant preservation of ejection fraction post-MI and an overall reduction in myocyte apoptosis and fibrosis.

A study from 2012 mentioned previously which used collagen VI knockout mice found that 3 days post-MI, knockout mice were observed to have increased and accelerated remodelling and apoptosis compared to WT mice (Luther et al., 2012). 2 weeks post-MI there was a reduction in the apoptosis observed in the knockout mice compared to the WT mice who experienced a more chronic apoptosis over time. Although these results indicate a protective effect of collagen VI deletion, for this paper it is hypothesised that the use of mice instead of rats may have caused differing results due to multiple, well documented differences between the two species (Milani-Nejad & Janssen, 2014). These results show a further need for more research to be done on discovering the function of collagen VI and its clear link between heart disease and remodelling which this paper aimed to achieve.

1.63 Biglycan and collagen VI

Biglycan is a proteoglycan from the small leucine rich proteoglycan (SLRP) family of proteins. It consists of two chondroitin sulfate and/or dermatan chain(s) which are bound covalently to a repeated leucine-rich amino acid chain shown in Figure 1.22 (Fisher et al., 1989). Proteoglycans are known to make up the part of the extracellular matrix where events such as cell adhesion, migration and proliferation are regulated (Wight et al., 1992). Biglycan is also linked to structural integrity of the aortic wall, blood coagulation and lipoprotein oxidation functions in arterial walls (Camejo et al., 1998). Specifically, research has linked biglycan to potentially having a vital role in atherosclerosis, with expression of biglycan increasing significantly in blood vessels when the formation of plaques occurred (Riessen et al., 1994).

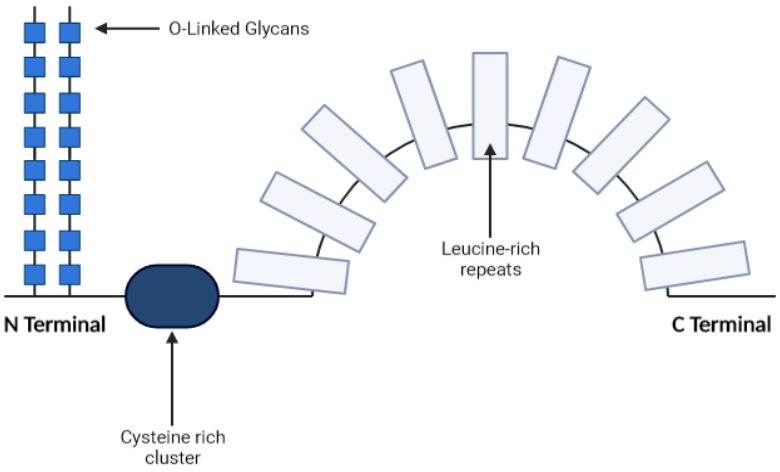

Figure 1.22: The structure of Biglycan

A diagram representing the structure of biglycan. Two glycan chains at the N-terminal of the molecule are attached to leucine-rich repeats and the C-terminal via a cysteine rich cluster, all of which can bind other molecules.

Figure created by B. A

In skeletal muscle, biglycan binds to both α- and γ-sarcoglycans within the costamere (Figure 1.3, red structure) and is known for linking the cytoskeleton and the extracellular matrix together along with regulating their expression in development whilst maintaining the integrity of the plasma membrane (Rafii et al., 2006). It's also very common that in skeletal muscle dystrophies biglycan is defective with many citing the known linkage between collagen VI and biglycan is damaged in muscle and neuromuscular dystrophies (Peat et al., 2008). Biglycan has been found to organise collagen VI into hexagonal-like networks resembling tissue structures (Wiberg et al., 2002) suggesting these structures may become disorganised in knockout rats. In human placental tissue, biglycan and decorin also have been found to bind close to the N-terminal region of the collagen VI triple helix and in coprecipitation experiments, biglycan and decorin bound to collagen VI and equally competed with the other with further confirmation that they both bound to the same site on collagen VI (Wiberg et al., 2001). A cancer study looking into collagen VI's interactions from rat chondrosarcoma tissue showed that both biglycan and decorin were bound to the N-terminus of collagen VI as shown in Figure 1.23 (Wiberg et al., 2003). Collagen VI's N-terminus serves as a binding site for small leucine rich repeat (LRR) proteoglycans, biglycan and decorin. Together these proteoglycans and collagen VI microfibrils form areas of assembly for fibrillogenesis and as scaffolds for the extracellular matrix.

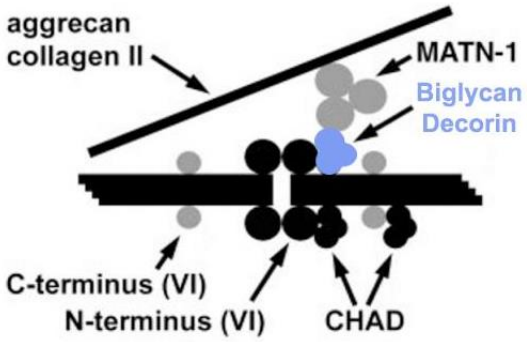

Figure 1.23: The confirmed model for supramolecular assembly in the extracellular matrix of connective tissue involving collagen VI.

This is the confirmed assembly unit which collagen VI is connected to. The collagen VI beaded filaments at both the N-terminus and C-terminus form a complex with small proteoglycans biglycan and decorin as well and other collagen II aggrecan networks and matrilin-1 (MATN-1) which are all thought to interact to influence and form extracellular matrix components.

Figure adapted from: (Wiberg et al., 2003)

It has also been shown that biglycan binds to the α-dystroglycan molecule in the costamere complex via these LRRs (Bowe et al., 2000) and when a mouse model with muscular dystrophy was used where dystrophin was absent, immunostaining skeletal muscle samples showed increased levels of biglycan compared to controls.

When skeletal myocytes from biglycan knockout mice were examined, there was an observed reduction in collagen synthesis and a higher rate of apoptosis compared to WT myocytes (Young et al., 2002). Collagen VI fibril structures were significantly disturbed and altered as when viewed using electron microscopy the fibrils had irregular shapes and different mean diameters being either much bigger or smaller than controls. In myocardial remodelling, proteoglycans such as biglycan can modify the bioavailability of a molecule called transforming growth factor-beta (TGF-β) via a negative feedback loop (Breuer et al., 1990). TGF-β is an important regulator of fibroblast proliferation and the synthesis of collagen and fibronectin in the extracellular matrix (Schönherr et al., 1993). This is important because a study has shown that if there is an elevated level of biglycan in the myocardium, it can change the equilibrium between biglycan and TGF-β, allowing for enhanced TGF-β in the tissue (Ahmed et al., 2003). Biglycan is also known to bind to a variety of extracellular signalling molecules such as TNF-α in macrophages to elicit a proinflammatory signal.

1.7 The collagen VI knockout animal model

As early as 1998, studies have been inactivating collagen VI genes in mice with the most common gene targeted being the *col6α1* gene (Bonaldo et al., 1998). The collagen VI knockout model was created due to its correlation to multiple skeletal myopathies observed in humans with the earliest being Bethlehem myopathy. Since then, the model has evolved from disruption of genes to full knockouts of the collagen VI genes in multiple animals including zebrafish, rats, mice with the main animal used for skeletal myopathy being mice. The Crossman lab was the first to produce the collagen VI knockout rats (Crossman et al., 2017). Whilst there are physiological similarities when comparing humans to mice for skeletal muscle myopathies, the presentation of human pathologies are what most researchers rely on with alternative splicing and gene editing commonly used in these models (Sztretye et al., 2020).

The rat is commonly used for heart research as their hearts are anatomically similar to human hearts on a smaller scale, however whilst there are similarities in heart disease progression between humans and rats, the model will never be a direct translation of the response to diseases in humans (Doggrell & Brown, 1998). Ideally for heart failure research in humans, samples would have to be repeated using other patients to form a large enough sample size to form any conclusions from any results achieved. For human research, this number of samples is considered unethical for researchers to take from patients, thus, animals provide a better model for discovery. There are human heart failure studies using samples from patients that exist, however with these studies, the rationale behind them requires multiple studies with animal models prior to human research approval, as well as long processes for ethical approval which can take years.

Recent data from the Crossman lab, it was observed that in collagen VI knockout rats, there was a larger calcium transient in isolated cardiac myocytes (Figure 1.24A– unpublished data Anna Krstic) compared to WT rats.

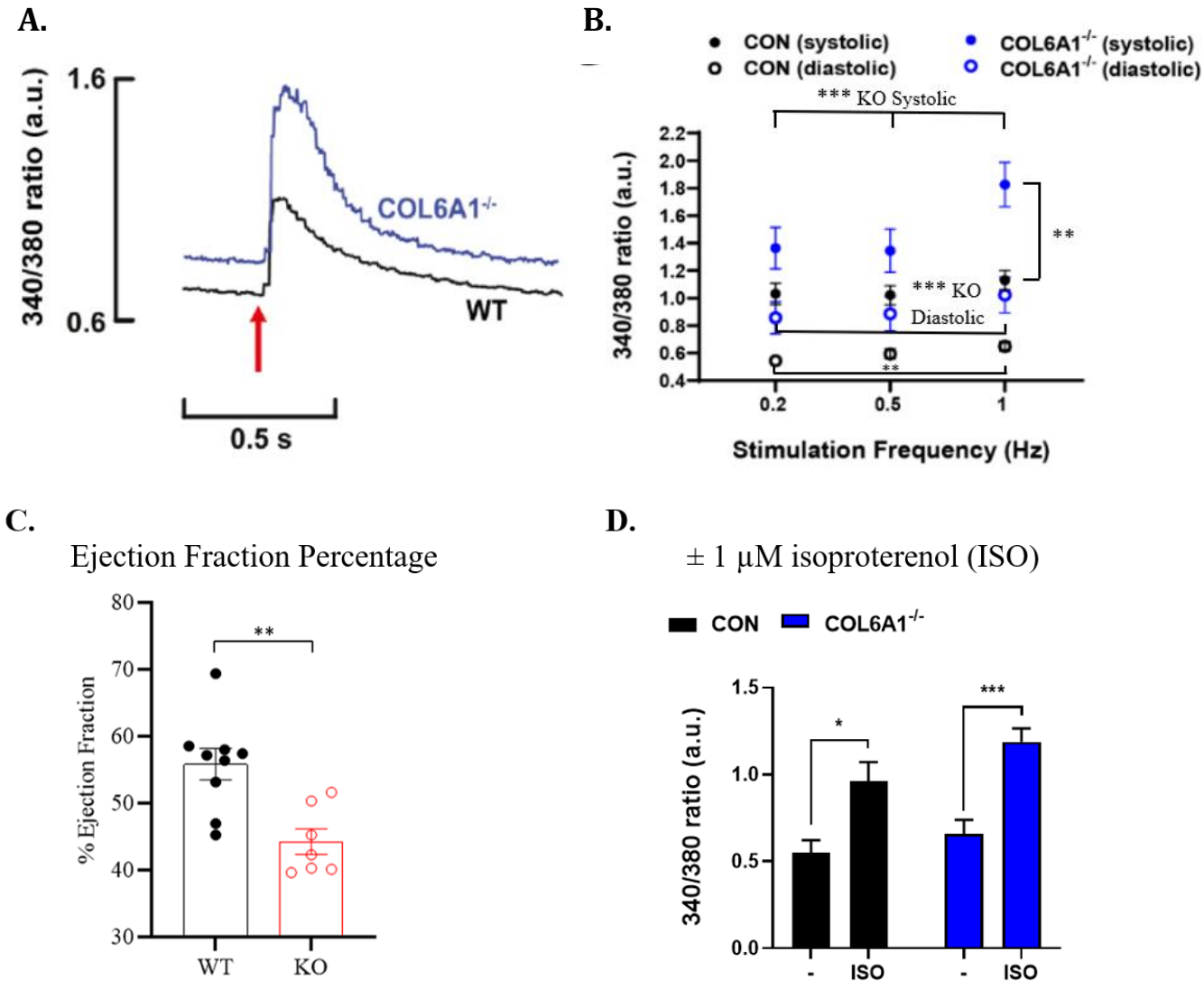

Figure 1.24: Observed calcium transients and ejection fractions from collagen VI KO rats.

Intracellular calcium is quantified into a 340nm/380nm ratio from Fura-2 AM loading cells for calcium fluorescence. In isolated cardiomyocytes, KO rats were observed to have an increased calcium transient compared to controls **A.** with the KO group also displaying higher amounts of calcium for each stimulation frequency tested with significant **(B.)**. When echoed **C.** the KO rats displayed a reduced ejection fraction when compared to the WT group. **D.** Shows the 340nm/380nm ratio before and after the addition of isoproterenol in the isolated cardiomyocytes.

Figures: (Unpublished data, Crossman lab).

Calcium changes observed in isolated cardiac myocytes with a Duchenne muscular dystrophy (DMD) mouse model (known as MDX) showed that there was increase in the influx and resting calcium concentration (Williams & Allen, 2007). This is vital as DMD is characterised by the lack of dystrophin. Such results may mimic what is expected to be found in this paper, as if collagen VI does hold dystrophin in place as hypothesised, then without it we may see similar occurrences with no dystrophin. The DMD paper noted what when in absence of dystrophin, myocytes showed an increase in stretch-activated channel expression and activity which lead to the increases in overall calcium. These increases in calcium

were therefore hypothesised in trabeculae when knocking out collagen VI in rats.

1.8 Hypothesis and thesis rationale

A reduced ejection fraction in COL6α1 knockout rats (Figure 1.24C) provides evidence to support impaired contractions. Further, mutations in COL6 are known to cause skeletal muscular dystrophies Bethlem myopathy and UCMD, both of which clinically present as muscle weakness with severity dependent on availability of COL6 (Baker et al., 2005). The hypothesis for this thesis is that myocardial force generation is diminished in the COL6α1 knockout rat due to a break in the link between the dystrophin and biglycan in the DGC. Evidence of a binding site found on collagen VI molecules in chondrosarcoma tissue for biglycan (Wiberg et al., 2003) has been found in prior research along with evidence of biglycan binding to α-dystroglycan molecules of the DGC (Bowe et al., 2000) in the costamere complex via the same leucine rich repeats that also bind COL6. MDX mice in which the dystrophin gene was knocked out also showed increased calcium in skeletal myocytes (Williams & Allen, 2007) similar to the unpublished results of COL6α1 knockout rat cardiomyocytes (Figure 1.24B) which further suggests dystrophin and collagen VI are within the same complex.

For this experiment, the hypothesis is that with increased cellular calcium transients shown in isolated myocytes from collagen VI knockout rats (unpublished research), the results from experiments using a full dissected trabeculae from knockouts would show a larger increased calcium transient than controls. Due to a hypothesised increased calcium transient, there is also a probability that extracellular calcium handling in knockouts will be compromised.

Due to the absence of collagen VI in the knockout animal model, there is a break in the link between the DGC that links to myocyte cytoskeleton that is hypothesised to result in a decreased amount of force per amount of calcium released.

1.9 Aims

1.91 – Aim 1: Trabecula experiments

The aim for the trabecula experiments conducted as a part of this thesis is to investigate the calcium handling, stress production and functioning of cardiac trabeculae from collagen VI knockout rats in comparison to wild type rats.

For stress production of the trabeculae, there are three probable outcomes for what occurs in knockout muscles with calcium mishandling:

1. Stress production overall does not change in comparison to controls and there is a resulting set of homeostatic modifications to functioning in order to account for the lack of collagen VI and the previously hypothesised increase in calcium transients.
2. A decreased amount of force due to the DGC break with potential larger calcium transients observed in single cell models.
3. There is no difference between knockout stress and calcium transient amplitudes compared to wild types.

1.92 - Aim 2: Immunohistochemical labelling

The aim for immunohistochemical labelling is to image biglycan relative to collagen VI in left ventricle cardiac tissue samples taken from collagen VI knockout rats and comparing them to wild types to attempt to identify changes occurring in the organisation of the extracellular and intracellular matrix where collagen VI is absent. Biglycan localises adjacent to collagen VI in cardiac myocytes and in knockouts it is hypothesised this is disrupted. In this instance, disorganisation of the DGC would also be assumed due to biglycan being unable to hold sarcoglycans to dystrophin in the absence of collagen VI. If this occurs, a further assumption can be made of coupled functioning changes in knockouts which might be confirmed through trabeculae experiments completed as part of this thesis or can further be investigated in future research.

CHAPTER 2 - METHODS

2.1 Tissue collection

2.11 - Trabeculae dissection

Rats were euthanised via inhalation of isoflurane with 100% O_2 as the carrier gas. Hearts from each rat are then taken out and placed into a Krebs–Henseleit buffer ([NaCl]=118.5mM, [KCl]=4.5mM, [NaH_2PO_4-H_2O]=0.33mM, [$MgCl_2$-$6H_2O$]=1mM, [$NaHCO_3$]=25mM, [$C_6H_{12}O_6$]=11mM) bath containing [Ca^{2+}]=0.25mM, [BDM]=25mM which is bubbled with carbogen throughout the experiment. The heart is cannulated through the aorta and is flushed with the KHB/BDM buffer to remove any remaining blood from vessels. The right atrium is opened so that the right ventricle opening becomes visible and is then opened by cutting laterally from the right ventricle opening to the apex of the heart whilst remaining against the septum. After opening and pinning, free-running trabeculae from the right ventricle are dissected with larger tissue pieces left on either end of the trabeculae for mounting. Setup of the dissection bench is shown in Figure 2.1 with flow direction of tubing labelled.

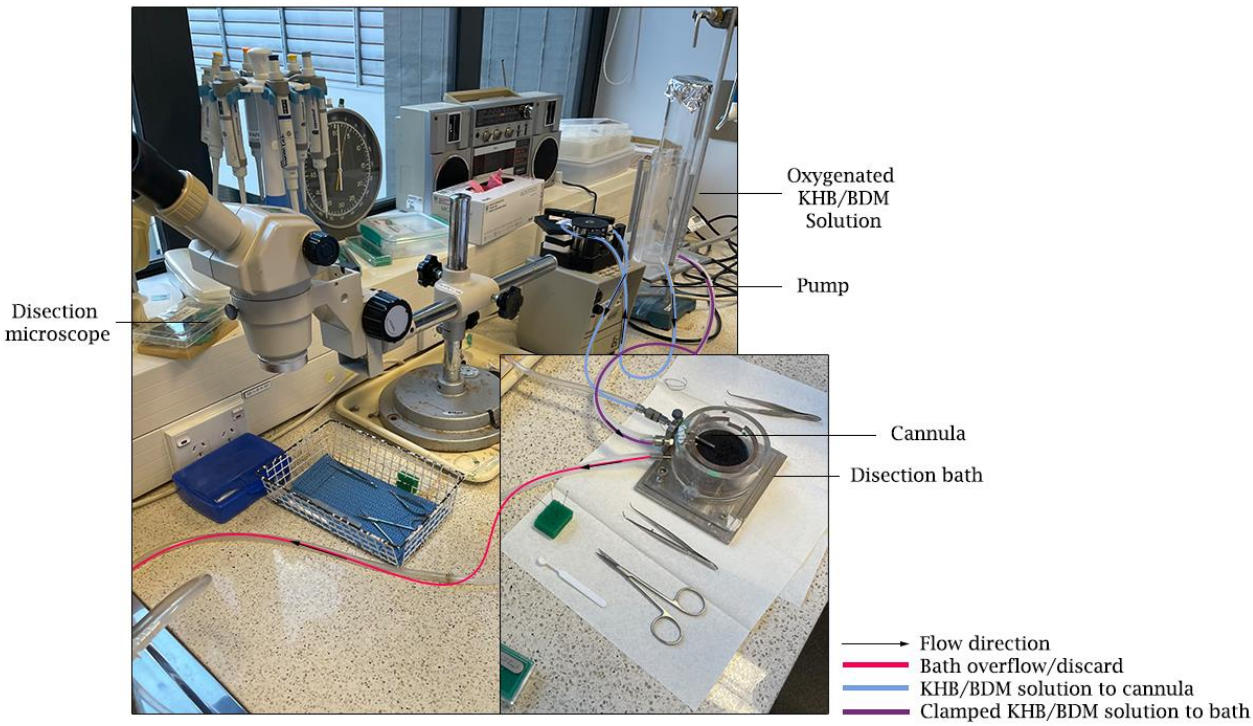

Figure 2.1: Diagram of dissection setup

Shown is the setup used for microdissection of trabeculae from rat hearts with the heart being cannulated in the dissection bath and oxygenated KHB/BDM solution (blue) flowing through a pump and into the heart. Overflow of the bath is pumped out of the dissection bath (pink) and a clamped tube connected straight to the bath (purple) is connected in case solution in the bath needed to be replaced quickly.

(Figure by B.A)

2.12 - Sections for immunolabeling

After dissecting multiple trabeculae for use in further electrophysiological experiments, sections of right ventricle, left ventricle and septum were taken. Samples were taken and fixed in 2% PFA for later use in immunohistochemical labelling.

2.2 Electrophysiological experiment trabeculae methods

2.21 - Mounting trabeculae

A chosen dissected trabecula is taken with a small spoon filled with buffer from the dissection bath and moved to the flow-through chamber. Prior to mounting, the flow-through chamber on the microscope where experiments occurred is circulated with the same concentration of KHB and BDM solution with carbogen.

The trabecula was then mounted to a force transducer (KX801, Kronex Tech. USA) via a wire hook and a snare on the opposite end in a flow-through chamber on the stage of an inverted microscope (Nikon Eclipse Te2000-U, Tokyo, Japan). The trabecula was then superfused with carbogenated, BDM-free KHB containing [CaCl2] =0.50mM.

A.

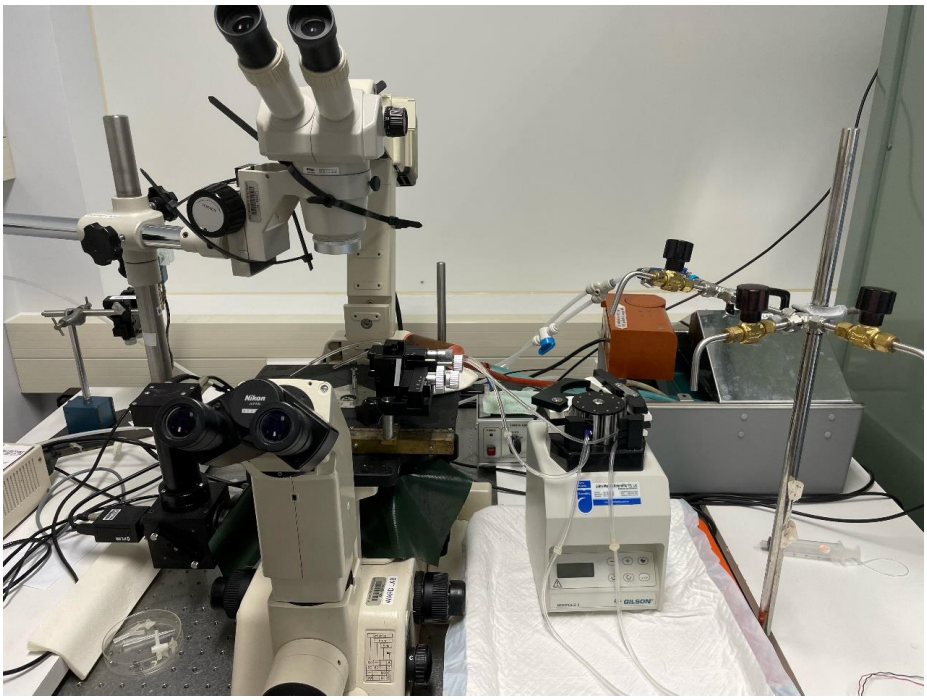

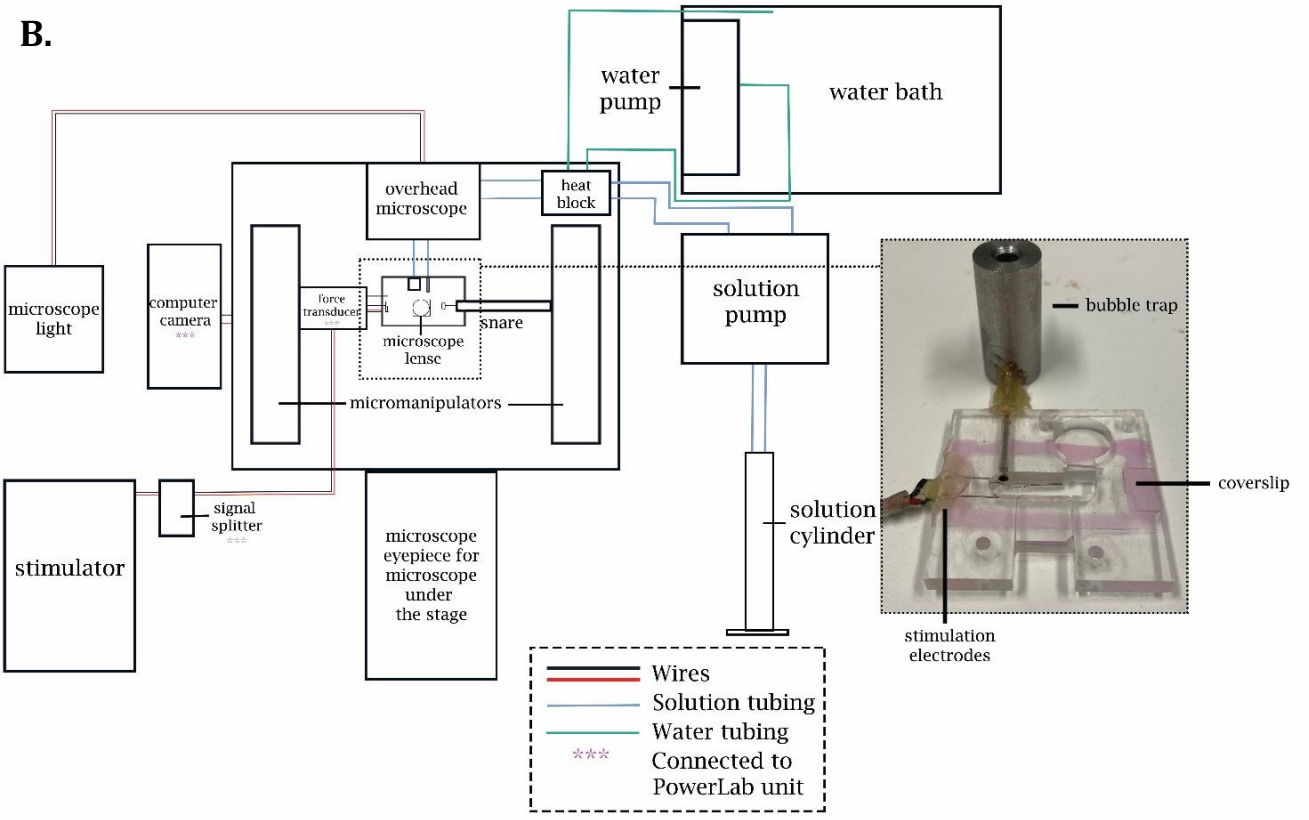

Figure 2.2: Photo and diagram of the force transducer and bath setup

A. An image of the setup for trabeculae experiments. **B.** Diagram of setup with wires (red/black lines), water tubing for heating up the heat block (green), oxygenated solution tubing (blue) and connections to PowerLab (purple asterisks) which would then connect to a computer running LabChart.
(Figure by B.A)

2.22 - Preparation prior to Fura-2 AM loading

A grass stimulator was used for stimulating the trabeculae for these experiments. The stimulator was set to repeat, 0.1HZ, 1 pulse-per-second, 5ms duration, 10V. The mounted trabecula is left for ten minutes at slackened length in the BDM solution. The BDM solution was then washed out with a control KHB solution ([NaCl] = 0.5mM, [$C_6H_{12}O_6$] =11mM) and stimulus was started at 10V with a frequency of 0.2Hz. Trabeculae length was increased until active force was maximal. After reaching maximal length (LMAX), voltage was increased until active force was maximal. This voltage was multiplied by 1.2x to ensure a supramax voltage was achieved. Calcium concentration was then increased to 1.5mM.

2.23 - Fura-2 AM loading and calcium transient visualisation

Prior to imaging and mounting, trabeculae will be loaded with Fura-2 solution. Trabeculae will

then be mounted between a wire basket extending from a force transducer. We will stimulate the field using 1Hz and 5Hz with 5-ms pulses at voltage 20% above threshold.

In order to view calcium transients for imaging we used a Fura-2 AM Cell Permanent Calcium Indicator (F1201) with the corresponding imaging calibration kit (F6774). To load the Fura-2, trabeculae was superfused at room temperature for 2 hours prior to experiments in 3.7mL of the same KHB (containing [1.5mM] = Ca^{2+}) solution trabeculae were stimulated in, with additions of 100µg Fura-2 AM, 40µL dimethyl sulfoxide (DMSO), 100µL PowerLoad™ (P10020) and 1µL anti-foam for imaging preparation. Trabeculae would then be illuminated via alternating excitation 340 and 380 nm wavelengths using an optoscan monochromator system (Cairn Research, Faversham, U.K.). The emitted fluorescence would be collected from the middle section of the trabeculae (~200 µm × 100 µm) and could then be converted to intracellular calcium concentration using a currently used equation described first by Grynkiewicz et al. (Grynkiewicz et al., 1985).

2.24 – Fura-2 AM calibration

In order to understand the fluorescence outputs in LabChart obtained from the OptoScan and Fura-2AM systems, an in vitro calibration of Fura-2 was completed. The imaging calibration kit (F6774) was used by putting 100µl of each of the calcium calibration buffers provided and 10µL of a 100µM Fura-2 (Potassium salt) stock into Eppendorf tubes, mixed well and added to one of two clear Perspex blocks with embedded wells in them and a coverslip on the bottom attached via a silicone glue. 9 wells were used which were; Fura-2 free/[Ca^{2+}] = 0µM, Fura-2 free/[Ca^{2+}] = 39µM, Fura-2/[Ca^{2+}] = 0µM, Fura-2/[Ca^{2+}] = 0.017µM, Fura-2/[Ca^{2+}] = 0.065µM, Fura-2/[Ca^{2+}] = 0.1µM, Fura-2/[Ca^{2+}] = 0.15µM, Fura-2/[Ca^{2+}] = 0.225µM, Fura-2/[Ca^{2+}] = 39µM. The microscope on the rig used for experiments was focused onto one well at a time and the OptoScan and LabChart was used to obtain fluorescence outputs for each. Shown in Figure 2.5 is the calibration curve based on fluorescence results.

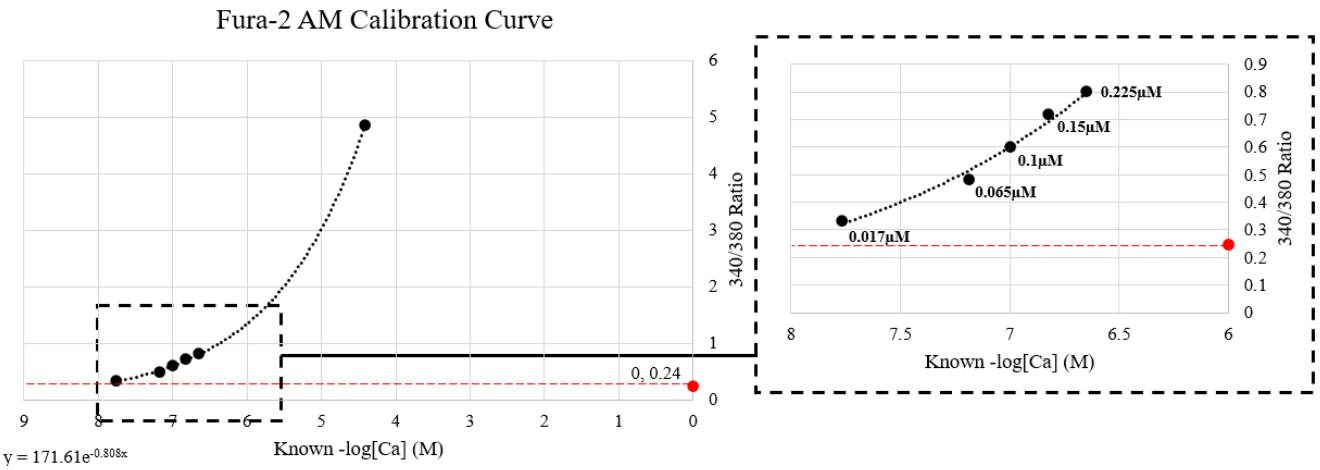

Figure 2.5: Obtained Fura-2 calcium calibration graph.

Shown is the calibration graph of Fura-2 at different calcium concentrations on the rig used for trabeculae experiments with the same sized window on the microscope as used when collecting fluorescence data during experiments. The red point indicates the output reading of the 340/380 ratio at 0mM Ca^{2+}. The magnified area of the curve is where the 340nm/380nm readings occurred for the experiments. Labels show the known calcium concentrations used for the calibration.

2.25 – Experimental protocols after Fura-2 AM loading

Experiments conducted were force/length relationship, transient measuring, extracellular calcium handling and isoproterenol response all conducted at 37°C. Force/length relationship was tested via finding L_{MAX} a second time with the length recorded, then reducing length until the force of the contractions from the trabeculae were half and a quarter of the total force from L_{MAX}. An example of finding L_{MAX} can be seen in Figure 2.3A, with the amplitude of the normalised force increasing as lengthening occurs to a plateau where L_{MAX} is reached.

Calcium and force measurements were conducted at 0.1Hz,1Hz, 2Hz and 5Hz in the control solution of KHB ([NaCl]=1.5mM, [$C_6H_{12}O_6$]=11mM, [Probenecid]=1mM). Each frequency was recorded for 2 minutes with 5Hz recorded until the force amplitude plateaued. Within each frequency recording the stimulus was also turned off for 30 seconds and turned on again, this was to test for potential differences in force and calcium transients upon re-stimulation. This can be seen in in Figure 2.3B with each break being a 30 second no-stimulus point within each frequency.

Extracellular calcium experiments were conducted at 1Hz beginning in a KHB solution ([NaCl]=1mM, [$C_6H_{12}O_6$]=11mM, [Probenecid]=1mM) with a calcium concentration of 1mM. After amplitudes plateaued, the calcium concentration in the solution was increased in 0.5mM increments up to 3mM. An example of what the output looked like is shown in Figure 2.3C. The

3mM solution was then washed out with the original KHB solution ([NaCl] = 1.5mM, [$C_6H_{12}O_6$] = 11mM, [Probenecid] = 1mM) and the trabecula was left to re-stabilise before recording for 2 minutes, then washing out into the same solution makeup with added 1mM isoproterenol. Recordings were continued until the active stress and 340nm/380nm ratio channels had plateaued as shown in Figure 2.3D.

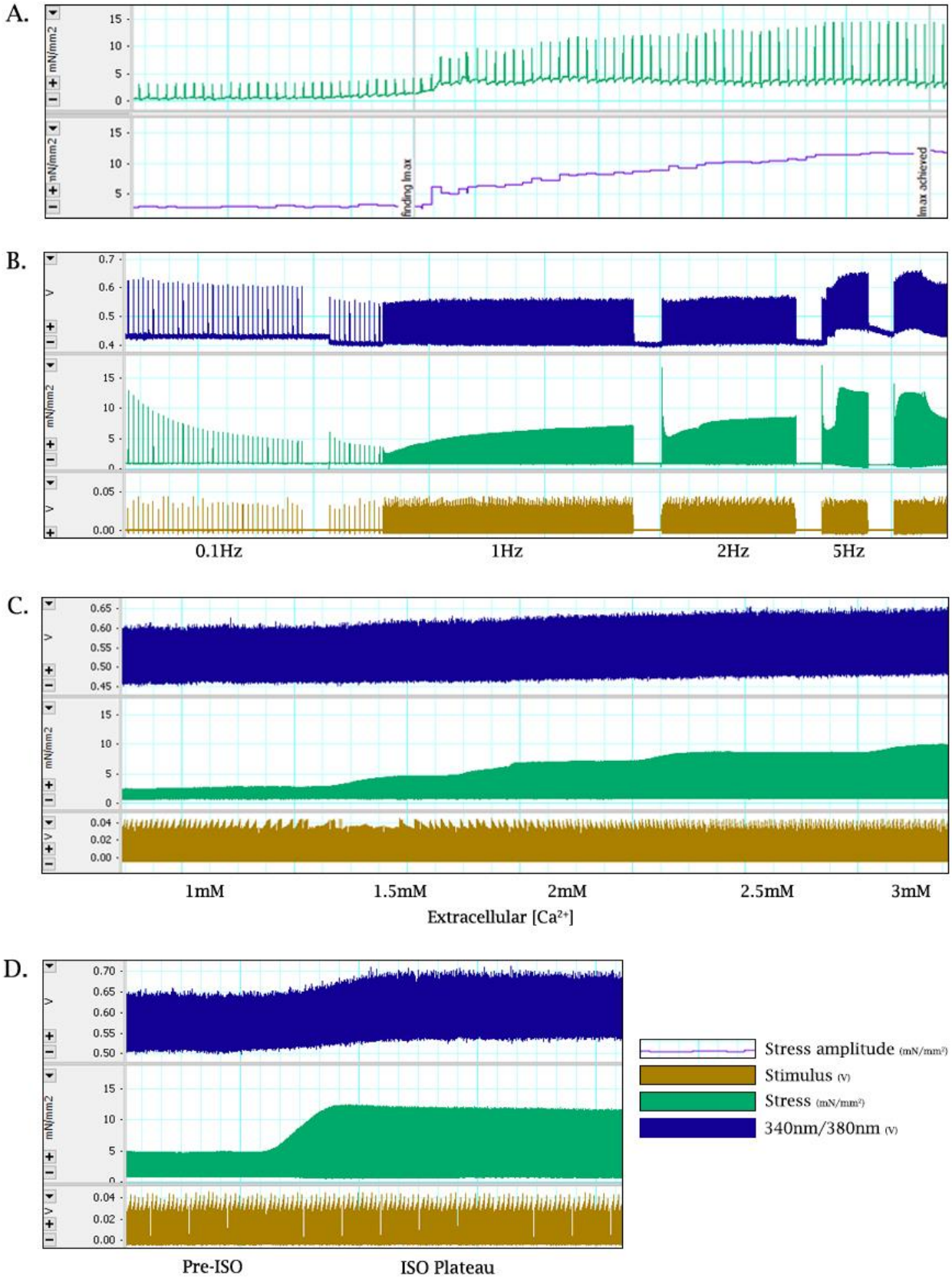

Figure 2.3: Experimental protocol examples.

A. Shows the lengthening process, with increasing the length of the trabecula there is an increasing amplitude of force shown, until a plateau is formed where length is documented as L_{MAX}. **B.** Shows zoomed out frequency testing with 30 second intervals of no stimulus between each frequency change. **C.** Increasing extracellular calcium concentration by 0.5mM when stress (green) would plateau up to 3mM. **D.** Showing a response to the addition of isoproterenol.

2.26 – Data acquisition

In order to view force, stress and intracellular calcium from the trabeculae experiments, all data acquisition was completed via the use of Labchart Pro 8 (AD Instruments, UK) and its corresponding modular Power Lab system which compiled the data from the Grass SD9 Stimulator (Grass Instruments, Warwick, Rhode Island), the force transducer (AE801, Kronex, Oakland, CA, USA) and the Cairn OptoScan Monochromator (Cairn Research Ltd., UK) for fluorescence data of 340,360 and 380 wavelengths. Figure 2.4A shows the output from an experiment with all channels active and 2.4B shows a zoomed-in single stress peak taken with the peak analysis function on LabChart.

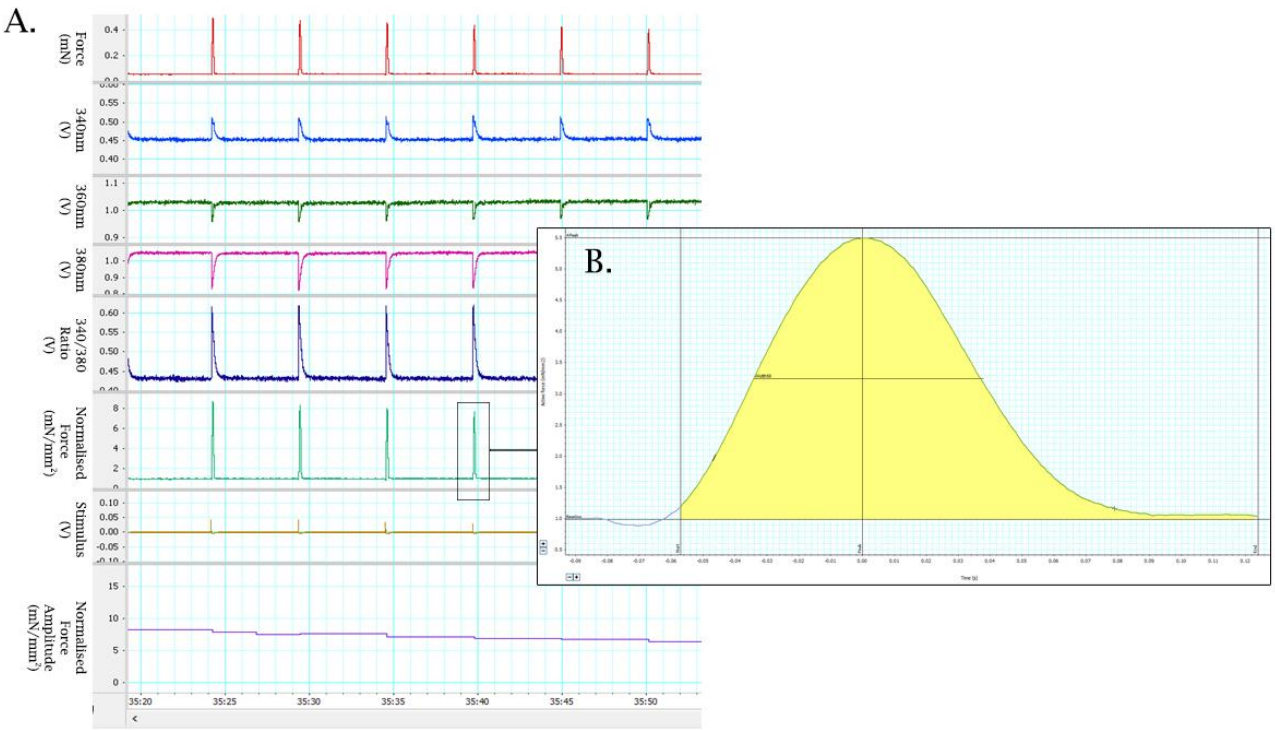

Figure 2.4: LabChart data output example.

A. This figure is an example of the LabChart inputs throughout a trabecula experiment. The normalised channel (green) uses a formula of the un-normalised force (red) divided by the cross-sectional area of the muscle. The normalised force amplitude (purple) is generally used for pre-the two experiment setup steps which are determining plateaus when lengthening to L_{max} and finding the supramaximal voltage for stimulus. **B.** An example of a zoomed normalised force peak via the peak analysis function package on LabChart. With each peak, LabChart selects the beginning of the curve, the peak of the curve and the end of the curve – which is then provided in a table format along with other analyses such as rate of rise, time to peak and overall time of peak.

Shown in Figure 2.5 are two curves from taken from an experiment as an example with each variable of the curve analysed after experiments labelled. For stress curves (Figure 2.5A), analysed was R-R intervals, diastolic and systolic stress and rate of rise. When analysing calcium transients (Figure 2.5B), the decay of the curve was recorded instead of rate of rise.

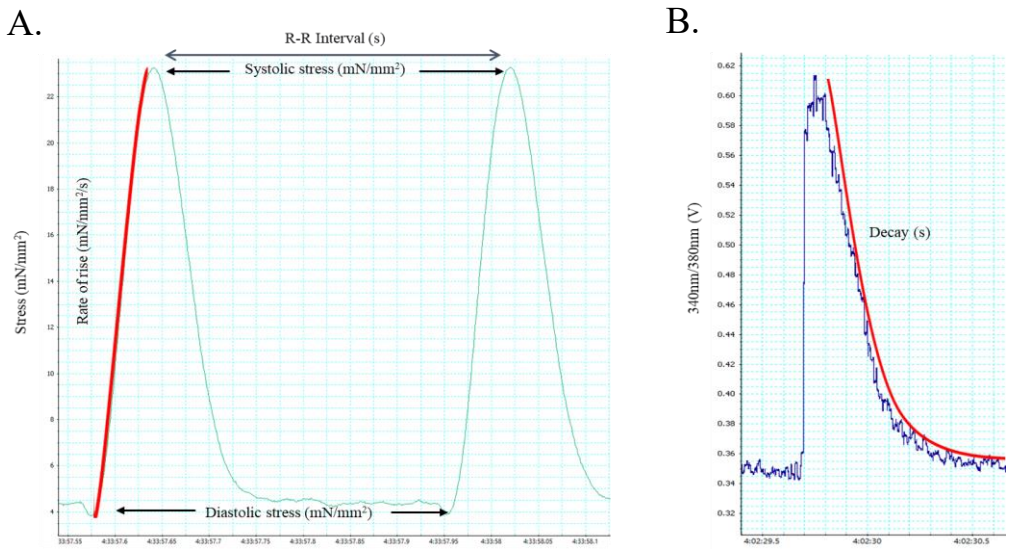

Figure 2.5: Stress and calcium transient curves for analysis.

A. For a stress curve, analysed was the R-R interval between two peaks (s), the diastolic and systolic stress in (mN/mm^2) and the rate of rise ($mN/mm^2/s$) of the curve. For each analysis, 10 peaks' data was analysed and averaged. **B.** When looking at calcium transients, the same analyses as the stress curves was done, except no rate of rise was looked at and only the decay (s) of the transient.

2.27 – Exclusion criteria for data analysis

Data from trabecula experiments was either included or excluded from analysis based on two main criteria. Firstly, was after loading the trabecula with Fura-2 AM, if the muscle was no longer responsive to stimulation it was excluded. Trabeculae which were unresponsive to stimulus would not contract and therefore the experiments would not provide any results to experimental procedures. Secondly if the normalised force produced after loading with Fura-2 AM and re-lengthening was under $5mN/mm^2$ at 0.1Hz, the animal's results were excluded. Trabeculae which were excluded this way proceeded through experimental protocol and were excluded upon analysis of traces. Ideally, exclusion criteria would only include trabeculae with active stress above $10mN/mm^2$, however with time constraints and the lack of sample numbers, using this criterion would exclude majority of the samples from analysis.

2.3 – Immunohistochemical labelling

2.31 – Sectioning

Frozen tissue samples fixed with 2% paraformaldehyde (PFA) were stored in -80°C until sectioning occurred. 10µm thick sections were taken from the RV of three rats from both the collagen VI knockout and wild type control groups on a cryostat (CM3050 S, Leica Biosystems).

2.32 – Immunohistochemistry imaging

There were seven slides in total (Figure 2.6), each with two sections on them and a blank for control. Sections were hydrated with 200µL phosphate-buffered saline (PBS) for 5 minutes.

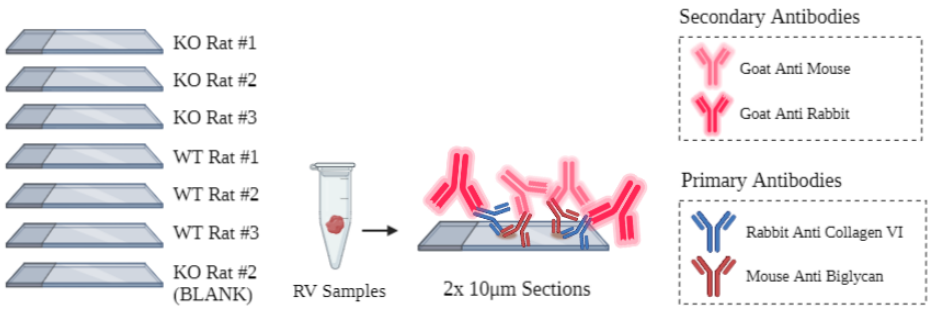

Figure 2.6: Diagram of slides created for labelling with primary and secondary antibodies.

Three rat's RV samples were sectioned onto slides for each group with one blank created for seven slides total. Primary antibodies attach to the collagen VI and biglycan on the sections and then secondary antibodies attach to the primary antibodies and fluoresce under specific wavelengths of light.

Then to permeate the membrane of the tissues, 100µL of a solution made up of 1% triton x-100 and PBS was left on sections at room temperature for 15 minutes. Sections were then washed three times with PBS and then three times again leaving the PBS on the sections for 5 minutes each time. For blocking, 50µL of Image iT FX signal enhancer was left on each section for 60 minutes at room temperature. Primary antibodies (both 1mg/ml); 10µL of rabbit anti collagen-6 (ab6588) and mouse anti biglycan (Abnova H0000633-M01) were both added to a solution of 1% BSA, 0.05% triton, 0.05% NaN3 in PBS to a concentration of 1:100. This solution was spun for one minute in a centrifuge at max speed for adequate mixing, then 100µL was added to each of the sections and left overnight at 4°C. The next day sections were washed three times with PBS and then three times again with PBS left on sections for 5 minutes at a time. 20µL of the secondary antibodies (which were originally diluted 1:1 in glycerol); goat anti rabbit (Alexa 594) and goat

anti mouse (Abberior STAR RED) were added to 1mL of PBS for a concentration of 1:100 and spun at max for one minute in the centrifuge to ensure homogeneity. 100µL of the solution was added to each section and left for 2 hours at room temperature. Sections were washed three times in PBS and again three times with 5 minutes in between and coverslips were then mounted onto slides with Abberior TDE solution D (97%) and were kept in 4°C for 24hrs prior to imaging.

2.4 – Animal handling and treatment

Prior to experiments, male rats were housed in the Vernon Jansen Unit animal resource unit at the Faculty of Medical and Health Sciences at the University of Auckland. Rats had comfortable conditions with *ad libitum* access to rodent chow and water, with the staff at the Vernon Jansen Unit monitoring them regularly.

2.41 – Ethics approval

This study was approved and monitored by the Animal Ethics Committee of the University of Auckland (AEC23882).

2.5 – Statistical analysis

For determining differences between control and knockout groups of animals, a repeated measures analysis of variance tests (ANOVA) was completed with assumptions of equal variance between repeated measures being tested with a Mauchly's test of sphericity. Where this test was violated ($p<0.05$) the Greenhouse-Geisser correction was used. The post-hoc tests used least significant difference (LSD).

CHAPTER 3 – RESULTS

3.1 – Physiological trabeculae experiments

Physiological trabeculae experiments were completed with both control rats and collagen VI knockout rats with animal weight and age along with averages presented in Table 1. The difference in age was due to timings and animals readily available and the difference in weight is likely due to knockout effects. Also included in Table 1 are whether trabeculae were included or excluded in analysis based on the exclusion criteria outlined in the methods section. Trabeculae were excluded if they were unresponsive to stimulus after loading with Fura-2 AM or if they showed a normalised active stress of under 5mN/mm^2 as this would suggest they were damaged prior to the experimental protocol.

Control Group	Age (weeks)	Weight (g)	Responsive after loading?	Stress more than 5mN after re-lengthening?	Excluded/ Included
	13.86	230	Yes	Yes	Included
	31.43	334	Yes	Yes	Included
	9.87	246	Yes	Yes	Included
	30.57	409	Yes	Yes	Included
	27.45	230	Yes	No	Excluded
	28.24	246	Yes	No	Excluded
	32.14	265	No	No	Excluded
Average (all animals n=7):	24.79	280			
Average (included animals n=4):	21.43	304.75			

Knockout Group	Age (weeks)	Weight (g)	Responsive after loading?	Stress more than 5mN after re-lengthening?	Excluded/ Included
	35.86	364	Yes	Yes	Included
	10.51	194	Yes	Yes	Included
	12.32	311	Yes	Yes	Included
	14.87	221	Yes	Yes	Included
	16.25	341	Yes	Yes	Included
	29.15	364	Yes	No	Excluded
	15.35	341	Yes	No	Excluded
	13.78	311	Yes	No	Excluded
	10.68	221	Yes	No	Excluded
	16.37	362	Yes	No	Excluded
Average (all animals):	17.51	303			
Average (included animals):	17.96	286.2			

Table 3.1: Data for each rat used for trabeculae experiments in each group.

Listed above are the ages, weights and tibia lengths of all animals used in both the control wild type group and the collagen VI knockout group. Of the animals included in analyses, the control group had a larger median age (+3.47 weeks), weight (+18.55g) and tibia length (+4.25mm).

The experimental stimulation frequencies chosen were 0.1 Hz, 1 Hz, 2 Hz, and 5 Hz. However, by

examining the R-R intervals of the recorded stimulus channel the actual stimulation frequencies were found to be: 0.2 Hz, 2 Hz, 2.6 Hz and 5.6 Hz respectively, shown in Table 3.2. R-R intervals were calculated from 10 peaks in each tested frequency in the stimulus channel for each experiment to calculate the actual mean stimulation frequency occurring across the experiments. The explanation for this difference between the setting and frequencies delivered was found to be an error in the dial used for selecting frequencies on the Grass stimulator. The actual frequencies delivered were used in the following results instead of the dial setting.

Original Frequency	Average R-R (s)	1/Average R-R	Rounded Actual Frequency
0.1	5.18±0.0009	0.19±3.4E-5	0.2
1	0.51±0.0001	1.94±3.8E-5	2
2	0.3±0.0068	2.55±2.1E-4	2.6
5	0.17±0.0023	5.64±3.8E-4	5.6

Table 3.2: Calculated stimulated frequencies from R-R intervals from stimulator.
Originally proposed stimulation frequencies were found to be different to actual stimulation frequency with 10 peaks' R-R from each stimulus in each experiment being calculated and averaged. Instead of 0.1Hz, 1Hz, 2Hz and 5Hz, rounded actual stimulation frequencies were found to be 0.2Hz, 2Hz, 2.5Hz and 5.5Hz respectively. ± Values are for standard error.

3.11 – Effect of differing stimulation frequency

Most of the KO and WT trabeculae showed a biphasic response to stimulus, as shown in Figures 3.2 and 3.3 are the active stress and 340nm/380nm ratios respectively, which were recorded with four stimulation frequencies; 0.2Hz, 2Hz, 2.6Hz and 5.6Hz in 1.5mM calcium concentration at 37°C. In Figure 3.1A, each trabecula's response to increasing frequency is shown, with most trabeculae showing a biphasic response with active stress higher at 0.2Hz and at 5.6 Hz with a dip at 2 and 2.6 Hz. The mean values are shown in Figure 3.1B. There was no statistically significant difference in active stress between the knockout and wild type groups across stimulation frequency although the variance was larger in the knockouts. Within the knockout group there were statistically significant differences in active stress between 0.2Hz and 2Hz (P=0.011), 2Hz and 2.6Hz (P=0.016) and 2.6Hz and 5.6Hz (P=0.009).

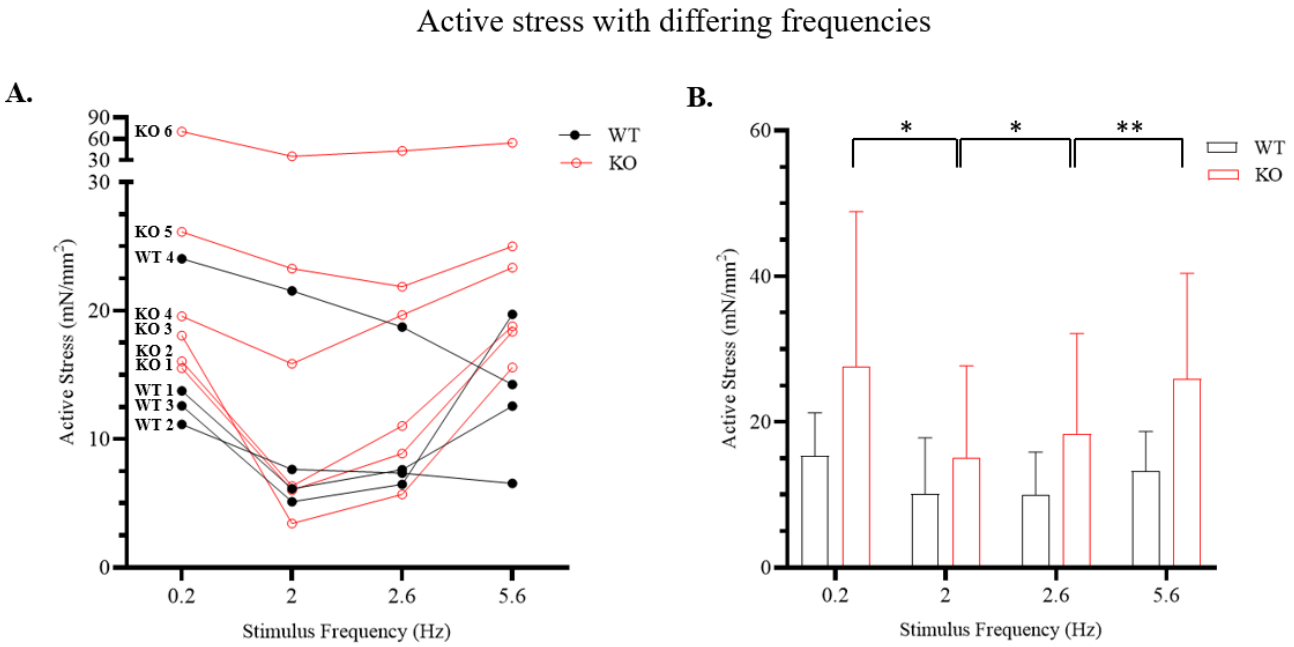

Figure 3.1: Active stress of trabeculae at increasing stimulation frequencies.

A. Active stress for each trabecula across four frequencies; 0.2Hz, 2Hz, 2.6Hz and 5.6Hz. **B.** Median active stress at each frequency for both wild type and knockout groups. There was no significant difference between KO and WT groups across the stimulation frequencies (P=0.267). Within the KO group, active stress between 0.2Hz and 2Hz were statistically significant (P=0.011), 2Hz and 2.5Hz were statistically different (P=0.016 and 2.5Hz to 5.5Hz (P=0.009). (Error bars represent mean and SEM).

There was no statistically significant difference between the rate of rise in stress in the knockout group compared to the control group (Figure 3.2). It's important to note that the small sample size and high variance values within the knockout group would result in statistical power being too low to determine any statistically significant differences in values between the two groups.

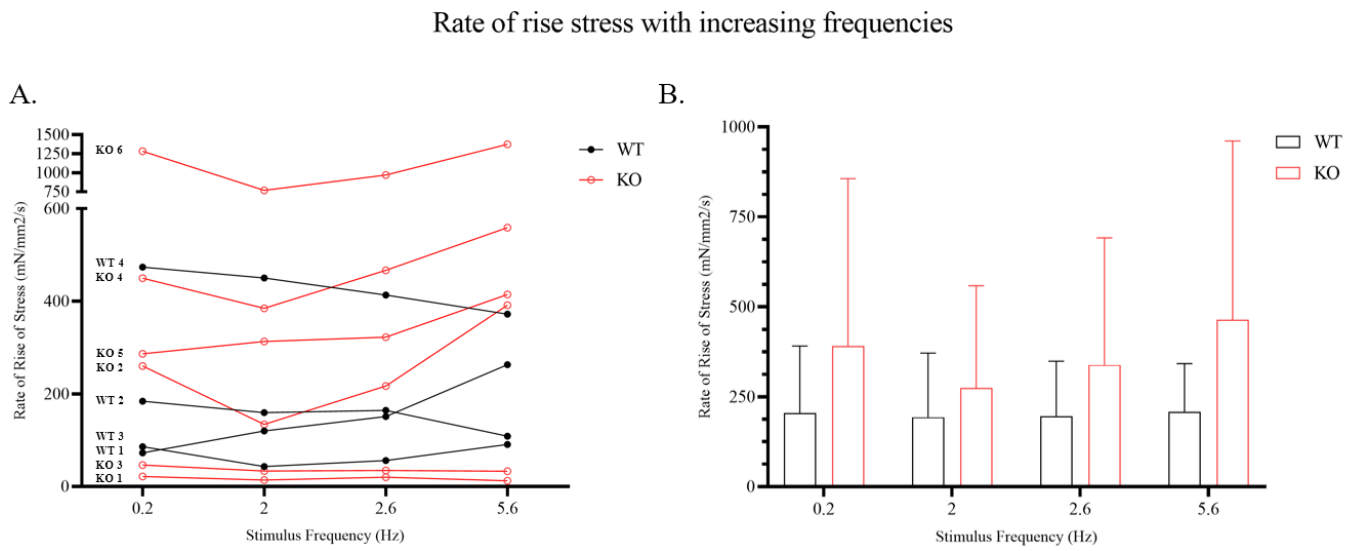

Figure 3.2: Rate of rise of stress at increasing frequencies of trabeculae.

A. This figure shows each trabecula's rate of rise over each frequency. **B.** Shown are both KO and WT rate of rises at each frequency. There was no statistically significant difference in the rate of rise of stress overall for each frequency between groups. (Error bars represent mean and SEM)

In Figure 3.3A, the active intracellular calcium shown as the 340nm/380nm ratio was similar in trends across both groups however, the knockout group showed more variability in recordings in comparison to the control group. With means (Figure 3.3B) for each group across all frequencies there was no statistical difference found between groups.

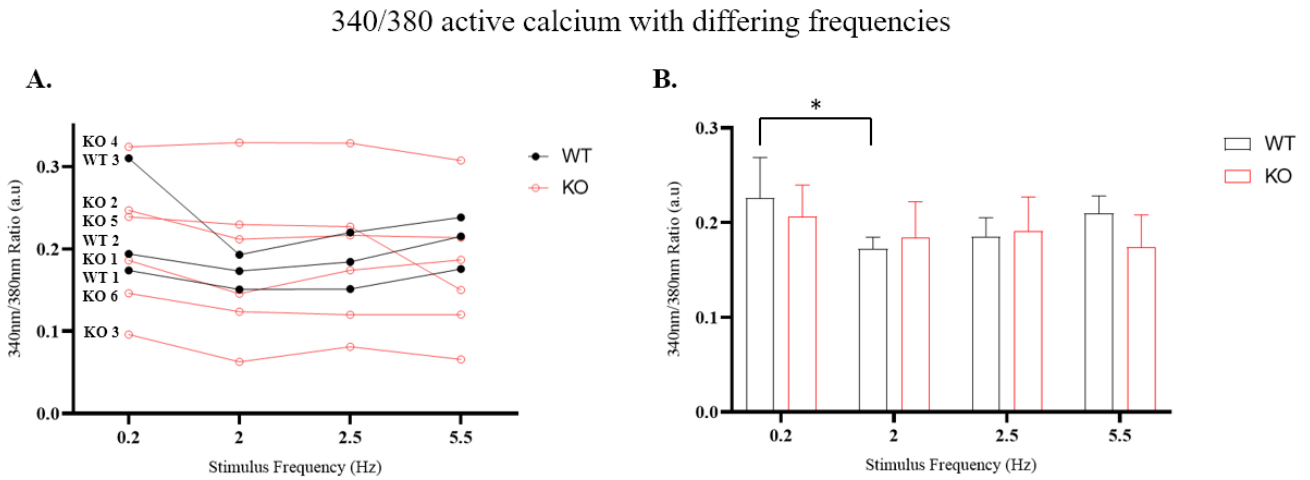

Figure 3.3: Active 340nm/380nm ratio from trabeculae at increasing frequencies.

A. 340mn/380mn ratio readings for both control and knockout groups. There was no statistically significant difference between the two groups of data. **B.** The mean ratio readings for each group at each frequency. Calcium readings here are similar for each group with no statistically significant difference found between groups. There is a statistically significant difference in the control group between the 0.2Hz and 2Hz stimulation frequencies (P=0.026). (Error bars represent mean and SEM)

To confirm the similar recordings for the 340nm/380nm ratio across the four tested stimulation frequencies which was unusual, when calculating active calcium (Figure 3.3), the 340nm/380nm recordings for each group split into diastolic and systolic values (Figure 3.4). There was an observed increase in diastolic and systolic calcium as the stimulation frequency increased which therefore explained the minimal change for the active calcium shown in Figure 3.3A. There was no statistically significant difference found between KO and WT groups shown in diastolic and systolic calcium, however within the KO and WT groups there was a statistically significant increase in diastolic calcium via the ratio between the 2.6Hz and 5.6Hz frequencies (P=0.006 and P=0.005 respectively).

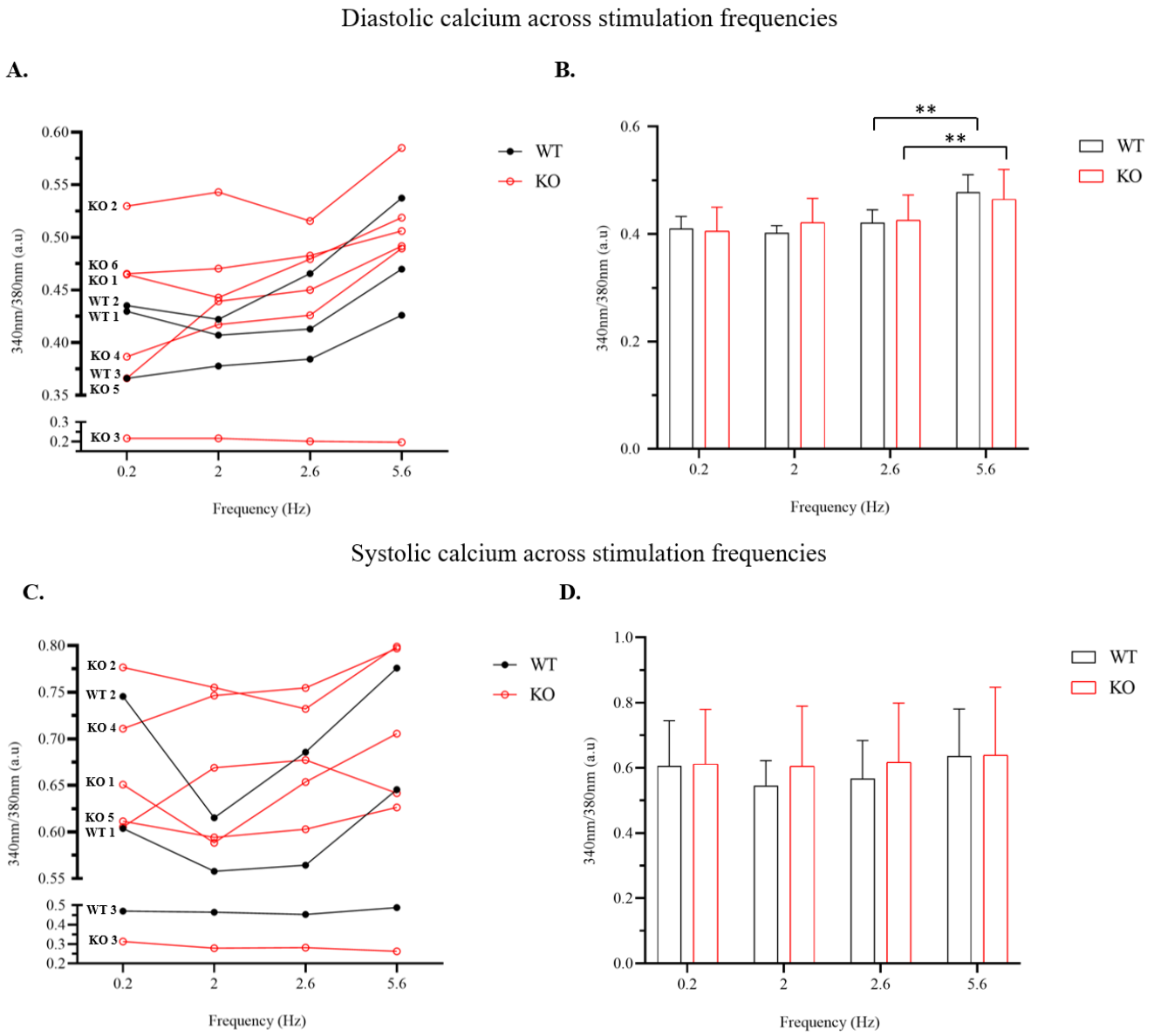

Figure 3.4: Diastolic and Systolic Calcium (340nm/380nm ratio) from trabeculae at increasing frequencies.

Shown here are the separate diastolic (**A.**) changes and means (**B.**) and systolic calcium (**C.**) changes and means (**D.**) as the 340nm/380nm ratio for both the KO and WT groups. There was no statistically significant difference found between the two groups for both diastolic and systolic calcium. Shown in **B.** within both KO (P=0.006) and WT (P=0.005) groups, there was a statistically significant increase in diastolic calcium between 2.6Hz and 5.6Hz. (Error bars represent mean and SEM)

When viewing calcium decay across the 0.2Hz, 2Hz, 2.6Hz and 5.6Hz frequencies, there was no significant differences between the groups (Figure 3.6). Within the knockout group there were statistically significant differences in calcium decay between 0.2Hz and 2Hz (P=0.009), 2Hz and 2.5Hz (P=0.014) and 2.6Hz and 5.6Hz (P<0.001). There was also the continuing prevalence of an increased variance in the knockout group with the control group showing similar recordings of calcium decay in comparison.

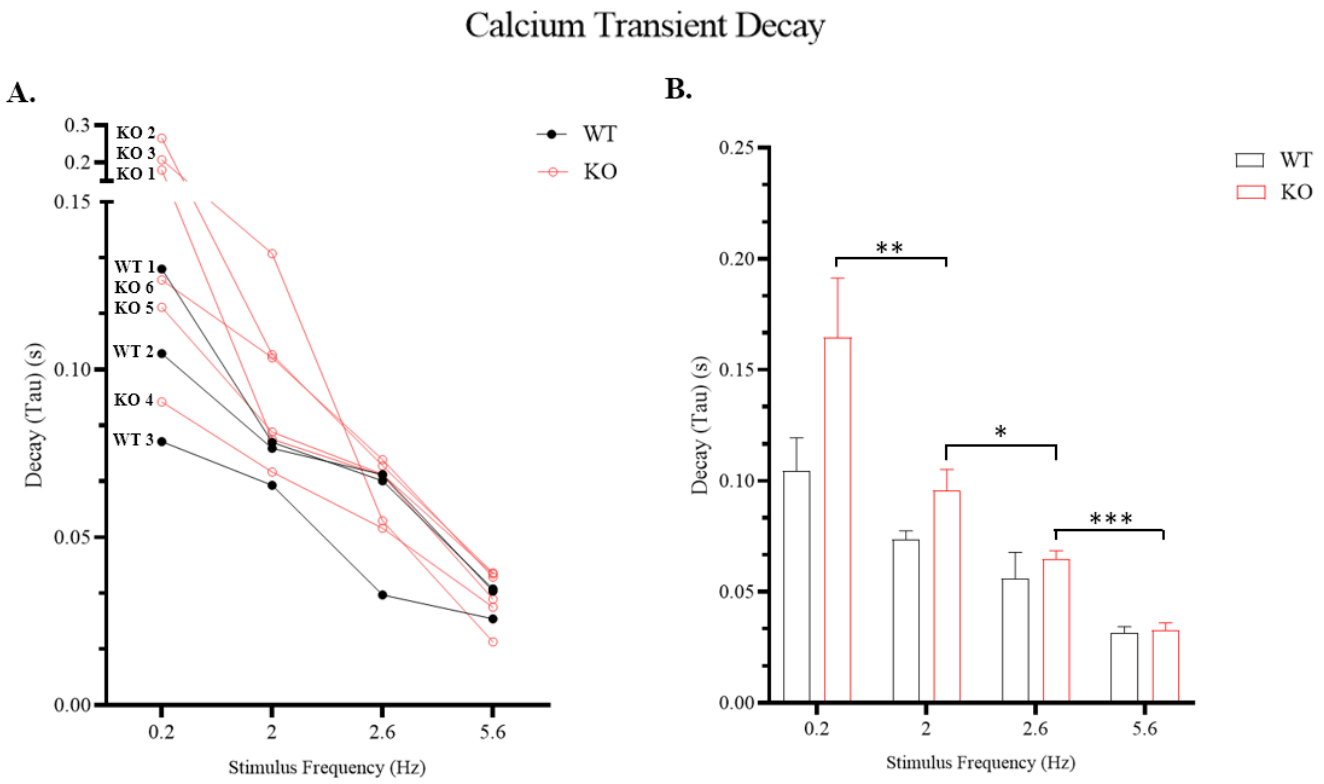

Figure 3.5: Calcium transient decay from trabeculae with increasing stimulation

Calcium decay was found to be the same in knockout trabeculae compared to controls with no statistically significant difference determined. Within the knockout group there were statistically significant differences in calcium decay between 0.2Hz and 2Hz (P=0.009), 2Hz and 2.5Hz (P=0.014) and 2.5Hz and 5.5Hz (P<0.001). There is also a high variance in decay times within the knockout group which is skewed to greater decay times than controls. (Error bars represent mean and SEM)

3.12 – Effect of increasing extracellular calcium concentration

When increasing the calcium concentration extracellularly in the solution circulated through trabeculae, there was an observed increase in active stress at each concentration increase shown in Figure 3.6A which was expected. There were statistically significant increases within the knockout group for active stress between extracellular calcium concentrations 1mM and 1.5mM (P=0.033), 1.5mM and 2mM (P=0.006), 2mM and 2.5mM (P=0.013), and 2.5mM and 3mM (P=0.026) (Figure 3.6B). The 340nm/380nm ratio readings (Figure 3.6C) obtained were unexpected as with increasing intracellular concentrations we would expect increasing intracellular calcium concentrations also which would show an increased 340nm/380nm ratio with each extracellular calcium increase. With extracellular calcium concentration and active stress increasing at each increase in concentration, the 340nm/380nm ratio not increasing across samples indicates a problem with the ratio measurements. Between and within groups there was no statistically significant difference in the 340nm/380nm ratio across all extracellular calcium

concentrations. There were no significant differences between extracellular calcium concentrations within the control group (Figure 3.6D).

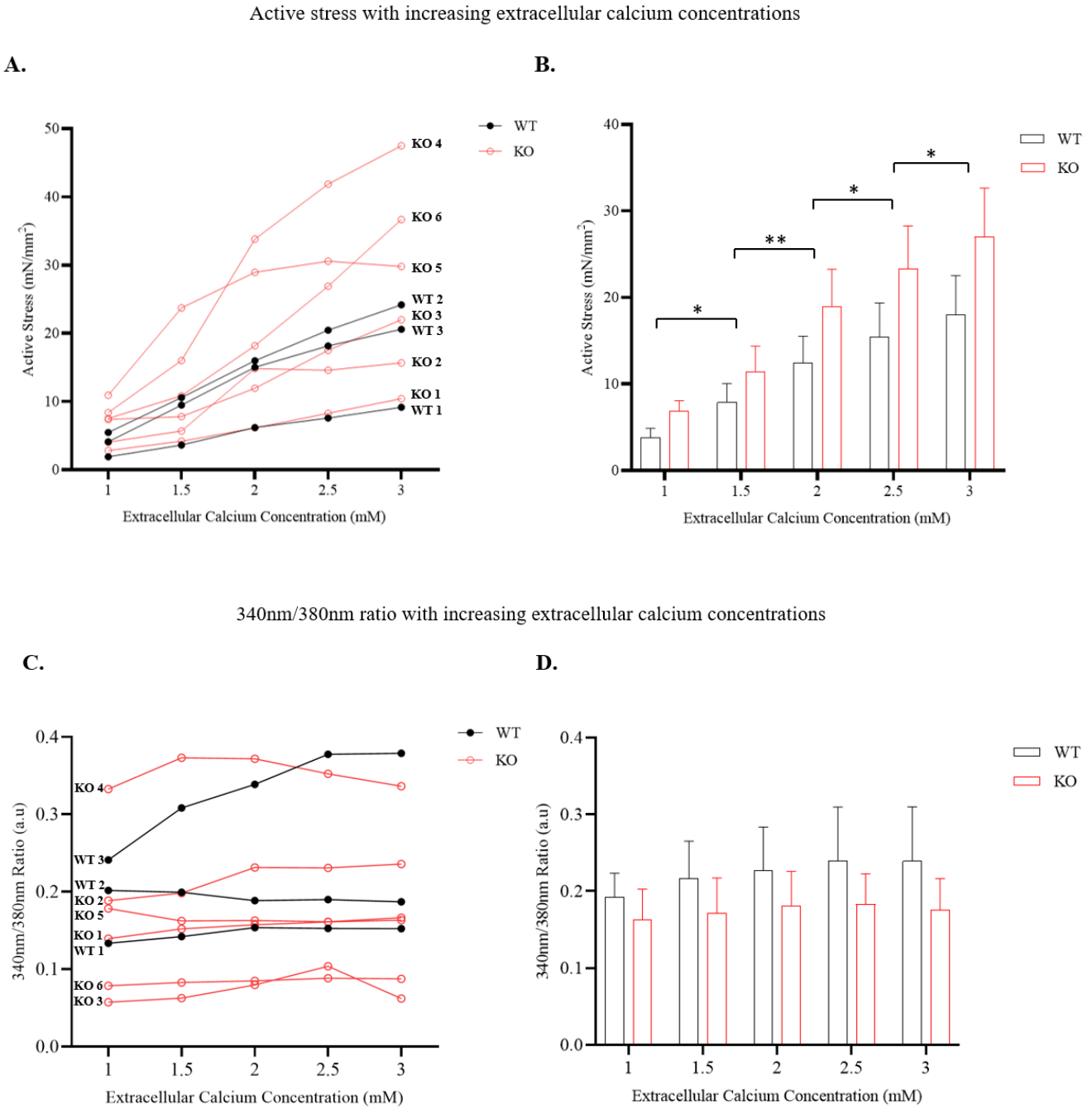

Figure 3.6: Active stress and calcium of trabeculae at increasing extracellular calcium concentrations.

A. Each trabecula's active stress at each extracellular calcium concentration; 1mM, 1.5mM, 2mM and 3mM. Active stress is shown to increase as the extracellular calcium concentration increases. **B.** There were no significant differences in active stress between the knockout and control groups. Within the knockout group, there were statistically significant increases between the active stress for 1mM and 1.5mM (P=0.033), 1.5mM and 2mM (P=0.006), 2mM and 2.5mM (P=0.013), and 2.5mM and 3mM (P=0.026). **C.** Shown is the 340nm/380nm ratio from trabeculae at increasing extracellular calcium concentrations. **D.** There were minimal changes are shown in each group's 340nm/380nm ratio readings, with no significant differences between or within groups. (Error bars represent mean and SEM)

3.13 – Effect of isoproterenol on active stress

The increase in active stress of trabeculae after adding the drug isoproterenol can be observed in Figure 3.8A. Each group showed increases in active stress post-addition of the isoproterenol, which was expected to occur, however statistical analysis of active stress between the groups showed no significant difference. Figure 3.8B shows the diastolic and systolic stress of both groups before and after the addition of 1mM isoproterenol. There was a statistically significant increase in diastolic stress with the control group compared to the knockout group both pre-addition ($P=0.028$) of isoproterenol and post ($P=0.002$). Within the control group, there was also a statistically significant increase in diastolic stress over the two timepoints ($P=0.016$) and within the knockout group there was a significant increase in systolic stress pre- isoproterenol and after addition ($P=0.008$).

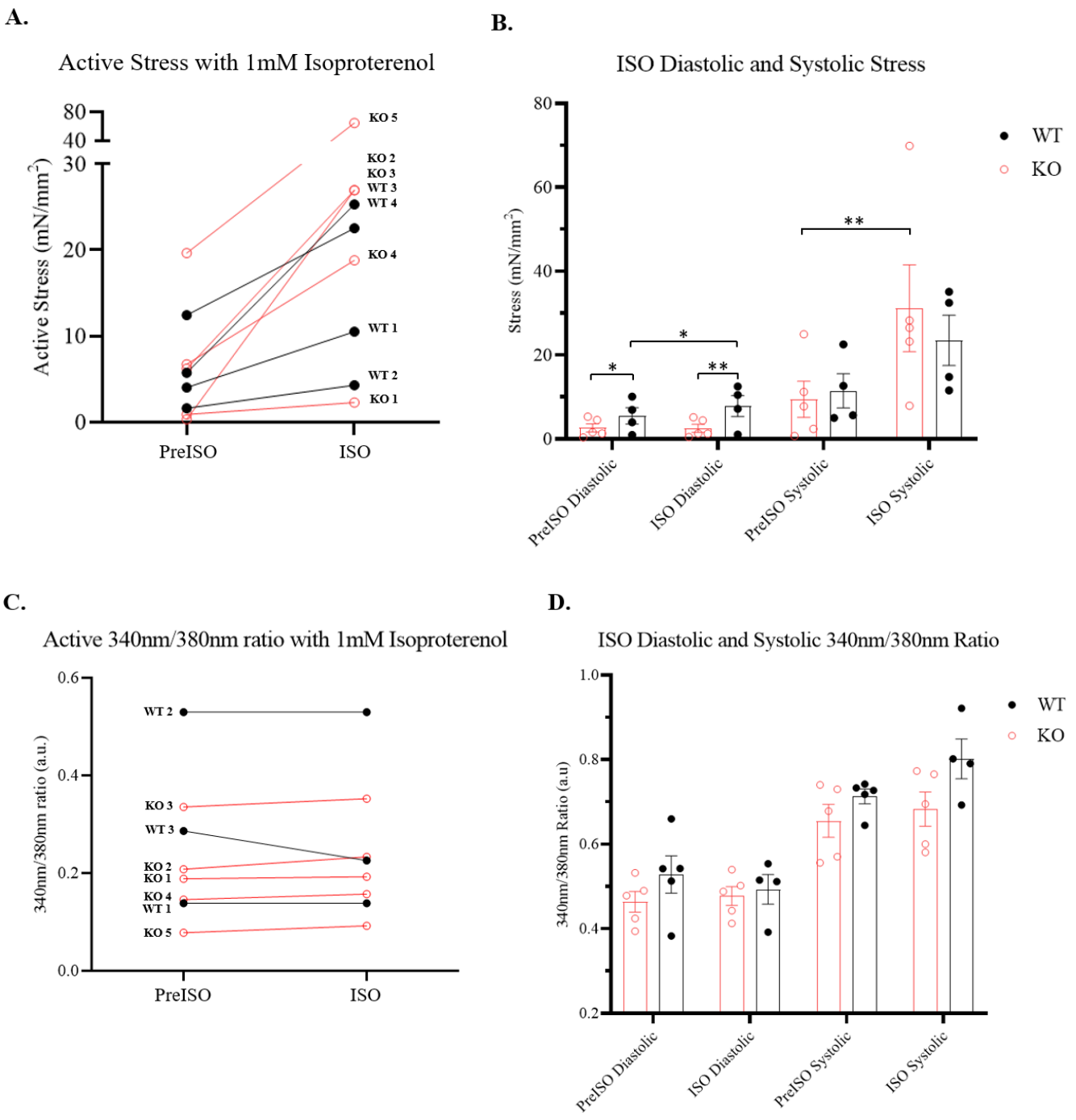

Figure 3.7: Active stress of trabeculae before and after the addition of 1mM isoproterenol

A. Active stress measurements of trabeculae before the addition of 1mM isoproterenol and the plateau of active stress after the addition of the isoproterenol. No statistical difference found between the groups. **B.** Shown is pre and post isoproterenol systolic and diastolic stress measurements for each group. There was a statistically significant increase in diastolic stress with the control group compared to the knockout group both pre-addition (P=0.028) of isoproterenol and post (P=0.002). There was also a statistically significant increase in diastolic stress over the two timepoints (P=0.016). Within the knockout group there was a significant increase in systolic stress pre isoproterenol and after addition (P=0.008). **C.** PreISO and ISO 340nm/380nm ratio for both knockout and wild type trabeculae. **D.** Systolic and diastolic calcium preISO and ISO. (Error bars represent mean and SEM)

3.14 – Arrhythmic features of Col6α1 -/- trabeculae

Within the knockout trabeculae, there were two animal experiments in which arrhythmic activity was present compared to none of the wild type trabeculae. Examples from each experiment trace from these two trabeculae are shown in Figure 3.8B and Figure 3.8C in comparison to a wild type trace (Figure 3.8A) with expected responses to stimulus. Shown in Figure 3.8A, it is expected that the stimulus occurs, then the calcium transient occurs which results in a contraction shortly after. With this knowledge, clear irregularities occurred at the lowest stimulation frequency of 0.2Hz for two of the six knockout trabeculae. Shown in Figures 3.8B and C are two different knockout trabecula traces from the 0.2Hz stimulation frequency. Observed are extra calcium transients and resulting contractions in between stimulations, with the first knockout (Figure 3.8B) showing an extra contraction for some stimuli, whilst the other knockout (Figure 3.8C) showed continuous contractions closer to a 1Hz frequency compared to the given stimulus shown in yellow which was 0.2Hz.

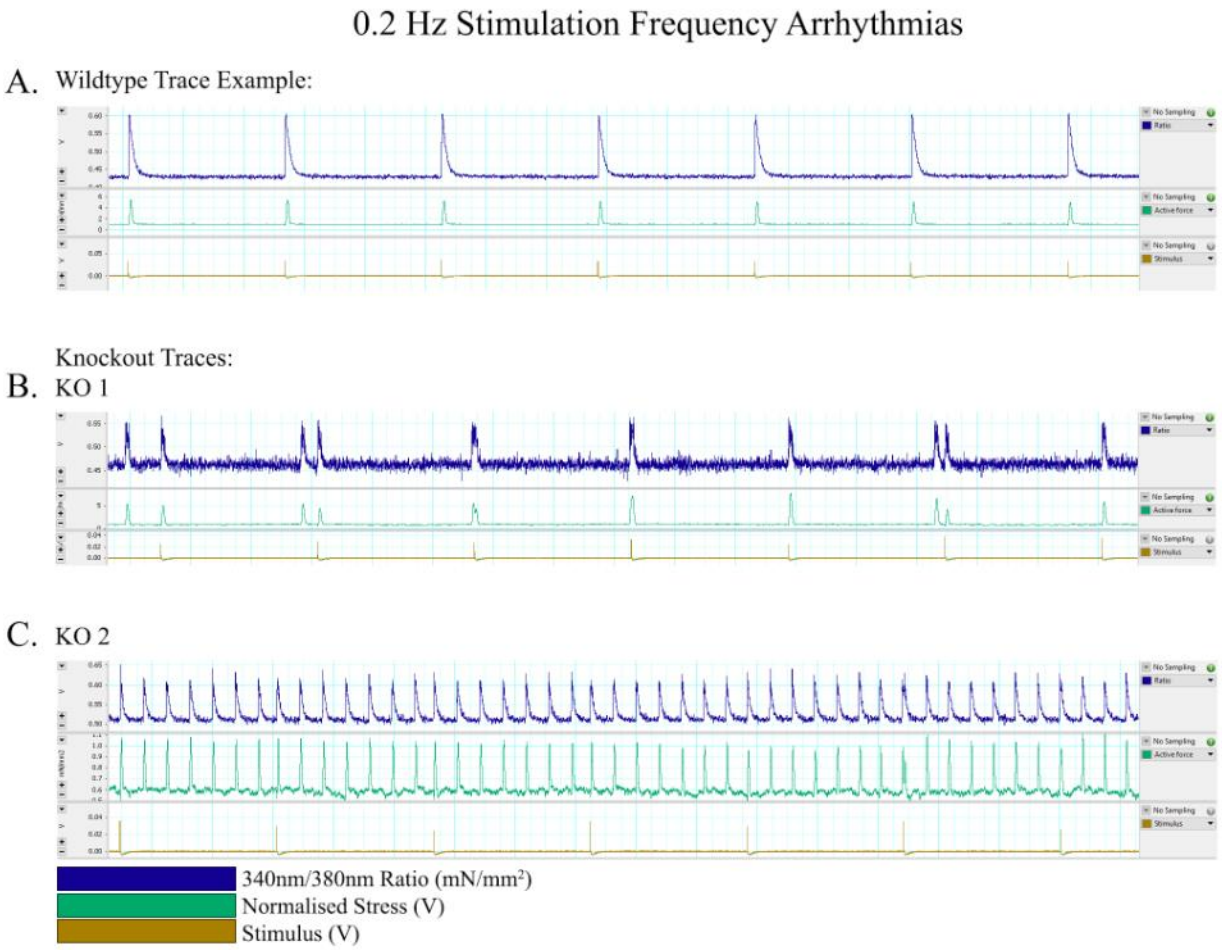

Figure 3.8: Trace examples of arrythmias from knockout trabeculae at 0.2 Hz stimulation frequency

A. A trace at 0.2Hz from a wild type trabecula as an example of a control response for comparison. **B.** Shows one of the knockout trabeculae at 0.2Hz appearing to be contracting irregularly with one stimulus and two contractions. **C.** Another knockout trabecula trace at 0.2Hz stimulation frequency showing contractions occurring outside of stimulations.

To quantify the irregularities, the standard deviation of the R-R intervals of the calcium transients during the four stimulation frequencies was graphed (Figure 3.9). When viewing trends in the standard deviation of R-R intervals from calcium transients, there was no statistically significant difference between or within groups (Figure 3.9), however increased variance in the knockout group was present, with R-R intervals trending to be larger in standard deviation compared to wild types.

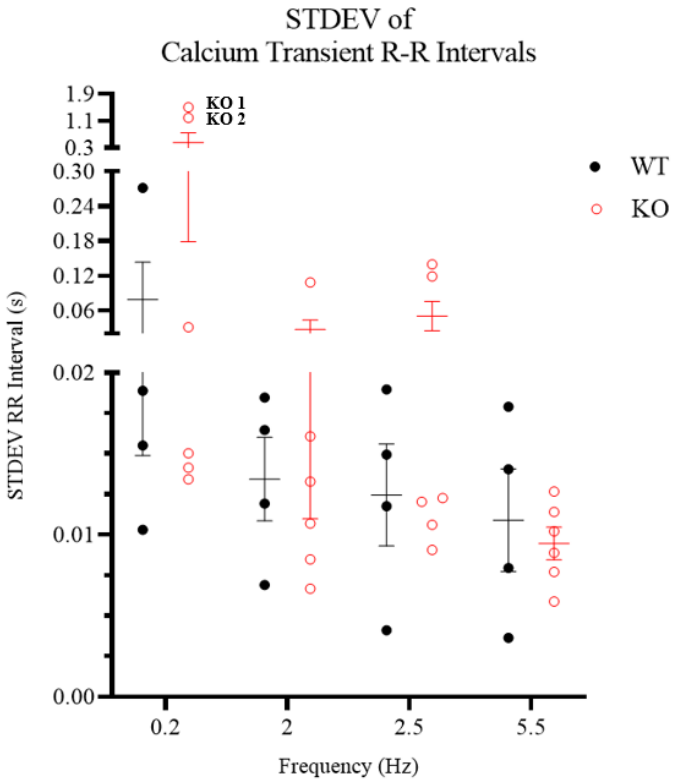

Figure 3.9: Standard deviation of the RR intervals of the calcium transients from trabeculae at increasing frequencies.

Shown is the standard deviation of each trabecula's R-R intervals of the calcium transients at each of the four stimulation frequencies. At the 0.1Hz frequency, there is a larger standard deviation of trabeculae compared to all other frequencies. The knockout trabeculae group displayed a larger mean standard deviation across the 0.1Hz, 1Hz and 2Hz frequencies compared to controls. At 5Hz, the control group displayed a larger mean standard deviation compared to the knockout group. (Error bars represent mean and SEM)

3.15 – Preliminary Investigative Imaging of Biglycan

Due to time constraints, imaging was only successfully completed on one knockout and one wild type animal. Shown in Figure 3.10 are two preliminary super resolution (STED) images of sections of LV; one from a Col6α1 knockout rat and one from a wild type rat for comparison. The green label shows collagen VI and the red label was used for identifying biglycan. In the knockout rat there was weakly positive collagen VI labelling in the extracellular space between myocytes, but collagen VI was absent

within t-tubules. Biglycan was found within the t-tubules in both knockout and wild type animals. In the wild type animals biglycan puncta were with ~100 nm of nearest collagen VI puncta.

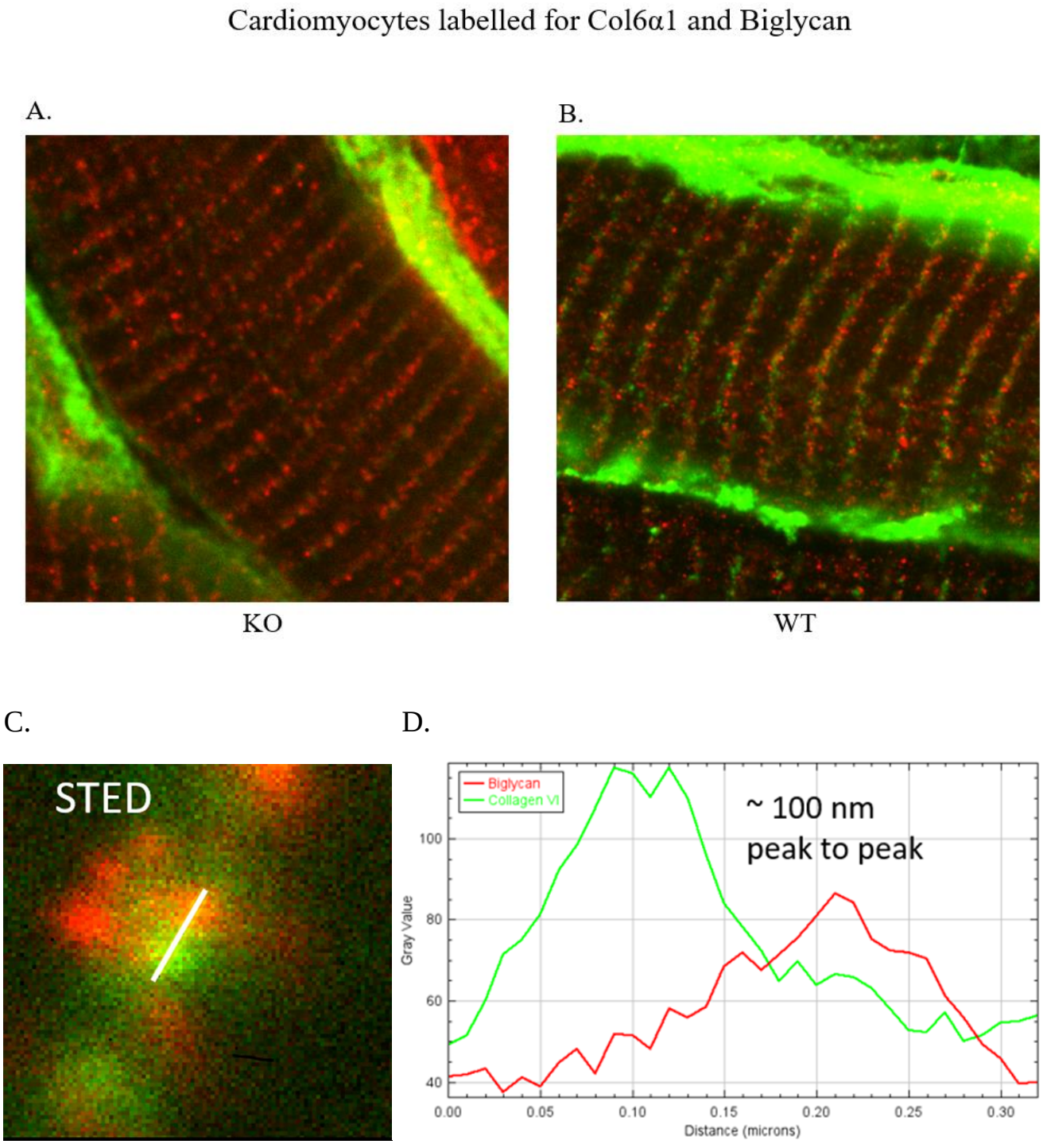

Figure 3.10: STED images of rat cardiomyocytes labelled for Col6α1 and Biglycan

Shown are super resolution (STED) images of two cardiomyocytes from the RV of: **A.** a Col6α1 knockout rat and **B.** a wild type rat. In both images biglycan is labelled in red (Aberrior STAR RED) and Col6α1 is labelled in green (ALEXA Fluor 594). **C.** STED close-up image of a collagen VI and biglycan molecule shows via analysis **(D.)** that both molecules are within binding range of each other at approximately a 100nm distance.

3.16 – Power Analysis

Due to a lack of significance found across statistical analysis of results, a power analysis was conducted to determine the number of animals required for future experiments to detect a 12.2 mN/mm^2 difference. This was the maximal mean difference in active force measured between knockouts and wild types, recorded at 0.2 Hz stimulation frequency (Figure 3.11A). The power analysis used mean difference and the standard deviation estimates in active force from knockouts and wild types at 0.2 Hz stimulation frequency. This analysis showed a minimum of 22 animals in each group would be required in order to have a statistical power of 0.7 or higher. Figure 3.11B shows the increase in power as the sample size increases.

A.

Power Analysis Table

					Test Assumptions			
Test for Mean Difference[a]	N1	N2	Actual Power[b]	Power	Std. Dev1	Std. Dev2	Mean Difference	Sig.
1	22	22	.700	.700	21.3	5.9	12.200	.05
2	25	25	.759	.750	21.3	5.9	12.200	.05
3	28	28	.808	.800	21.3	5.9	12.200	.05
4	32	32	.859	.850	21.3	5.9	12.200	.05
5	37	37	.906	.900	21.3	5.9	12.200	.05

a. Two-sided test.

b. Based on noncentral t-distribution.

B.

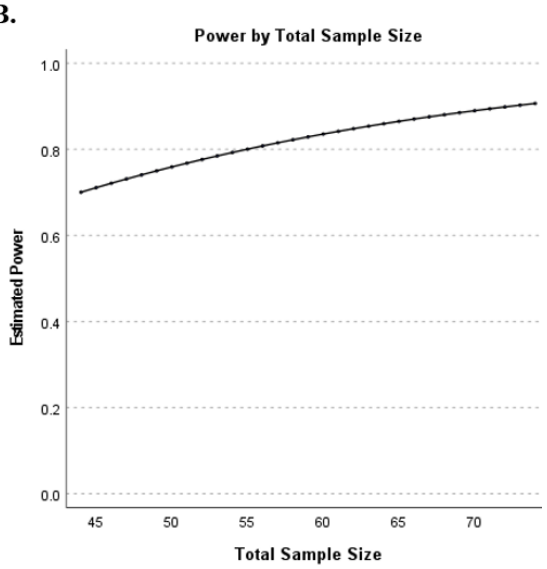

Figure 3.11: Power analysis and sample sizes.

A. A power analysis table using means from the experiments at the 0.1Hz frequency to determine approximate sample sizes and their corresponding statistical power. In order to obtain a power of 0.8 for our analyses, there would have needed to be a minimum of 28 animals in each group. **B.** Shown is a graph of the estimated power with total sample size increases. As shown as total sample size increases, so too does statistical power.

CHAPTER 4 – DISCUSSION

Previous data from the collagen VI knockout rat model demonstrated a reduced ejection fraction compared to wild type animals (shown in Figure 1.24). In comparison, isolated cardiac myocytes from knockout animals demonstrated increased systolic calcium at 1Hz frequency compared to wild type animals (Figure 1.24). An increase in calcium, with all other variables equivalent, should increase force and therefore ejection fraction suggesting that the knockout out animals have diminished force transmission. This data generated the hypothesis that trabeculae from collagen VI knockout rats would have a decreased calcium force relationship leading to reduced force and therefore diminished ejection fraction. Furthermore, this would likely be driven by the loss of collagen VI connection to the dystrophin-glycoprotein complex impacting the force that can be generated during contraction. Preliminary imaging of collagen VI and biglycan in a wild type sample shows localization adjacent to biglycan within t-tubules indicating that biglycan is a likely linking collagen VI to dystrophin-glycoprotein complex in partial support of this hypothesis (Figure 3.10). However, the physiological data from this thesis does not support this hypothesis. Although a major caveat is that the study is underpowered due to larger than expected variance particularly in the knockout animals that will be discussed in depth in the limitations section. However, this large variance suggests an alternative hypothesis in that variability in force generation within the collagen VI knockout heart may drive a dyssynchronous contraction that diminishes the ejection fraction.

4.1 - Effects of stimulation frequency on Col6α1 -/- trabeculae

4.11 - Active stress and rate of rise

In general, the active force generated by individual trabeculae followed a biphasic force frequency response previous observed in rat trabeculae (Layland & Kentish, 1999). This response was statistically demonstrated in knockout trabeculae and to lesser extent in wild types, however, the low sample number would likely increase sampling error that could mask this trend in the wild types. There was an increase in mean active stress observed in the knockout animal group compared to the control group, although not statistically significant, due to low statistical power we cannot exclude this as a potential feature (Figure 3.1B). Overall, there was no statistical difference between the knockout and wild type trabeculae, however, there was some evidence of an increased variance in stress from the knockout trabeculae compared to the wild type. The presence of increased collagen VI within t-tubules in the human heart failure setting (Crossman et al., 2017) suggests that the increased amount may diminish calcium release, presumably through disruption of the cardiac dyads. However, the finding from knockout isolated myocytes also indicates that the absence of collagen VI increases the amplitudes of calcium transients

(Figure 1.24B). With no statistically significant changes in calcium shown in knockouts compared to controls across all frequencies from trabeculae experiments (Figure 3.3), there may be other reasons for the variation of stress shown in knockouts compared to wild types. However, there was evidence of poorly functioning spectral excitation of the calcium dye Fura-2 that indicates changes in Ca^{2+} can't be excluded.

The active stress measured for wild type animals was lower than expected, with average active stress starting around 20mN/mm^2 (Figure 3.1). In experiments with similar protocols, with one example being a rat trabeculae study, the mean active stress at 2Hz for control trabeculae was found to be above 40kPa (40mN/mm^2) at 1mM calcium concentration (Han et al., 2010). In Han et al (2010) a 1mM calcium concentration was used which is less than what was used in this thesis (1.5mM), trabeculae would be expected to have an increased active stress comparatively, which was not the case. Whilst the stress recordings were not high, the trend across frequencies for most trabeculae shown in Figure 3.1A were consistent with the known standard force frequency relationship for rats shown in Figure 1.6. The corresponding active stress with each frequency within the knockout group displayed a trend similar to the original rat FFR trend (Figure 1.6). This was also the same for the rate of rise of stress in each group shown in Figure 3.2, with no difference between the groups and a low rate of rise overall due to low stress.

There is a number of potential reasons for why the observed stress across all experiments was lower than expected. One of the main reasons for the lack in stress was the potential for the trabeculae to be damaged before Fura-2 AM loading. Such damage can occur at every step of the dissection and mounting phase and whilst it is difficult to pinpoint where the damage occurred, dissection is known as the hardest part of the experiment and therefore, is assumed to be the point of damage for the trabeculae. Damage can occur due to an increase in time taken from cull to cannulation, which would result in no oxygen or BDM being perfused into the heart for that time. The result of this is clotting of any remaining blood within the heart which could damage the trabeculae before dissection has occurred. The lack of oxygenated solution in the heart can also result in a hypoxic response from cells, which when damaged experience apoptosis and further tissue necrosis if enough time had occurred. This was potentially the case for an excluded animal, as when being mounted in the KHB/glucose oxygenated solution was unresponsive to any external stimulation. Force generation through contraction in cardiomyocytes requires a high level of metabolism to occur and without enough oxygen, there becomes increased levels of anaerobic metabolism within cells (Bevere et al., 2022). The accumulation of metabolic glycolysis products - lactate and protons, inhibit glycolysis which in turn stops the anaerobic metabolism from occurring overall leading to cell death (Das et al., 1987). Another study detailing the Langendorff-

perfused isolated heart model using wild type mice had a mechanical setup which was the same as the setup for experiments conducted with rats for this paper (Reichelt et al., 2009). When dissecting trabeculae from mice hearts, researchers concluded that whilst the model does provide a reliable analysis of contractile function; age, sex and the calcium concentration of the perfusion liquid can significantly affect the variability in contractile function and therefore force in ischemic responses. Within the 2009 study, male mice which were 24 weeks in age had an increased left ventricular developed pressure (LVDP) compared to male mice who were 8 weeks of age as well as reductions in tolerance and significant declines in recovery which were evident at 16 weeks and reduced again at 20-24 weeks in males. Whilst not looking at ischemic responses, variations in age is present for the rats used in this study (shown in Table 3.1) with one rat aged at approximately 10.5 weeks compared to a rat who was 35.9 weeks in the knockout group which may contribute to the higher variability in active stress. There is, however, similar variability in ages within the wild type rats which have lower contractile variability suggesting the higher variability of contractility in knockout is a consequence of the absence of collagen VI.

In a study using two groups of rats where one group had an excess myocardial collagen volume fraction and the other having a reduced myocardial collagen volume fraction (total collagen was measured with the protocol), both groups displayed differing papillary function (Matsubara et al., 2000). Within the excess collagen group, the passive tension length curve had shifted upwards indicating an increase in passive stiffness of papillary muscles in comparison to the reduced collagen group which experienced the opposite, with passive tension shifting downwards indicating a decreased passive stiffness. The decrease in passive stiffness was concluded to be strongly correlated to the loss of collagen with an association to cardiomyocyte hypertrophy due to its assumed link to ventricular dilation (Janicki, 1992) and an increase in active stiffness also present. These findings may explain the increased variability in active stress shown by the knockouts, as with no Col6α1 present, trabeculae may have experienced similar changes in both passive and active stiffness. If trabeculae experienced a decrease in passive stiffness, there would be an observed decrease in diastolic stress in comparison to the wild type trabeculae. Similarly, if there was an increase in the calcium transient in knockout trabeculae there would be an observed increase in systolic stress when compared to the wild type trabeculae. A decreased diastolic stress and an increased systolic stress together would result in an increased active stress overall, which was a trend shown in the knockout trabeculae and could therefore explain both the trend for greater active stress and increased variability shown in knockout trabeculae across all experiments in this thesis.

Fibrosis is commonly named when explaining increases myocardial stiffness and impaired contractions in the heart. Fibrosis in heart failure literature is known to impair contractions (Kania et al., 2009), but is commonly overlooked for other aspects of cardiomyocytes and remodelling. Research of heart failure indicates that the reduction in the contractile force of the heart is due at least partially to increases in fibrosis and scaring after injury (van Spreeuwel et al., 2017). Upon depletion of collagen VI in human intestinal cells (smooth muscle cells), significant increases in cell spreading have been observed which was found to coincide with an upregulation of the expression of fibronectin (Groulx et al., 2011). Not only was expression of fibronectin upregulated, but its deposition increased as well with a larger amount of phosphorylation occurring on myosin light chains which caused increased fibrosis. Cultured fibroblasts from collagen VI knockout mice also showed the same increase in deposition amount and organisation of fibronectin compared to controls similar to that of patients with Bethlem myopathy (Sabatelli et al., 2001). Fibronectin is an extracellular matrix adhesin protein known for causing fibrosis in injury and heart disease (K. S. Song et al., 2001) with many studies targeting the protein for inhibition for improving cardiac functioning after injury (Valiente-Alandi et al., 2018). If a similar phenomenon occurs in a rat model where collagen VI was knocked out, there becomes an increase in fibronectin which causes the proliferation of myofibroblasts resulting in increased fibrosis in the heart. Increased variance of active stress shown in the knockout trabeculae compared to the wild type trabeculae may be the result of increased fibronectin and corresponding regional fibrosis experienced in the knockout myocardium.

Alternatively, increased variance in active stress may be due changes in dyadic structure. The absence of collagen VI in knockouts may disturb membrane structure through loss of connection to the dystrophin glycoprotein complex. If collagen VI does hold dystrophin in place across the membrane, then in knockouts there would be an assumed increase in disorganised plasma membranes which could disrupt the structure and spacing of the cardiac dyads. Another possibility is the lack of physical connection in collagen VI knockouts between collagen, biglycan and dystrophin could diminish force generation. In that instance collagen VI knockout cardiomyocytes would also have inefficient cell signalling between the extracellular matrix and cytosol of cells as well as reduced efficiency of signals via the sarcolemma and t-tubule system. The increase in incorrect signalling and membrane disorganisation may result in the observed larger variation of active stress in the knockout trabeculae shown in Figure 3.1.

If there was disorganization of dystrophin due to the absence of collagen VI in knockout trabeculae, there may have already been damage to the sarcolemma before experiments occurred leading to influx of Ca^{2+} that could trigger arrhythmia and apoptosis. A study in MDX mice

observed onset of myonecrosis in skeletal tissue - the necrosis of myofibers which began at two weeks of age in mice and peaked between three and four weeks of age before approximately eighty percent of the myofibers were regenerated (McGeachie et al., 1993). It has been proposed that myonecrosis is triggered by increased calcium influx into skeletal cells through sarcolemma micro-tears (Burr & Molkentin, 2015). A similar mechanism may be in play within the myocardium of collagen VI knockouts. An alternative hypothesis is that stretch activated channels are activated in MDX mice. Transient receptor potential canonical (TRPC) channels are cation channels on the plasma membrane and has roles in multiple modulation pathways for all types of cells in the body (Eder & Molkentin, 2011). Both TRPC3 and TRPC6 channels have been associated with the modulation of the pathological cardiac response via systolic mechanosensing shown in pressure overloaded mice (Kuwahara et al., 2006; Nakayama et al., 2006). One study these two channels TRPC3 and TRPC6 via knockout mice models and in a cardiac muscle dystrophy model to determine whether there was relevance for future DMD studies (Seo et al., 2014). In the dystrophic hearts there was an excess of stress-stimulated contractility and arrythmias which when suppressed by protein kinase G (PKG) (a known potent negative modulator of cardiac systolic mechanosensing) reversed this phenotype. Perhaps this is the same for the collagen VI knockout trabeculae, with stretch activated channels being active explaining the variance in active stress displayed and the trend for higher active stress in comparison to wild type trabeculae. Lower stiffness in the knockouts as indicated by reduced passive stress would make the myocytes more prone to stretching increasing calcium load. This could lead to variability in contractility as some cells would increase contractility while others could become calcium overloaded triggering apoptosis.

Animal studies of dystrophin mutations show similar features to collagen VI knockouts which suggest effects be through DGC. Therefore, we can use research from Duchenne muscular dystrophy (DMD) and Becker muscular dystrophy (BMD), two X-linked muscular dystrophies which both affect the synthesis of dystrophin, to model what occurs in the heart because of incorrect amounts of dystrophin, with DMD patients having no dystrophin and BMD patients having reduced synthesis of dystrophin to determine any similarities in active stress variance compared to the knockouts from this thesis. In MDX mice myocardium, there was a reduction in membrane-associated neuronal nitric oxide synthase (nNOS), which without dystrophin in DMD was thought to incorrectly gather within the cytosol instead of the sarcolemma (Bia et al., 1999). For DMD patients, after contraction of the myocardium there was not enough nitric oxide (NO) which would normally diffuse through the membrane into the vasculature compared to controls, and this can result in myocardial ischemia (Sander et al., 2000). Ischemia due to lack of NO is thought to be one probable reason for cardiomyopathy in DMD patients (Hainsey et al., 2003).

Inducible nitric oxide synthase (iNOS) is a calcium independent enzyme and can be induced by a range of molecules including cytokines to consistently create NO until its degraded (Lind et al., 2017). Researchers from the same 1999 paper hypothesised that the MDX hearts having iNOS activity seven times higher than normal was an attempt by cells to have the adequate amount of NO required to avoid said ischemia from occurring. Studies on effects of ischemic myocardium in humans have also shown ischemia and reperfusion injuries being linked to ventricular remodelling, mechanical dysfunction and tissue necrosis which are all known occurrences in heart failure patients (Wainwright, 2004). A loss of NO in cells as a result of ischemia may also cause fibrosis which would then reduce the contractile ability of the myocardium and as discussed above. With collagen VI knockout trabeculae, having a reduction in dystrophin may have decreased the amount of NO able to diffuse into cells. Further, depending on the thickness of the muscle, this may have caused ischemia or stress within the muscles, potentially causing regional fibrosis causing the observed increased variance in active stress between each experiment.

Another potential reason for the increased variance shown in active stress by the knockout trabeculae may be due to errors in calcium release, either at the wrong times or incorrect amounts of calcium. If calcium release and reuptake is inconsistent between contractions, resulting contractions would also become inconsistent resulting in arrythmias, or the active stress variance seen in knockout trabeculae. It is common for DMD patients to exhibit electrocardiographic abnormalities including many premature ventricular contractions attributed to fibrosis (Chenard et al., 1993) (Finsterer & Stöllberger, 2003). Leaky or orphaned RyRs in DMD have been noted as being responsible for some abnormalities. Earlier, it was introduced that orphaned RyRs in the failing myocardium were misplaced due to dyad separation across the membrane, making the distance between dyads becoming suboptimal due to t-tubule remodelling in heart failure (L.-S. Song et al., 2006). It is possible that this occurred in the collagen VI knockout trabeculae as there was not only arrythmias in some trabecula, but also the varied stress trend shown in the group overall.

4.12 - Intracellular calcium and decay

Surprisingly a biphasic response in calcium was not observed in trabeculae in response to stimulation frequency as would be expected given the biphasic nature of the stimulation-force relationship (Luo et al., 2006). Although similarly, there was an increased variability in the knockout trabeculae's active calcium, diastolic and systolic calcium in comparison to the wild type trabeculae (Figure 3.3 and Figure 3.4). However, this did not correlate with active stress as

evidenced in the trabecula labelled KO6 which had the second lowest active calcium ratio (Figure 3.3A) but the highest active stress (Figure 3.1A). Upon examination, the change in Fura-2 340nm/380nm ratio for all trabeculae was lower than reported by other authors (Janssen & de Tombe, 1997) but similar to a previous student project on the same experimental rig. This could be due to poor Fura-2 loading or technical issue with the microscope setup. This led me to closely examine the Fura-2 340nm/380nm calcium calibration curve.

Upon re-measuring the calibration curve, using the window size similar to that used in the trabeculae experiments, demonstrated a calibration curve with less sensitivity than previous Authors both within our lab and from other laboratories but similar to the previous student project mentioned above (see Appendix 2). As Fura-2 is ratio metric dye changes in the fluorescence ratio should be independent of dye concentration. The most likely explanation of reduce ratio would be if the excitation wavelengths were not at the optimal position (340 and 380 nm). This would compromise the accurate assessment of Ca^{2+} values in this thesis. For example, for trabecula KO3 the 340/380 ratio (Figure 3.3) was below 0.24V reading for 0 calcium (red line in methods Figure 2.5) which indicated a calcium concentration less than zero millimolar which is theoretically not possible. This indicates increased noise creating an erroneous measurement. It is likely in this trabecula, lower than average Fura-2 loading resulted in noisy fluorescence signal that resulted in measurement below the standard curve. In future, there would be a proposed realignment of the microscope to increase the sensitivity of the calcium detection prior to further experiments.

As expected, based on minimal change in the active calcium, there was a minimal increase in diastolic and systolic calcium with increasing frequency. Although there was evidence of a small increase in diastolic calcium at the highest frequency of 5.6Hz. Diastolic calcium increases are a common sign in experiments of damage to trabeculae which furthers the reasoning that trabeculae used in experiments may have been damaged pre-experimental procedure. The increased diastolic calcium may be due to an inability to remove enough calcium within the cells after stimulation and contraction occurs, leading to an increase overall in diastolic calcium. An older study noted that even though the sodium-calcium exchangers were responsible for approximately 77% of sarcolemmal calcium removal in rat cardiomyocytes, there were background (B-type) calcium channels that passively allow calcium to enter cardiomyocytes in the absence of sodium and under resting potential (Coulombe et al., 1989). Activity of these B-type channels were found to be enhanced in human atrial cardiomyocytes upon metabolic poisoning and increasing the amount of free-radicals within cells (Antoine et al., 1998). With assumed damaged cardiomyocytes in trabeculae from dissection being used for experiments, there is a possibility of this metabolic

poisoning increasing the levels of diastolic calcium via the B-type calcium channels.

There were no statistical differences in calcium transient decay identified between the knockout and control group, however, within the knockout group there were significant differences in calcium transient decay between the frequencies (Figure 3.5). As the stimulation frequencies increased, the calcium transient decay time decreased. This was expected as with a faster rate of stimulation, calcium current would be faster, and this would make the calcium transients quicker within cells which would allow for overall faster contractions of the sarcomeres within the cardiomyocyte.

Two of the six collagen VI knockout trabeculae showed spontaneous beating resulting in irregular contractions on the trace that did not line up to the stimulus frequency of 0.2Hz. Shown in Figure 3.8A is a section from a wild type trabeculae trace at 0.2Hz which shows the expected stimulus peak (yellow) first with the calcium transient (blue) occurring after the stimulus with a resulting contraction (green) of the muscle. Calcium transients and contractions are only expected when a stimulus occurs as shown in the trace. Figure 3.8B and Figure 3.8C show sections of two different knockout trabeculae with spontaneous contractions at 0.2Hz stimulation frequency. These irregularities were not observed in any of the wild type trabeculae, which indicates spontaneous contractions are due to the lack of collagen VI. To quantify the potential difference in contraction frequency between the knockout and wild type trabeculae, the standard deviation of the calcium transients R-R interval were analysed (Figure 3.9). This was done to determine if there was a more variable but subtle differences in R-R intervals in the knockout animals.

There was no statistically significant difference between the standard deviation of knockout and wild type trabeculae's calcium transient R-R intervals for each tested frequency (Figure 3.9), with the variance in knockout trabeculae without spontaneous contractions similar to the variance in the wild-type trabeculae. In knockout trabeculae spontaneous contraction also occurred without stimulus during thirty seconds of no stimulus between frequencies tested - suggesting irregularities in calcium handling from these muscles. For every wild type trabecula used in experiments regardless of exclusion criteria, irregular contractions or contractions with no stimulus never occurred - supporting the hypothesis that the increased variance in active stress, the arrythmias, and variable calcium handling are all attributed to the lack of collagen VI in the knockout trabeculae.

4.2 - Effects of extracellular calcium on Col6α1 -/- trabeculae

Overall stress increases across the increased concentration of extracellular calcium in solution were expected and obtained, however changes observed in the 340nm/380nm ratio were unexpected as they were expected to increase as extracellular calcium increased and they did not or there was a minimal increase. The unexpected observations are likely explained by the errors in measuring calcium which were discussed above.

4.21 - Active Stress in increasing extracellular calcium

For both knockout and wild type trabeculae groups, active stress increased as extracellular calcium increased (Figure 3.6A). There was no statistically significant difference in active stress between groups (Figure 3.6B), however there was still a noticeable increase in variance displayed by the knockout group compared to the control group. Within the knockout group there was significant increases in active stress with increasing extracellular calcium concentration. A similar trend was seen in the wild type trabeculae which was expected based on previous studies with wild type trabeculae (Han et al., 2009). Although this was not significant this is mostly likely explained by low N number. With more extracellular calcium being available to cells, it is expected more trigger calcium would be available for faster activation of more RyRs via L-type channels resulting in increased sarcolemmal calcium release. Furthermore, higher extracellular cellular would increase the load of the sarcoplasmic reticulum through store-operated Ca^{2+} entry (SOCE) and increase the amount of Ca^{2+} available for release during the Ca^{2+} transient (Bootman & Rietdorf, 2017). With greater releases of calcium, more myosin can bind in sarcomeres allowing for a stronger contraction of more sarcomeres across cardiomyocytes.

Spontaneous contractions shown in two of the six knockouts (Figure 3.8) at 0.2Hz provide evidence of potential calcium mishandling within the cardiomyocytes. However, the assumed calcium mishandling in knockout trabeculae did not occur when increasing extracellular calcium. If the spontaneous contractions were caused by calcium mishandling, for example if calcium could not be efficiently removed by the cardiomyocytes in diastole and caused secondary contractions after stimulus, that increasing extracellular calcium concentration would trigger the same effect. However, the spontaneous contractions in the knockout animals were at most 1 Hz frequency but the extracellular calcium experiments were paced at 2 Hz. This would override the spontaneous contractions.

4.22 - Active calcium in increasing extracellular calcium

It was expected that there would be an increase in intracellular calcium shown based on the increase of active stress observed. This intracellular calcium increase was not observed when reviewing the 340nm/380nm ratio readings from the corresponding experiments (Figure 3.6C). The main reason believed for the unexpected calcium results was due to errors with the experimental setup as discussed earlier, as there was no significant difference across both the knockout and control groups (Figure 3.6D). It is known that small alterations of intracellular calcium in cardiomyocytes can drastically change contraction and relaxation of the heart (Barry & Bridge, 1993), and these changes had likely been obscured due to a poorly functioning calcium imaging system. A well calibrated calcium setup would be required to assess the relationship between stress and intracellular calcium.

Whilst not different between groups, there was a notable variation of readings in the 340nm/380nm ratio in the knockout group (Figure 3.6D) with results at 1mM extracellular calcium concentration ranging from 0.057 to 0.373. Other than mentioned problems with the experimental setup, increased variance could be due to mishandling of calcium in the knockout trabeculae. A study using MDX mice discovered that there was altered calcium homeostasis in the form of increased calcium sparks and a reduction in a protein called junctophilin-2 (JPH-2) in isolated ventricular cardiomyocytes (Kurt W. Prins et al., 2016). JPH-2 is located on the plasma membrane and functions to hold RyRs in the correct alignment to t-tubules forming the dyad. Observed in MDX cardiomyocytes were signs of cardiomyopathy with older mice displaying a reduction in t-tubule integrity hypothesised to be due to decreased levels of JPH-2. The Crossman's lab unpublished research demonstrates similar alterations in calcium handling in the collagen VI knockout rats, therefore, the knockout trabeculae used for our experiments may have been experiencing a lack of JPH-2 or may have unaligned RyRs which would provide the same calcium mishandling results as cardiomyocytes with a lack of JHP-2. Instances of calcium mishandling have been observed in multiple instances in MDX models with another study showing that increased calcium transients in older mice was also accompanied by increased expression of RyRs and an overall increase in the function of Na^{+}/Ca^{2+} exchangers along the plasma membrane in isolated ventricular cardiomyocytes (Williams & Allen, 2007). It is not uncommon in skeletal muscle dystrophy research to find evidence of incorrect calcium handling in myocytes (Wang et al., 2005). Another example evidenced from a study with adolescent DMD patients showing observed sarcolemmal instability leading to calcium mishandling and overload in cardiomyocytes (Law et al., 2020).

4.3 - Effects of isoproterenol on Col6α1 -/- trabeculae

Isoproterenol functions to increase heart contractility, heart rate and peripheral vasodilation in patients via secondary messenger systems triggered by binding to beta-1 (primarily in the heart) and beta-2 adrenergic receptors (Michael W Szymanski & Davinder P Singh, 2022). For trabeculae experiments, isoproterenol was used to stimulate this pathway and determine if there were differences in response between the knockout and wild type muscles. For each trabecula, isoproterenol increased active stress but this effect was not statistically significant due to large within group variability in baseline stress and response. Again, this variability was greater in the knockout. A significant lower diastolic stress was found in the knockout and wild type trabeculae before and after isoproterenol in addition (Figure 3.7B). This result is likely due to absence of collagen VI reducing mechanical stiffness of the heart as discussed as an explanation for increased variance of active stress. There was no significant difference in diastolic or systolic calcium ratios between groups (Figure 3.8C) likely due to errors in Ca^{2+} measurement.

The reason we expect systolic calcium to increase with the addition of isoproterenol is because the trabecula increases contractile force as shown in Figure 3.8A to almost double active stress in some trabecula. With a stronger contractile force, it is expected that more troponin is bound to calcium ions which reveal more myosin binding sites on actin filaments for myosin filaments to bind to which would produce stronger contractions. Knockout trabeculae were expected to show increased calcium ratios overall due to previous research conducted in collagen VI knockout isolated cardiomyocytes (Figure 1.24AB). It is likely with a higher statistical power there would be a statistical difference in systolic calcium between timepoints and in line with the increase in calcium shown in knockouts myocytes from precious research, as the active stress between timepoints increased for knockouts significantly (Figure 3.7B) in comparison to the lack of increase in active calcium observed.

In a study comparing MDX mice and heterozygous mice in which approximately fifty percent of cardiomyocytes had the dystrophin gene, after three months of being treated with isoproterenol, the MDX cardiomyocytes displayed significant impairments in sarcolemma integrity compared to no change in heterozygous mice (Yue et al., 2004). Researchers found that both mouse model hearts functioned adequately in a stress-free environment, and it was only upon stressing the hearts with isoproterenol that changes occurred. Hemodynamic evaluation of heart functioning after isoproterenol showed indications that the MDX mice had systolic dysfunction with a reduction in peak systolic pressure and maximal rate of pressure change in the left ventricle, along with impaired relaxation shown as an increase in the minimum diastolic rate of pressure change (Yue et al., 2004). In the knockout trabeculae, these findings may further the idea that there is an overall lack control of contraction and relaxation in systole and diastole in comparison with wild type trabeculae which would result in experiments displaying the higher

variability of results in comparison to wild type trabeculae.

4.4 – Preliminary Investigative Imaging of Biglycan

Preliminary imaging of biglycan in sections of cardiac tissue from one knockout and one wild type sample showed that biglycan was located in the t-tubules and on the cell surface (Figure 3.10). Shown in Figure 3.10C was that biglycan puncta were located approximately 100 nm from collagen VI puncta (Figure 3.10D) which is within binding distance for two molecules. This finding supports the hypothesis that biglycan links DGC to the extracellular matrix through collagen VI, however due to time constraints no further analysis or imaging could be completed.

4.5 - Limitations

Due to experimental protocols with multiple calcium concentrations, frequencies and lengths, the effect of time and stress was likely to have deteriorated trabecula integrity. The testing of the addition of isoproterenol to the solution perfusing the trabecula was at the end of the entire experimental protocol which lasted around six hours. It was common for trabecula to not respond as expected near the end of the protocol and therefore, in future reducing the protocol to testing one or two variables is recommended for these experiments. Kurihara & Konishi (1987) observed a decreased tension and therefore force in a similar trabecula protocol near the end of their experiment when compared to the beginning.

When reviewing 340nm/380nm ratio results from experiments, there were small changes observed when changing our variables (extracellular calcium, stimulation frequency, isoproterenol) normally expected to increase the calcium transient. Based on the Fura-2 AM calibration (Figure 2.5) changes in the standard curve calcium also resulted in small changes in fluorescence ratio. This indicates the system was functioning poorly with low sensitivity. If the system was performing correctly, the calcium calibration would produce larger changes in ratio readings. An improved calcium detection system would likely improve the ability to analyse changes in calcium concentration within trabeculae. Calcium detection could also be improved with a refined loading protocol as there were also instances of leakage of Fura-2 AM out of cells after the initial loading of the dye that would reduce detection sensitivity. The addition of probenecid was to stop leakage occurring, as probenecid is commonly used in calcium transient experiments since it is an inhibitor of anion transport (Robbins et al., 2012). Fura-2 AM leaking was thought to be due to either the incorrect amount probenecid added to solution after loading which would prevent the dye running out of cells due to the increase in temperature from room temperature to thirty-seven degrees in the bath and/or not enough time for the cells to perfuse in the solution. In future experiments, waiting a longer time after the addition of probenecid before the water bath was turned on for raising the solution temperature would be beneficial, as it would confirm all cells had perfused in the probenecid solution adequately to reduce the potential leakage of indicator.

The statistical power of the analysis from experiments was low indicating a much larger sample size would be required to detect differences between knockout and wild type. Shown in Figure 3.1A is a power analysis for an independent sample means test using means from the stimulation frequency of 0.1Hz, as this frequency had the largest mean difference in active stress between the knockout and control groups. Listed are the number of animals required per group (N1 and N2) required to obtain increasing power. Ideally, the standard strived for would be a power of 0.8 or an 80% chance of success when analysing data which is the most common power used in similar research papers. Shown is Figure 3.2B is a graph of estimated power and the total sample size required. As shown, the larger the sample, the greater the statistical power to detect a difference.. The number of experiments required for a power of

0.8 was not the number used in this thesis, with a minimum of 28 animals for each group required, undertaking this many experiments successfully would have taken more time than was allocated. These results mean that even though the sample size used for experiments was not large enough for statistical power, any difference between the knockout and control groups should not be excluded regardless of statistical outcome, as the tests used may have failed due to a low power.

The low power was largely driven by increased variance of the stress in the knockout trabeculae group in comparison to controls. Although, when conducting a Levene's test to determine equality of variances between those groups, the results showed that differences was deemed statistically insignificant (Appendix 1). Importantly, the significance value was P=0.059, which was close to being evidence of a statistically significant difference between our two groups of animals ($P<0.05$). A modest increase of N number would likely improve statistical power and the increase in variance in trabeculae function could be the more important parameter to determine.

4.6 - Conclusions

It was hypothesised that collagen VI binds to dystrophin within the DGC and holds it in place along the plasma membrane at the correct intervals for optimal dyad placement and cell signalling. This would mean that without collagen VI in cardiomyocytes there would be assumed disorganisation similar to that of muscle dystrophies where there was little to no dystrophin genes in cells such as DMD where there are no genes at all or BMD where there was reduced synthesis of dystrophin in cells (Bia et al., 1999). Spontaneous contractions and arrhythmic activity were observed in two of six knockout trabeculae compared to none in the wild type trabeculae which should be investigated further and is hypothesised to be result of either calcium mishandling and/or an increased contractility phenotype in the collagen VI knockouts. With not enough statistical power, differences between knockout trabeculae and wild type trabeculae in stress and intracellular calcium were not found, however, a near significant increase in variability overall from knockout trabeculae shows there may well be differences between the two groups in function. These findings demonstrated the requirement for further research and experimental design with larger sample size where enough trabeculae can be tested in order to increase statistical power to determine if there are significant trends in the knockout trabeculae, which would further the knowledge around the functioning of collagen VI.

In future research, experiments should be completed on a larger scale with more samples as well as more time between experiments for correct management and handling of equipment so that mechanical errors such as misalignment of machinery and complete calibrations can be undertaken to ensure correct excitation wavelengths are used. Having more time to improve on dissection technique paired with a

shorter protocol would have increased the likelihood of healthy trabeculae which would provide clearer results not impeded by potential muscle damage.

Appendix

Appendix 1 - Independent Samples Test using sample data from all experiments.

Independent Samples Test

		Levene's Test for Equality of Variances		t-test for Equality of Means							
						Significance		Mean	Std. Error	95% Confidence Interval of the Difference	
		F	Sig.	t	df	One-Sided p	Two-Sided p	Difference	Difference	Lower	Upper
Act_Force	Equal variances assumed	3.795	.059	2.316	38	.013	.026	9.56825	4.13172	1.20402	17.93249
	Equal variances not assumed			2.698	31.976	.006	.011	9.56825	3.54684	2.34337	16.79314

Independent Samples Effect Sizes

				95% Confidence Interval	
		Standardizer[a]	Point Estimate	Lower	Upper
Act_Force	Cohen's d	12.80168	.747	.088	1.397
	Hedges' correction	13.06147	.733	.087	1.369
	Glass's delta	6.06228	1.578	.719	2.408

a. The denominator used in estimating the effect sizes.
Cohen's d uses the pooled standard deviation.
Hedges' correction uses the pooled standard deviation, plus a correction factor.
Glass's delta uses the sample standard deviation of the control group.

Figure 5.1: Levene's test for equality of variance for active stress.

Shown is the Levene's test for equality of variance using all active force data points. This analysis shows that the larger variance in the knockout group is close to the $p<0.05$ criteria of statistical significance.

Appendix 2 - *In vitro* Fura-2 AM Calibration Curves

A.

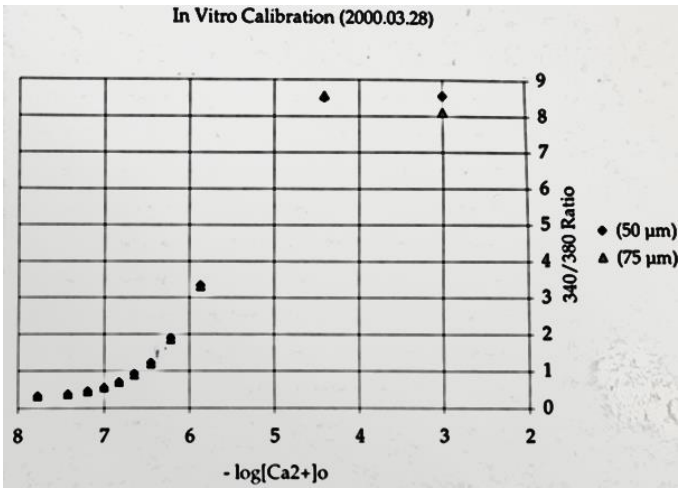

B.

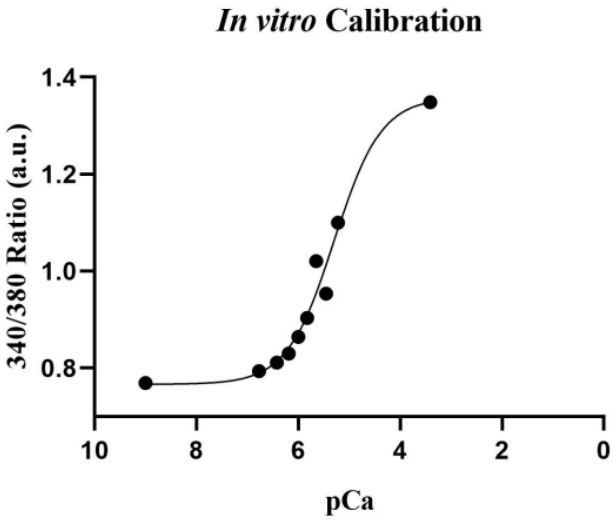

Figure 5.2: *In vitro* calibration curves of Fura-2 AM from previous uses

A. Shows the original in vitro calibration curve of the rig with an older monochromator (Dr Marie Louise Ward). This curve follows the curve obtained when in vitro calibration of Fura-2 AM was completed again for the experiments in this paper however, shown in **B.** is the last student's calibration using the same concentration kit and equipment including the new monochromator which is a sigmoidal curve rather than an exponential shape.

Figure 5.2B taken from (150): Yi Dan Liang. (2022). Impact of Dyskalaemia on Calcium Transients, Isometric Force and Excitability in isolated Right Ventricular Trabeculae. The University of Auckland.

References

Abu-Khousa, M., Fiegle, D. J., Sommer, S. T., Minabari, G., Milting, H., Heim, C., Weyand, M., Tomasi, R., Dendorfer, A., Volk, T., & Seidel, T. (2020). The Degree of t-System Remodeling Predicts Negative Force-Frequency Relationship and Prolonged Relaxation Time in Failing Human Myocardium. *Frontiers in Physiology*, *11*.

Ahmed, M. S., Øie, E., Vinge, L. E., Yndestad, A., Andersen, G. Ø., Andersson, Y., Attramadal, T., & Attramadal, H. (2003). Induction of myocardial biglycan in heart failure in rats—an extracellular matrix component targeted by AT1 receptor antagonism. *Cardiovascular Research*, *60*(3), 557–568. https://doi.org/10.1016/j.cardiores.2003.08.017

Allamand, V., Briñas, L., Richard, P., Stojkovic, T., Quijano-Roy, S., & Bonne, G. (2011). ColVI myopathies: where do we stand, where do we go? *Skeletal Muscle*, *1*(1), 1–14.

Anastasi, G., Cutroneo, G., Gaeta, R., Di Mauro, D., Arco, A., Consolo, A., Santoro, G., Trimarchi, F., & Favaloro, A. (2009). Dystrophin-glycoprotein complex and vinculin-talin-integrin system in human adult cardiac muscle. *International Journal of Molecular Medicine*, *23*(2), 149–159.

Antoine, S., Lefèvre, T., Coraboeuf, E., Nottin, R., & Coulombe, A. (1998). B-type Ca2+ channels activated by chlorpromazine and free radicals in membrane of human atrial myocytes. *Journal of Molecular and Cellular Cardiology*, *30*(12), 2623–2636.

Atherton, J. J., Sindone, A., De Pasquale, C. G., Driscoll, A., MacDonald, P. S., Hopper, I., Kistler, P., Briffa, T. G., Wong, J., Abhayaratna, W. P., Thomas, L., Audehm, R., Newton, P. J., O'Loughlin, J., Connell, C., & Branagan, M. (2018). National Heart Foundation of Australia and Cardiac Society of Australia and New Zealand: Australian clinical guidelines for the management of heart failure 2018. *Medical Journal of Australia*, *209*(8), 363–369.

Baartscheer, A., Schumacher, C. A., Belterman, C. N. W., Coronel, R., & Fiolet, J. W. T. (2003). SR calcium handling and calcium after-transients in a rabbit model of heart failure. *Cardiovascular Research*, *58*(1), 99–108. https://doi.org/10.1016/S0008-6363(02)00854-4

Backx, P. H., Gao, W. D., Azan-Backx, M. D., & Marban, E. (1995). The relationship between contractile force and intracellular [Ca2+] in intact rat cardiac trabeculae. *The Journal of General Physiology*, *105*(1), 1–19. https://doi.org/10.1085/jgp.105.1.1

Baker, N. L., Mörgelin, M., Peat, R., Goemans, N., North, K. N., Bateman, J. F., & Lamandé, S. R. (2005). Dominant collagen VI mutations are a common cause of Ullrich congenital muscular dystrophy. *Human Molecular Genetics*, *14*(2), 279–293. https://doi.org/10.1093/hmg/ddi025

Baldock, C., Sherratt, M. J., Shuttleworth, C. A., & Kielty, C. M. (2003). The supramolecular organization of collagen VI microfibrils. *Journal of Molecular Biology*, *330*(2), 297–307.

Barry, W. H., & Bridge, J. H. (1993). Intracellular calcium homeostasis in cardiac myocytes. *Circulation*, *87*(6), 1806–1815. https://doi.org/10.1161/01.CIR.87.6.1806

Benjamin, E. J., Blaha, M. J., Chiuve, S. E., Cushman, M., Das, S. R., Deo, R., De Ferranti, S. D., Floyd, J., Fornage, M., & Gillespie, C. (2017). Heart disease and stroke statistics—2017 update: a report from the American Heart Association. *Circulation*, *135*(10), e146–e603.

Berliner, D., Hänselmann, A., & Bauersachs, J. (2020). The treatment of heart failure with reduced ejection fraction. *Deutsches Ärzteblatt International*, *117*(21), 376.

Bernardi, P., & Bonaldo, P. (2008). Dysfunction of mitochondria and sarcoplasmic reticulum in the pathogenesis of collagen VI muscular dystrophies. *Annals of the New York Academy of Sciences*, *1147*(1), 303–311.

Bers, D. (2001). *Excitation-contraction coupling and cardiac contractile force* (Vol. 237). Springer Science & Business Media.

Bers, D. M. (2000). Calcium Fluxes Involved in Control of Cardiac Myocyte Contraction. *Circulation Research*, *87*(4), 275–281. https://doi.org/10.1161/01.RES.87.4.275

Bevere, M., Morabito, C., Mariggiò, M. A., & Guarnieri, S. (2022). The oxidative balance orchestrates the main keystones of the functional activity of cardiomyocytes. *Oxidative Medicine and Cellular Longevity*, *2022*.

Bhat, S. S., Ali, R., & Khanday, F. A. (2019). Syntrophins entangled in cytoskeletal meshwork: Helping to hold it all together. *Cell Proliferation*, *52*(2), e12562.

Bia, B. L., Cassidy, P. J., Young, M. E., Rafael, J. A., Leighton, B., Davies, K. E., Radda, G. K., & Clarke, K. (1999). Decreased Myocardial nNOS, Increased iNOS and Abnormal ECGs in Mouse Models of Duchenne Muscular Dystrophy. *Journal of Molecular and Cellular Cardiology*, *31*(10), 1857–1862. https://doi.org/https://doi.org/10.1006/jmcc.1999.1018

Bloom, M. W., Greenberg, B., Jaarsma, T., Januzzi, J. L., Lam, C. S. P., Maggioni, A. P., Trochu, J.-N., & Butler, J. (2017). Heart failure with reduced ejection fraction. *Nature Reviews Disease Primers*, *3*(1), 1–19.

Bonaldo, P., Braghetta, P., Zanetti, M., Piccolo, S., Volpin, D., & Bressan, G. M. (1998). Collagen VI deficiency induces early onset myopathy in the mouse: an animal model for Bethlem myopathy. *Human Molecular Genetics*, *7*(13), 2135–2140.

Bootman, M. D., & Rietdorf, K. (2017). *Tissue Specificity: Store-Operated Ca2+ Entry in Cardiac Myocytes* (pp. 363–387). https://doi.org/10.1007/978-3-319-57732-6_19

Borlaug, B. A. (2014). The pathophysiology of heart failure with preserved ejection fraction. *Nature Reviews Cardiology*, *11*(9), 507–515.

Borlaug, B. A., Jaber, W. A., Ommen, S. R., Lam, C. S. P., Redfield, M. M., & Nishimura, R. A. (2011). Diastolic relaxation and compliance reserve during dynamic exercise in heart failure with preserved ejection fraction. *Heart*, *97*(12), 964–969.

Borlaug, B. A., & Kass, D. A. (2011). Ventricular–vascular interaction in heart failure. *Cardiology Clinics*, *29*(3), 447–459.

Bowe, M. A., Mendis, D. B., & Fallon, J. R. (2000). The small leucine-rich repeat proteoglycan biglycan binds to α-dystroglycan and is upregulated in dystrophic muscle. *The Journal of Cell Biology*, *148*(4), 801–810.

Braunwald, E. (1997). Cardiovascular medicine at the turn of the millennium: triumphs, concerns, and opportunities. *New England Journal of Medicine*, *337*(19), 1360–1369.

Breuer, B., Schmidt, G., & Kresse, H. (1990). Non-uniform influence of transforming growth factor-β on the biosynthesis of different forms of small chondroitin sulphate/dermatan sulphate proteoglycan. *Biochemical Journal*, *269*(2), 551–554. https://doi.org/10.1042/bj2690551

Camejo, G., Hurt-Camejo, E., Wiklund, O., & Bondjers, G. (1998). Association of apo B lipoproteins with arterial proteoglycans: Pathological significance and molecular basis. *Atherosclerosis*, *139*(2), 205–222. https://doi.org/https://doi.org/10.1016/S0021-9150(98)00107-5

Campbell, K. P., & Kahl, S. D. (1989). Association of dystrophin and an integral membrane glycoprotein. *Nature*, *338*(6212), 259–262.

Campbell, R. T., Jhund, P. S., Castagno, D., Hawkins, N. M., Petrie, M. C., & McMurray, J. J. V. (2012). What have we learned about patients with heart failure and preserved ejection fraction from DIG-PEF, CHARM-preserved, and I-PRESERVE? *Journal of the American College of Cardiology*, *60*(23), 2349–2356.

Chan, D. Z. L., Kerr, A., Grey, C., Selak, V., Lee, M. A. W., Lund, M., Poppe, K., & Doughty, R. N. (2022). Contrasting trends in heart failure incidence in younger and older New Zealanders, 2006–2018. *Heart*, *108*(4), 300. https://doi.org/10.1136/heartjnl-2021-319853

Chan, W. C., Wright, C., Riddell, T., Wells, S., Kerr, A. J., Gala, G., & Jackson, R. (2008). Ethnic and socioeconomic disparities in the prevalence of cardiovascular disease in New Zealand. *The New Zealand Medical Journal (Online)*, *121*(1285).

Chenard, A. A., Becane, H. M., Tertrain, F., De Kermadec, J. M., & Weiss, Y. A. (1993). Ventricular arrhythmia in Duchenne muscular dystrophy: prevalence, significance and prognosis. *Neuromuscular Disorders*, *3*(3), 201–206.

Cheng, H., & Lederer, W. J. (2008). Calcium Sparks. *Physiological Reviews*, *88*(4), 1491–1545. https://doi.org/10.1152/physrev.00030.2007

Chirinos, J. A., Zhao, L., Reese-Petersen, A. L., Cohen, J. B., Genovese, F., Richards, A. M., Doughty, R. N., Díez, J., González, A., & Querejeta, R. (2022). Endotrophin, a collagen VI formation–derived peptide, in heart failure. *NEJM Evidence*, *1*(10), EVIDoa2200091.

Chung, J.-H., Biesiadecki, B. J., Ziolo, M. T., Davis, J. P., & Janssen, P. M. L. (2016). Myofilament calcium sensitivity: role in regulation of in vivo cardiac contraction and relaxation. *Frontiers in Physiology*, *7*, 562.

Contard, F., Koteliansky, V., Marotte, F., Dubus, I., Rappaport, L., & Samuel, J. L. (1991). Specific alterations in the distribution of extracellular matrix components within rat myocardium during the

development of pressure overload. *Laboratory Investigation; a Journal of Technical Methods and Pathology*, *64*(1), 65–75.

Coulombe, A., Lefèvre, I. A., Baro, I., & Coraboeuf, E. (1989). Barium-and calcium-permeable channels open at negative membrane potentials in rat ventricular myocytes. *The Journal of Membrane Biology*, *111*, 57–67.

Cowie, M. R., Wood, D. A., Coats, A. J. S., Thompson, S. G., Poole-Wilson, P. A., Suresh, V., & Sutton, G. C. (1999). Incidence and aetiology of heart failure; a population-based study. *European Heart Journal*, *20*(6), 421–428.

Crossman, D. J., Shen, X., Jüllig, M., Munro, M., Hou, Y., Middleditch, M., Shrestha, D., Li, A., Lal, S., & Dos Remedios, C. G. (2017). Increased collagen within the transverse tubules in human heart failure. *Cardiovascular Research*, *113*(8), 879–891.

Das, D. K., Engelman, R. M., Rousou, J. A., & Breyer, R. H. (1987). Aerobic vs anaerobic metabolism during ischemia in heart muscle. *Annales Chirurgiae et Gynaecologiae*, *76*(1), 68–76.

Doggrell, S. A., & Brown, L. (1998). Rat models of hypertension, cardiac hypertrophy and failure. *Cardiovascular Research*, *39*(1), 89–105.

Eder, P., & Molkentin, J. D. (2011). TRPC channels as effectors of cardiac hypertrophy. *Circulation Research*, *108*(2), 265–272.

Endoh, M. (2004). Force-frequency relationship in intact mammalian ventricular myocardium: physiological and pathophysiological relevance. *European Journal of Pharmacology*, *500*(1–3), 73–86. https://doi.org/10.1016/j.ejphar.2004.07.013

Fatemifar, F., Feldman, M. D., Oglesby, M., & Han, H.-C. (2018). Comparison of Biomechanical Properties and Microstructure of Trabeculae Carneae, Papillary Muscles, and Myocardium in the Human Heart. *Journal of Biomechanical Engineering*, *141*(2). https://doi.org/10.1115/1.4041966

Feher, J. J. (2017). *Quantitative human physiology: an introduction*. Academic press.

Finsterer, J., & Stöllberger, C. (2003). The heart in human dystrophinopathies. *Cardiology*, *99*(1), 1–19.

Fisher, L. W., Termine, J. D., & Young, M. F. (1989). Deduced protein sequence of bone small proteoglycan I (biglycan) shows homology with proteoglycan II (decorin) and several nonconnective tissue proteins in a variety of species. *Journal of Biological Chemistry*, *264*(8), 4571–4576. https://doi.org/https://doi.org/10.1016/S0021-9258(18)83781-4

Fitzgerald, J., Rich, C., Zhou, F. H., & Hansen, U. (2008). Three novel collagen VI chains, α4 (VI), α5 (VI), and α6 (VI). *Journal of Biological Chemistry*, *283*(29), 20170–20180.

Frank, O. (1895). Zur dynamik des herzmuskels. *Zeitschr. Biol.*, *32*, 370–437.

Gao, W. D., Perez, N. G., & Marban, E. (1998). Calcium cycling and contractile activation in intact mouse cardiac muscle. *The Journal of Physiology*, *507*(1), 175–184. https://doi.org/10.1111/j.1469-7793.1998.175bu.x

García-Pelagio, K. P., Bloch, R. J., Ortega, A., & González-Serratos, H. (2006). Elastic Properties of the Sarcolemma-Costamere Complex of Muscle Cells in Normal Mice. *AIP Conference Proceedings*, *854*(1), 51–53.

Goodenough, D. A., & Paul, D. L. (2009). Gap junctions. *Cold Spring Harbor Perspectives in Biology*, *1*(1), a002576.

Groulx, J.-F., Gagné, D., Benoit, Y. D., Martel, D., Basora, N., & Beaulieu, J.-F. (2011). Collagen VI is a basement membrane component that regulates epithelial cell–fibronectin interactions. *Matrix Biology*, *30*(3), 195–206.

Grynkiewicz, G., Poenie, M., & Tsien, R. Y. (1985). A new generation of Ca2+ indicators with greatly improved fluorescence properties. *Journal of Biological Chemistry*, *260*(6), 3440–3450. https://doi.org/10.1016/S0021-9258(19)83641-4

Hainsey, T. A., Senapati, S., Kuhn, D. E., & Rafael, J. A. (2003). Cardiomyopathic features associated with muscular dystrophy are independent of dystrophin absence in cardiovasculature. *Neuromuscular Disorders*, *13*(4), 294–302.

Han, J.-C., Taberner, A. J., Nielsen, P. M. F., Kirton, R. S., Ward, M.-L., & Loiselle, D. S. (2010). Energetics of stress production in isolated cardiac trabeculae from the rat. *American Journal of Physiology-Heart and Circulatory Physiology*, *299*(5), H1382–H1394.

Heijman, J., Voigt, N., Nattel, S., & Dobrev, D. (2014). Cellular and molecular electrophysiology of atrial fibrillation initiation, maintenance, and progression. *Circulation Research*, *114*(9), 1483–1499.

Heinzel, F. R., Bito, V., Biesmans, L., Wu, M., Detre, E., Von Wegner, F., Claus, P., Dymarkowski, S., Maes, F., & Bogaert, J. (2008). Remodeling of T-tubules and reduced synchrony of Ca2+ release in myocytes from chronically ischemic myocardium. *Circulation Research*, *102*(3), 338–346.

Ho, K. K. L., Pinsky, J. L., Kannel, W. B., & Levy, D. (1993). The epidemiology of heart failure: the Framingham Study. *Journal of the American College of Cardiology*, *22*(4), A6–A13.

Hong, T., Yang, H., Zhang, S.-S., Cho, H. C., Kalashnikova, M., Sun, B., Zhang, H., Bhargava, A., Grabe, M., Olgin, J., Gorelik, J., Marbán, E., Jan, L. Y., & Shaw, R. M. (2014). Cardiac BIN1 folds T-tubule membrane, controlling ion flux and limiting arrhythmia. *Nature Medicine*, *20*(6), 624–632. https://doi.org/10.1038/nm.3543

Horn, M. A., & Trafford, A. W. (2016). Aging and the cardiac collagen matrix: Novel mediators of fibrotic remodelling. *Journal of Molecular and Cellular Cardiology*, *93*, 175–185.

Howe, K., Ross, J. M., Loiselle, D. S., Han, J.-C., & Crossman, D. J. (2021). Right-sided heart failure is also associated with transverse tubule remodeling in the left ventricle. *American Journal of Physiology-Heart and Circulatory Physiology*, *321*(5), H940–H947.

Ibrahim, M., Al Masri, A., Navaratnarajah, M., Siedlecka, U., Soppa, G. K., Moshkov, A., Abou Al-Saud, S., Gorelik, J., Yacoub, M. H., & Terracciano, C. M. N. (2010). Prolonged mechanical

unloading affects cardiomyocyte excitation-contraction coupling, transverse-tubule structure, and the cell surface. *The FASEB Journal*, *24*(9), 3321.

Ibrahim, M., Kukadia, P., Siedlecka, U., Cartledge, J. E., Navaratnarajah, M., Tokar, S., Van Doorn, C., Tsang, V. T., Gorelik, J., & Yacoub, M. H. (2012). Cardiomyocyte Ca 2+ handling and structure is regulated by degree and duration of mechanical load variation. *Journal of Cellular and Molecular Medicine*, *16*(12), 2910–2918.

Irwin, W. A., Bergamin, N., Sabatelli, P., Reggiani, C., Megighian, A., Merlini, L., Braghetta, P., Columbaro, M., Volpin, D., & Bressan, G. M. (2003). Mitochondrial dysfunction and apoptosis in myopathic mice with collagen VI deficiency. *Nature Genetics*, *35*(4), 367–371.

Itzhaki, I., Rapoport, S., Huber, I., Mizrahi, I., Zwi-Dantsis, L., Arbel, G., Schiller, J., & Gepstein, L. (2011). Calcium handling in human induced pluripotent stem cell derived cardiomyocytes. *PloS One*, *6*(4), e18037.

J, M. A., F, B. J., B, D. J., Kai, G., George, F., Scott, D. P., Raymond, M., Christian, R., Reinhard, G., H, R. A., Neelima, S., Peralta, S. A., & C, P. G. (2003). Targeted Disruption of the Murine Bin1/Amphiphysin II Gene Does Not Disable Endocytosis but Results in Embryonic Cardiomyopathy with Aberrant Myofibril Formation. *Molecular and Cellular Biology*, *23*(12), 4295–4306. https://doi.org/10.1128/MCB.23.12.4295-4306.2003

Janicki, J. S. (1992). Myocardial collagen remodeling and left ventricular diastolic function. *Brazilian Journal of Medical and Biological Research= Revista Brasileira de Pesquisas Medicas e Biologicas*, *25*(10), 975–982.

Janssen, P. M., & de Tombe, P. P. (1997). Uncontrolled sarcomere shortening increases intracellular Ca2+ transient in rat cardiac trabeculae. *American Journal of Physiology-Heart and Circulatory Physiology*, *272*(4), H1892–H1897.

Jideama, N. M., Crawford, B. H., Hussain, A. K. M. A., & Raynor, R. L. (2006). Dephosphorylation specificities of protein phosphatase for cardiac troponin I, troponin T, and sites within troponin T. *International Journal of Biological Sciences*, *2*(1), 1–9. https://doi.org/10.7150/ijbs.2.1

Jones, P. P., MacQuaide, N., & Louch, W. E. (2018). Dyadic plasticity in cardiomyocytes. *Frontiers in Physiology*, *9*, 1773.

Kania, G., Blyszczuk, P., & Eriksson, U. (2009). Mechanisms of cardiac fibrosis in inflammatory heart disease. *Trends in Cardiovascular Medicine*, *19*(8), 247–252.

Kanzaki, Y., Terasaki, F., Okabe, M., Fujita, S., Katashima, T., Otsuka, K., & Ishizaka, N. (2010). Three-Dimensional Architecture of Cardiomyocytes and Connective Tissue in Human Heart Revealed by Scanning Electron Microscopy. *Circulation*, *122*(19), 1973–1974. https://doi.org/10.1161/CIRCULATIONAHA.110.979815

Kaprielian, R. R., Stevenson, S., Rothery, S. M., Cullen, M. J., & Severs, N. J. (2000). Distinct patterns of dystrophin organization in myocyte sarcolemma and transverse tubules of normal and diseased human myocardium. *Circulation*, *101*(22), 2586–2594.

Karsdal, M. (2019). *Biochemistry of collagens, laminins and elastin: structure, function and biomarkers*. Academic Press.

Kemp, C. D., & Conte, J. V. (2012). The pathophysiology of heart failure. *Cardiovascular Pathology*, *21*(5), 365–371. https://doi.org/https://doi.org/10.1016/j.carpath.2011.11.007

Konhilas, J. P., Irving, T. C., & de Tombe, P. P. (2002). Frank-Starling law of the heart and the cellular mechanisms of length-dependent activation. *Pflügers Archiv-European Journal of Physiology*, *445*(3), 305.

Konstandin, M. H., Toko, H., Gastelum, G. M., Quijada, P., De La Torre, A., Quintana, M., Collins, B., Din, S., Avitabile, D., & Völkers, M. (2013). Fibronectin is essential for reparative cardiac progenitor cell response after myocardial infarction. *Circulation Research*, *113*(2), 115–125.

Kuo, H.-J., Maslen, C. L., Keene, D. R., & Glanville, R. W. (1997). Type VI collagen anchors endothelial basement membranes by interacting with type IV collagen. *Journal of Biological Chemistry*, *272*(42), 26522–26529.

Kurt W. Prins, L, A. M., Huiliang, Z., Wang, W., & M, M. J. (2016). Microtubule-Mediated Misregulation of Junctophilin-2 Underlies T-Tubule Disruptions and Calcium Mishandling in mdx Mice. *JACC: Basic to Translational Science*, *1*(3), 122–130.

Kuwahara, K., Wang, Y., McAnally, J., Richardson, J. A., Bassel-Duby, R., Hill, J. A., & Olson, E. N. (2006). TRPC6 fulfills a calcineurin signaling circuit during pathologic cardiac remodeling. *The Journal of Clinical Investigation*, *116*(12), 3114–3126. https://doi.org/10.1172/JCI27702

Lam, C. S. P., Gamble, G. D., Ling, L. H., Sim, D., Leong, K. T. G., Yeo, P. S. D., Ong, H. Y., Jaufeerally, F., Ng, T. P., & Cameron, V. A. (2018). Mortality associated with heart failure with preserved vs. reduced ejection fraction in a prospective international multi-ethnic cohort study. *European Heart Journal*, *39*(20), 1770–1780.

Landstrom, A. P., Weisleder, N., Batalden, K. B., Bos, J. M., Tester, D. J., Ommen, S. R., Wehrens, X. H. T., Claycomb, W. C., Ko, J.-K., & Hwang, M. (2007). Mutations in JPH2-encoded junctophilin-2 associated with hypertrophic cardiomyopathy in humans. *Journal of Molecular and Cellular Cardiology*, *42*(6), 1026–1035.

Lapidos, K. A., Kakkar, R., & McNally, E. M. (2004). The Dystrophin Glycoprotein Complex. *Circulation Research*, *94*(8), 1023–1031. https://doi.org/10.1161/01.RES.0000126574.61061.25

Law, M. L., Cohen, H., Martin, A. A., Angulski, A. B. B., & Metzger, J. M. (2020). Dysregulation of Calcium Handling in Duchenne Muscular Dystrophy-Associated Dilated Cardiomyopathy: Mechanisms and Experimental Therapeutic Strategies. *Journal of Clinical Medicine*, *9*(2). https://doi.org/10.3390/jcm9020520

Lawson, C. A., Zaccardi, F., Squire, I., Ling, S., Davies, M. J., Lam, C. S. P., Mamas, M. A., Khunti, K., & Kadam, U. T. (2019). 20-year trends in cause-specific heart failure outcomes by sex, socioeconomic status, and place of diagnosis: a population-based study. *The Lancet Public Health*, *4*(8), e406–e420.

Layland, J., & Kentish, J. C. (1999). Positive force- and [Ca2+]-frequency relationships in rat ventricular trabeculae at physiological frequencies. *American Journal of Physiology-Heart and Circulatory Physiology*, *276*(1), H9–H18. https://doi.org/10.1152/ajpheart.1999.276.1.H9

Lee, D. S., Gona, P., Albano, I., Larson, M. G., Benjamin, E. J., Levy, D., Kannel, W. B., & Vasan, R. S. (2011). A systematic assessment of causes of death after heart failure onset in the community: impact of age at death, time period, and left ventricular systolic dysfunction. *Circulation: Heart Failure*, *4*(1), 36–43.

Lekavich, C. L., Barksdale, D. J., Neelon, V., & Wu, J.-R. (2015). Heart failure preserved ejection fraction (HFpEF): an integrated and strategic review. *Heart Failure Reviews*, *20*, 643–653.

Li, N., Chiang, D. Y., Wang, S., Wang, Q., Sun, L., Voigt, N., Respress, J. L., Ather, S., Skapura, D. G., & Jordan, V. K. (2014). Ryanodine receptor–mediated calcium leak drives progressive development of an atrial fibrillation substrate in a transgenic mouse model. *Circulation*, *129*(12), 1276–1285.

Lilly, L. S. (2012). *Pathophysiology of heart disease: a collaborative project of medical students and faculty*. Lippincott Williams & Wilkins.

Lind, M., Hayes, A., Caprnda, M., Petrovic, D., Rodrigo, L., Kruzliak, P., & Zulli, A. (2017). Inducible nitric oxide synthase: good or bad? *Biomedicine & Pharmacotherapy*, *93*, 370–375.

Lipsett, D. B., Frisk, M., Aronsen, J. M., Norden, E. S., Buonarati, O. R., Cataliotti, A., Hell, J. W., Sjaastad, I., Christensen, G., & Louch, W. E. (2019). Cardiomyocyte substructure reverts to an immature phenotype during heart failure. *The Journal of Physiology*, *597*(7), 1833–1853.

Louch, W. E., Sejersted, O. M., & Swift, F. (2010). There Goes the Neighborhood: Pathological Alterations in T-Tubule Morphology and Consequences for Cardiomyocyte C a **2**+ Handling. *Journal of Biomedicine and Biotechnology*, *2010*.

Lu, F., Ma, Q., Xie, W., Liou, C. L., Zhang, D., Sweat, M. E., Jardin, B. D., Naya, F. J., Guo, Y., & Cheng, H. (2022). CMYA5 establishes cardiac dyad architecture and positioning. *Nature Communications*, *13*(1), 2185.

Lu, F., & Pu, W. T. (2020). The architecture and function of cardiac dyads. *Biophysical Reviews*, *12*(4), 1007–1017.

Luo, J., Xuan, Y.-T., Gu, Y., & Prabhu, S. D. (2006). Prolonged oxidative stress inverts the cardiac force–frequency relation: role of altered calcium handling and myofilament calcium responsiveness. *Journal of Molecular and Cellular Cardiology*, *40*(1), 64–75.

Luther, D. J., Thodeti, C. K., Shamhart, P. E., Adapala, R. K., Hodnichak, C., Weihrauch, D., Bonaldo, P., Chilian, W. M., & Meszaros, J. G. (2012). Absence of type VI collagen paradoxically improves

cardiac function, structure, and remodeling after myocardial infarction. *Circulation Research*, *110*(6), 851–856.

Maron, B. J., Ferrans, V. J., & Roberts, W. C. (1975). Ultrastructural features of degenerated cardiac muscle cells in patients with cardiac hypertrophy. *The American Journal of Pathology*, *79*(3), 387.

Matsubara, L. S., Matsubara, B. B., Okoshi, M. P., Cicogna, A. C., & Janicki, J. S. (2000). Alterations in myocardial collagen content affect rat papillary muscle function. *American Journal of Physiology-Heart and Circulatory Physiology*, *279*(4), H1534–H1539. https://doi.org/10.1152/ajpheart.2000.279.4.H1534

Mercadier, J. J., Lompré, A. M., Duc, P., Boheler, K. R., Fraysse, J. B., Wisnewsky, C., Allen, P. D., Komajda, M., & Schwartz, K. (1990). Altered sarcoplasmic reticulum Ca2(+)-ATPase gene expression in the human ventricle during end-stage heart failure. *The Journal of Clinical Investigation*, *85*(1), 305–309. https://doi.org/10.1172/JCI114429

Meyer, H. V, Dawes, T. J. W., Serrani, M., Bai, W., Tokarczuk, P., Cai, J., de Marvao, A., Henry, A., Lumbers, R. T., & Gierten, J. (2020). Genetic and functional insights into the fractal structure of the heart. *Nature*, *584*(7822), 589–594.

Michael W Szymanski, & Davinder P Singh. (2022, September 27). *Isoproterenol*. StatPearls [Internet].

Milani-Nejad, N., & Janssen, P. M. L. (2014). Small and large animal models in cardiac contraction research: advantages and disadvantages. *Pharmacology & Therapeutics*, *141*(3), 235–249.

Morgan, J. P., Erny, R. E., Allen, P. D., Grossman, W., & Gwathmey, J. K. (1990). Abnormal intracellular calcium handling, a major cause of systolic and diastolic dysfunction in ventricular myocardium from patients with heart failure. *Circulation*, *81*(2 Suppl), III21-32. http://europepmc.org/abstract/MED/2153479

Murphy, S. P., Ibrahim, N. E., & Januzzi, J. L. (2020). Heart failure with reduced ejection fraction: a review. *Jama*, *324*(5), 488–504.

Nakayama, H., Wilkin, B. J., Bodi, I., & Molkentin, J. D. (2006). Calcineurin-dependent cardiac hypertrophy is activated by TRPC in the adult mouse heart. *The FASEB Journal: Official Publication of the Federation of American Societies for Experimental Biology*, *20*(10), 1660.

Natera-de Benito, D., Alarcon, M., Ortez, C., Nascimento, A., Jou, C., Medina, J., Vigo, M., Codina, A., Frongia, A., Colomer, J., & Jimenez-Mallebrera, C. (2017). Clinical and genetic characterization of collagen VI-related myopathies: difficulties in phenotypic characterization in the first years of life. *Neuromuscular Disorders*, *27*, S105. https://doi.org/10.1016/j.nmd.2017.06.052

Naugle, J. E., Olson, E. R., Zhang, X., Mase, S. E., Pilati, C. F., Maron, M. B., Folkesson, H. G., Horne, W. I., Doane, K. J., & Meszaros, J. G. (2006). Type VI collagen induces cardiac myofibroblast differentiation: implications for postinfarction remodeling. *American Journal of Physiology-Heart and Circulatory Physiology*, *290*(1), H323–H330.

Oono, T., Specks, U., Eckes, B., Majewski, S., Hunzelmann, N., Timpl, R., & Krieg, T. (1993). Expression of type VI collagen mRNA during wound healing. *Journal of Investigative Dermatology*, *100*(3), 329–334.

Page, E., & McCallister, L. P. (1973). Quantitative electron microscopic description of heart muscle cells: application to normal, hypertrophied and thyroxin-stimulated hearts. *The American Journal of Cardiology*, *31*(2), 172–181.

Panadés-de Oliveira, L., Rodríguez-López, C., Cantero Montenegro, D., Marcos Toledano, M. del M., Fernández-Marmiesse, A., Esteban Pérez, J., Hernández Lain, A., & Domínguez-González, C. (2019). Bethlem myopathy: a series of 16 patients and description of seven new associated mutations. *Journal of Neurology*, *266*(4), 934–941. https://doi.org/10.1007/s00415-019-09217-z

Peat, R. A., Gécz, J., Fallon, J. R., Tarpey, P. S., Smith, R., Futreal, A., Stratton, M. R., Lamandé, S. R., Yang, N., & North, K. N. (2008). Exclusion of biglycan mutations in a cohort of patients with neuromuscular disorders. *Neuromuscular Disorders*, *18*(8), 606–609.

Pfeffer, M. A., Shah, A. M., & Borlaug, B. A. (2019). Heart failure with preserved ejection fraction in perspective. *Circulation Research*, *124*(11), 1598–1617.

Polyakova, V., Loeffler, I., Hein, S., Miyagawa, S., Piotrowska, I., Dammer, S., Risteli, J., Schaper, J., & Kostin, S. (2011). Fibrosis in endstage human heart failure: severe changes in collagen metabolism and MMP/TIMP profiles. *International Journal of Cardiology*, *151*(1), 18–33.

Querejeta, R., López, B., González, A., Sánchez, E., Larman, M., Martínez Ubago, J. L., & Díez, J. (2004). Increased collagen type I synthesis in patients with heart failure of hypertensive origin: relation to myocardial fibrosis. *Circulation*, *110*(10), 1263–1268.

Rafii, M. S., Hagiwara, H., Mercado, M. L., Seo, N. S., Xu, T., Dugan, T., Owens, R. T., Hook, M., McQuillan, D. J., & Young, M. F. (2006). Biglycan binds to α-and γ-sarcoglycan and regulates their expression during development. *Journal of Cellular Physiology*, *209*(2), 439–447.

Rando, T. A. (2001). The dystrophin–glycoprotein complex, cellular signaling, and the regulation of cell survival in the muscular dystrophies. *Muscle & Nerve*, *24*(12), 1575–1594.

Reese-Petersen, A. L., Gonzalez, A., Lopez, B., Ravassa, S., Karsdal, M., Genovese, F., & Diez, J. (2021). Endotrophin is significantly associated with disease severity and increased risk of adverse outcome in HFpEF but not in HFrEF patients. *European Heart Journal*, *42*(Supplement_1), ehab724.0732. https://doi.org/10.1093/eurheartj/ehab724.0732

Ricard-Blum, S. (2011). The collagen family. *Cold Spring Harbor Perspectives in Biology*, *3*(1), a004978.

Riddell, T. (2005). *Heart failure hospitalisations and deaths in New Zealand: patterns by deprivation and ethnicity*.

Riessen, R., Isner, J. M., Blessing, E., Loushin, C., Nikol, S., & Wight, T. N. (1994). Regional differences in the distribution of the proteoglycans biglycan and decorin in the extracellular matrix of

atherosclerotic and restenotic human coronary arteries. *The American Journal of Pathology*, *144*(5), 962–974. http://europepmc.org/abstract/MED/8178945

Robbins, N., Koch, S. E., Tranter, M., & Rubinstein, J. (2012). The History and Future of Probenecid. *Cardiovascular Toxicology*, *12*(1), 1–9. https://doi.org/10.1007/s12012-011-9145-8

Sabatelli, P., Bonaldo, P., Lattanzi, G., Braghetta, P., Bergamin, N., Capanni, C., Mattioli, E., Columbaro, M., Ognibene, A., & Pepe, G. (2001). Collagen VI deficiency affects the organization of fibronectin in the extracellular matrix of cultured fibroblasts. *Matrix Biology*, *20*(7), 475–486.

Sabatelli, P., Gualandi, F., Gara, S. K., Grumati, P., Zamparelli, A., Martoni, E., Pellegrini, C., Merlini, L., Ferlini, A., & Bonaldo, P. (2012). Expression of collagen VI α5 and α6 chains in human muscle and in Duchenne muscular dystrophy-related muscle fibrosis. *Matrix Biology*, *31*(3), 187–196.

Sacconi, L., Ferrantini, C., Lotti, J., Coppini, R., Yan, P., Loew, L. M., Tesi, C., Cerbai, E., Poggesi, C., & Pavone, F. S. (2012). Action potential propagation in transverse-axial tubular system is impaired in heart failure. *Proceedings of the National Academy of Sciences*, *109*(15), 5815–5819.

Samarel, A. M. (2005). Costameres, focal adhesions, and cardiomyocyte mechanotransduction. *American Journal of Physiology-Heart and Circulatory Physiology*, *289*(6), H2291–H2301.

Sander, M., Chavoshan, B., Harris, S. A., Iannaccone, S. T., Stull, J. T., Thomas, G. D., & Victor, R. G. (2000). Functional muscle ischemia in neuronal nitric oxide synthase-deficient skeletal muscle of children with Duchenne muscular dystrophy. *Proceedings of the National Academy of Sciences*, *97*(25), 13818–13823.

Savji, N., Meijers, W. C., Bartz, T. M., Bhambhani, V., Cushman, M., Nayor, M., Kizer, J. R., Sarma, A., Blaha, M. J., & Gansevoort, R. T. (2018). The association of obesity and cardiometabolic traits with incident HFpEF and HFrEF. *JACC: Heart Failure*, *6*(8), 701–709.

Schaper, J., Froede, R., Hein, S. T., Buck, A., Hashizume, H., Speiser, B., Friedl, A., & Bleese, N. (1991). Impairment of the myocardial ultrastructure and changes of the cytoskeleton in dilated cardiomyopathy. *Circulation*, *83*(2), 504–514.

Schobesberger, S., Wright, P., Tokar, S., Bhargava, A., Mansfield, C., Glukhov, A. V, Poulet, C., Buzuk, A., Monszpart, A., & Sikkel, M. (2017). T-tubule remodelling disturbs localized β2-adrenergic signalling in rat ventricular myocytes during the progression of heart failure. *Cardiovascular Research*, *113*(7), 770–782.

Schönherr, E., Järveläinen, H. T., Kinsella, M. G., Sandell, L. J., & Wight, T. N. (1993). Platelet-derived growth factor and transforming growth factor-beta 1 differentially affect the synthesis of biglycan and decorin by monkey arterial smooth muscle cells. *Arteriosclerosis and Thrombosis: A Journal of Vascular Biology*, *13*(7), 1026–1036. https://doi.org/10.1161/01.ATV.13.7.1026

Seo, K., Rainer, P. P., Lee, D., Hao, S., Bedja, D., Birnbaumer, L., Cingolani, O. H., & Kass, D. A. (2014). Hyperactive Adverse Mechanical Stress Responses in Dystrophic Heart Are Coupled to

Transient Receptor Potential Canonical 6 and Blocked by cGMP–Protein Kinase G Modulation. *Circulation Research*, *114*(5), 823–832. https://doi.org/10.1161/CIRCRESAHA.114.302614

Song, K. S., Kim, H. K., Shim, W., & Jee, S. H. (2001). Plasma fibronectin levels in ischemic heart disease. *Atherosclerosis*, *154*(2), 449–453. https://doi.org/https://doi.org/10.1016/S0021-9150(00)00490-1

Song, L.-S., Sobie, E. A., McCulle, S., Lederer, W. J., Balke, C. W., & Cheng, H. (2006). Orphaned ryanodine receptors in the failing heart. *Proceedings of the National Academy of Sciences*, *103*(11), 4305–4310.

Starling, E. H., & Visscher, M. (1927). The regulation of the energy output of the heart. *The Journal of Physiology*, *62*(3), 243.

Steinberg, B. A., Zhao, X., Heidenreich, P. A., Peterson, E. D., Bhatt, D. L., Cannon, C. P., Hernandez, A. F., & Fonarow, G. C. (2012). Trends in patients hospitalized with heart failure and preserved left ventricular ejection fraction: prevalence, therapies, and outcomes. *Circulation*, *126*(1), 65–75.

Sun, Y., Lee, S.-M., Ku, B.-J., & Moon, M.-J. (2020). Fine structure of the intercalated disc and cardiac junctions in the black widow spider Latrodectus mactans. *Applied Microscopy*, *50*, 1–9.

Sutanto, H., Lyon, A., Lumens, J., Schotten, U., Dobrev, D., & Heijman, J. (2020). Cardiomyocyte calcium handling in health and disease: Insights from in vitro and in silico studies. *Progress in Biophysics and Molecular Biology*, *157*, 54–75.

Sztretye, M., Szabó, L., Dobrosi, N., Fodor, J., Szentesi, P., Almássy, J., Magyar, Z. É., Dienes, B., & Csernoch, L. (2020). From mice to humans: an overview of the potentials and limitations of current transgenic mouse models of major muscular dystrophies and congenital myopathies. *International Journal of Molecular Sciences*, *21*(23), 8935.

Takeuchi, A., & Matsuoka, S. (2022). Spatial and Functional Crosstalk between the Mitochondrial Na+-Ca2+ Exchanger NCLX and the Sarcoplasmic Reticulum Ca2+ Pump SERCA in Cardiomyocytes. *International Journal of Molecular Sciences*, *23*(14), 7948.

Torr, E. E., Ngam, C. R., Bernau, K., Tomasini-Johansson, B., Acton, B., & Sandbo, N. (2015). Myofibroblasts exhibit enhanced fibronectin assembly that is intrinsic to their contractile phenotype. *Journal of Biological Chemistry*, *290*(11), 6951–6961.

Trafford, A. W., Díaz, M. E., & Eisner, D. A. (1999). A novel, rapid and reversible method to measure Ca buffering and time-course of total sarcoplasmic reticulum Ca content in cardiac ventricular myocytes. *Pflügers Archiv*, *437*(3), 501–503. https://doi.org/10.1007/s004240050808

Travers, J. G., Kamal, F. A., Robbins, J., Yutzey, K. E., & Blaxall, B. C. (2016). Cardiac fibrosis: the fibroblast awakens. *Circulation Research*, *118*(6), 1021–1040.

Valiente-Alandi, I., Potter, S. J., Salvador, A. M., Schafer, A. E., Schips, T., Carrillo-Salinas, F., Gibson, A. M., Nieman, M. L., Perkins, C., & Sargent, M. A. (2018). Inhibiting fibronectin attenuates fibrosis and improves cardiac function in a model of heart failure. *Circulation*, *138*(12), 1236–1252.

Van Oort, R. J., Garbino, A., Wang, W., Dixit, S. S., Landstrom, A. P., Gaur, N., De Almeida, A. C., Skapura, D. G., Rudy, Y., & Burns, A. R. (2011). Disrupted junctional membrane complexes and hyperactive ryanodine receptors after acute junctophilin knockdown in mice. *Circulation*, *123*(9), 979–988.

van Spreeuwel, A. C. C., Bax, N. A. M., van Nierop, B. J., Aartsma-Rus, A., Goumans, M.-J. T. H., & Bouten, C. V. C. (2017). Mimicking cardiac fibrosis in a dish: fibroblast density rather than collagen density weakens cardiomyocyte function. *Journal of Cardiovascular Translational Research*, *10*, 116–127.

Vatta, M., Stetson, S. J., Perez-Verdia, A., Entman, M. L., Noon, G. P., Torre-Amione, G., Bowles, N. E., & Towbin, J. A. (2002). Molecular remodelling of dystrophin in patients with end-stage cardiomyopathies and reversal in patients on assistance-device therapy. *The Lancet*, *359*(9310), 936–941. https://doi.org/https://doi.org/10.1016/S0140-6736(02)08026-1

Velagaleti, R. S., & Vasan, R. S. (2007). Heart failure in the twenty-first century: is it a coronary artery disease or hypertension problem? *Cardiology Clinics*, *25*(4), 487–495.

Wainwright, C. L. (2004). Matrix metalloproteinases, oxidative stress and the acute response to acute myocardial ischaemia and reperfusion. *Current Opinion in Pharmacology*, *4*(2), 132–138. https://doi.org/https://doi.org/10.1016/j.coph.2004.01.001

Wall, R., Bell, A., Devlin, G., & Lawrenson, R. (2013). Diagnosis and treatment of heart failure in Maori and New Zealand Europeans at the Waikato hospital. *The New Zealand Medical Journal (Online)*, *126*(1368).

Wang, X., Ju, J., Chen, Z., Lin, Q., Zhang, Z., Li, Q., Zhang, J., Xu, H., & Chen, K. (2022). Associations between calcium channel blocker therapy and mortality in heart failure with preserved ejection fraction. *European Journal of Preventive Cardiology*, *29*(9), 1343–1351.

Wang, X., Weisleder, N., Collet, C., Zhou, J., Chu, Y., Hirata, Y., Zhao, X., Pan, Z., Brotto, M., Cheng, H., & Ma, J. (2005). Uncontrolled calcium sparks act as a dystrophic signal for mammalian skeletal muscle. *Nature Cell Biology*, *7*(5), 525–530. https://doi.org/10.1038/ncb1254

Weber, K. T., Janicki, J. S., Shroff, S. G., Pick, R., Chen, R. M., & Bashey, R. I. (1988). Collagen remodeling of the pressure-overloaded, hypertrophied nonhuman primate myocardium. *Circulation Research*, *62*(4), 757–765.

Wiberg, C., Hedbom, E., Khairullina, A., Lamandé, S. R., Oldberg, Å., Timpl, R., Mörgelin, M., & Heinegård, D. (2001). Biglycan and decorin bind close to the n-terminal region of the collagen VI triple helix. *Journal of Biological Chemistry*, *276*(22), 18947–18952.

Wiberg, C., Heinegård, D., Wenglén, C., Timpl, R., & Mörgelin, M. (2002). Biglycan organizes collagen VI into hexagonal-like networks resembling tissue structures. *Journal of Biological Chemistry*, *277*(51), 49120–49126.

Wiberg, C., Klatt, A. R., Wagener, R., Paulsson, M., Bateman, J. F., Heinegård, D., & Mörgelin, M. (2003). Complexes of Matrilin-1 and Biglycan or Decorin Connect Collagen VI Microfibrils to Both Collagen II and Aggrecan *. *Journal of Biological Chemistry*, *278*(39), 37698–37704. https://doi.org/10.1074/jbc.M304638200

Wight, T. N., Kinsella, M. G., & Qwarnström, E. E. (1992). The role of proteoglycans in cell adhesion, migration and proliferation. *Current Opinion in Cell Biology*, *4*(5), 793–801. https://doi.org/https://doi.org/10.1016/0955-0674(92)90102-I

Williams, I. A., & Allen, D. G. (2007). Intracellular calcium handling in ventricular myocytes from mdx mice. *American Journal of Physiology-Heart and Circulatory Physiology*, *292*(2), H846–H855.

Wu, H.-D., Xu, M., Li, R.-C., Guo, L., Lai, Y.-S., Xu, S.-M., Li, S.-F., Lü, Q.-L., Li, L.-L., & Zhang, H.-B. (2012). Ultrastructural remodelling of Ca2+ signalling apparatus in failing heart cells. *Cardiovascular Research*, *95*(4), 430–438.

Young, M. F., Bi, Y., Ameye, L., & Chen, X.-D. (2002). Biglycan knockout mice: new models for musculoskeletal diseases. *Glycoconjugate Journal*, *19*, 257–262.

Yue, Y., Skimming, J. W., Liu, M., Strawn, T., & Duan, D. (2004). Full-length dystrophin expression in half of the heart cells ameliorates β-isoproterenol-induced cardiomyopathy in mdx mice. *Human Molecular Genetics*, *13*(15), 1669–1675. https://doi.org/10.1093/hmg/ddh174

Zhang, H.-B., Li, R.-C., Xu, M., Xu, S.-M., Lai, Y.-S., Wu, H.-D., Xie, X.-J., Gao, W., Ye, H., & Zhang, Y.-Y. (2013). Ultrastructural uncoupling between T-tubules and sarcoplasmic reticulum in human heart failure. *Cardiovascular Research*, *98*(2), 269–276.

Zile, M. R., Baicu, C. F., & Gaasch, W. H. (2004). Diastolic heart failure—abnormalities in active relaxation and passive stiffness of the left ventricle. *New England Journal of Medicine*, *350*(19), 1953–1959.